TRANSLATION

COLLECTION OF ARTICLES ON THE INTERNATIONAL GEOPHYSICAL YEAR ISSUE 2

FOREIGN TECHNOLOGY DIVISION

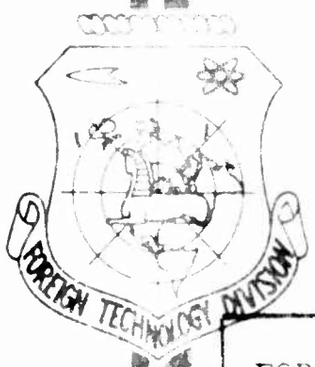

AIR FORCE SYSTEMS COMMAND

WRIGHT-PATTERSON AIR FORCE BASE

OHIO

DISCLAIMER NOTICE

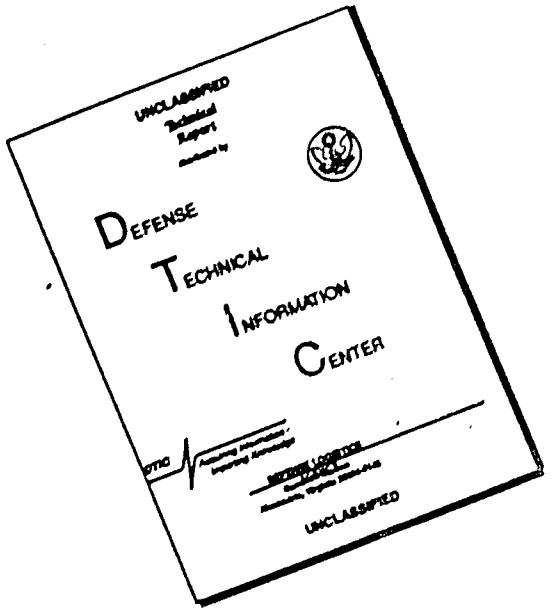

THIS DOCUMENT IS BEST QUALITY AVAILABLE. THE COPY FURNISHED TO DTIC CONTAINED A SIGNIFICANT NUMBER OF PAGES WHICH DO NOT REPRODUCE LEGIBLY.

UNEDITED ROUGH DRAFT TRANSLATION

COLLECTION OF ARTICLES ON THE INTERNATIONAL GEOPHYSICAL YEAR ISSUE 2

English pages: 150

TT5000763-772

PREPARED BY:

TRANSLATION DIVISION
FOREIGN TECHNOLOGY DIVISION
WP-AFB, OHIO.

+2

Ministerstvo Vysshego i Srednego Spetsial'nogo
Obrazovaniya USSR

Kievskiy Ordena Lenina Gosudarstvennyy
Universitet im. T. G. Shevchenko

SBORNIK
RABOT
PO MEZHDUNARODNOMU
GEOFIZICHESKOMU GODU

Vyp. II

Izdat[illegible] Kievskogo Universiteta
1963

[illegible] pages

TABLE OF CONTENTS

The present collection of articles consists of scientific papers prepared by members of the staff of the Kiev Astronomical Laboratory, on the basis of observations carried out as part of the International Geophysical Year program.

The material is intended for specialists-astronomers, as well as for post-graduates and students specializing in the study of astronomy.

Editor-in-Chief:

Asst. Prof. A.F. Bogorodskiy

PHOTOGRAPHIC OBSERVATIONS OF METEORS IN 1958 AT THE KIEV ASTRONOMICAL LABORATORY

V.V. Benyukh, S.P. Vil'chinskaya,
A.A. Demenko, Yu.N. Krivutsa, Ye.V. Sandakova,
A.K. Terent'yeva, L.M. Sherbaum

Photographic observations of the meteors were carried out – as in the previous year – at two base line stations of Kiev University (points A and B).

A meteor patrol of the AC-11 type, with fixed cameras, was used for photographing the meteors. At one of the stations, a device was used containing a three-blade obdurator in front of the camera lenses, which made it possible to determine the instant of the meteor's passage.

A description of the patrol camera, the coordinates of the observation points and other general information as to the methodology of the observations, were reported by us earlier [Ref. 1]. In the present article we shall give the results of the processing of 21 base line photographs of meteors. Measurements of the photographs were carried out by means of measuring machine KIM-3, in two positions of the reversing prisms.

Equatorial coordinates of the bearing point stars were taken from the AGK_2 catalog or the Boss Catalog, and based on the 1950.0 equinox. In th coordinates of the stars, their proper motion was also taken into account, this information being derived from the EBL_2 catalog.

Coordinates of the meteor points were determined by the Deutsch method, including terms of the second order. The methodology of compu-

tation of the radiants, altitudes and velocities will be outlir d in the next collection of articles to be published on the sul ject of the IGY.

The velocities as computed were slightly adjusted to obtain smooth curves. The drag effect was determined on the basis of these adjusted curves. Correction of observed meteor velocity to account for atmospheric resistance, rotation, and earth gravitation, as well as determination of the true radiant was carried out by use of the usual formulas.

Photometry was carried out with photographs taken with shutterless cameras, to determine the mass of meteor particles and the density of the atmosphere in the meteor zone.

The star magnitude of the meteor points was determined either by comparison with the brightness of an artificial meteor (Nos. 17, 19, 24, 29, 33), or by comparison with brightness of star trails. In both cases, serving as standards of comparison were stars of the A_0-A_9 class, as listed in the Henry Draper catalog. Corrections were introduced to account for atmospheric absorption. Stellar brightness was computed on the basis of its value at the equator. Photometric errors of field were also allowed for. In cases when the comparison was by direct juxtaposition of meteor and star trails, allowance was made for the difference in angular velocities of the stars and meteors, by using the well-known formula

$$\Delta m = -2.5 \lg \frac{w_m}{w_*},$$

where w_m is the angular velocity of the meteor, and w_* – the angular velocity of the star, adjusted to the equator.

In cases of comparison with the brightness of an artificial meteor, the stellar magnitude of the meteor points was determined from a char-

acteristic curve constructed on the basis of artificial brightness sources traveling with a velocity equal to that of the meteor. Classification of such artificial sources was carried out on the basis of comparison with the stars already listed.

A similar methodology for determining meteor brightness in terms of stellar magnitude can be found in [1].

The absolute value of the size of the meteors was determined by the following formula:

$$m_{100} = m - 5 \lg r + 10,$$

where r is the distance (in kms) from point B to the point of the meteor train. This distance was calculated by the formula

$$r_i = H_i \sec z_i,$$

where H_1 and z_1 are, respectively, the altitude and zenith distance of the points being observed. The altitude of the meteor points with respect to the horizon of point B was determined by linear interpolation for this point.

All brightness values obtained were converted to the international visual system.

Each point of a meteor train, depending on its brightness, was reduced to one of the formulas below:

for meteors of	– $3^m.0$ or brighter	$\Delta m = 0^m,00 + 0^m,26CI;$
"	– $1^m.0$ to – $3^m.0$	$\Delta m = -0^m,21 + 0^m,19CI;$
"	– $1^m.0$ and fainter	$\Delta m = -0^m,06 + 0^m,12CI.$

The above adjustments were determined on the basis of a study [2] of 150 stars of the Seares catalog. The stellar magnitude of these stars was determined by the same methodology as the one being used at Kiev. An equation was drawn up, in this general form: $\Delta m = a + bCI$, where Δm is the difference between stellar magnitude as recorded by Seares and at Kiev. The coefficients a and b were found by the method of least squares. The equation just cited was used only in the case of stars of

TABLE 1

General Information on Photometeors in 1958)

№ метеора	Дата 1958	Мировое время	Принадл. к потоку	Видимый $t_{1950.0}$	Радиант $\delta_{1950.0}$	Исправленный радиант $\alpha_{1950.0}$	Исправленный радиант $\delta_{1950.0}$	$M_{ph.max}$	r	Число перерывов	v_∞	$H_н$	$H_к$	H_1	W_1 (км·сек$^{-1}$)	H_2	W_2	Sin Q	Примечания
1	2	3	4	5	6	7				8									9
14	март 25	23h34m ± 10	Спорадич.	319° 06'	42°53'	248°02'	42° 48'	—0.9	1°.7	11	40.0	102.8	97.3	102.4	01	98.5	70	0.305	Очень слабый
15	апр., 17	0 36 ± 8	Спорадич.	23 14	-00 26	—	—	—0.5	3.8	12	34.0	90.9	89.0	—	—	—	—	—0.418	Слабый
16	авг., 11	19 22 29s	Персеиды	239 33	57 23	42 10	57 07	—3.7	6.3	15	60.7	98.6	95.5	—	—	—	—	0.205	
17	авг., 11	21 32 50	Персеид	269 03	58 54	45 10	58 54	—3.9	7.4	23	59.8	106 3	91.0	97.4	02	91.2	22	0.199	
18	авг., 11	21 59 38	Персеид	274 43	56 44	46 50	56 04	—3.5	12.7	24	[illegible]	112.3	91.7	109.6	01	92.8	22	0.156	
19	авг., 11	22 38 11	Персеид	282 45	56 50	47 28	56 53	—4.0	7.0	18	60.6	109.0	95.5	—	—	—	—	0.154	
20	авг., 12	19 52 02	Персеид	243 41	58 20	46 26	58 07	—2.0	12.0	26	60.5	110.2	95.8	—	—	—	—	0.136	
21	авг., 12	21 09 24	Персеид	259 28	58 24	49 55	58 19	—2.3	8.0	16	60.0	106.9	97.7	—	—	—	—	0.168	В пункте *A*
22	авг., 13	21 36 45	Персеид	271 04	56 14	46 01	56 14	—1.8		9	61.1	105.4	101.7	—	—	—	—	0.200	слабый
23	авг., 13	22 54 55	Персеид	291 44	58 25	44 40	58 32	—4.0	7.4	17	62.0	110.9	97.2	—	—	—	—	0.159	
24	авг., 14	0 07 00	Персеид	306 36	59 05	47 50	59 14	—4.3	3.0	24	60.4	111.3	95.5	97.1	33	96.1	105	0.235	
25	авг., 16	20 41 —14	Персеид	255 17	61 31	51 08	61 25	—1.8	11.0	21	58.1	106.7	97.6	—	—	—	—	0.192	Болид. В
26	сент., 11	23 52 55	Спорадич.	311 49	49 00	67 22	49 04	ярче —7.0	16.7	29	66.5	113.4	< 83.5	—	—	—	—	0.278	пункте *A*
27	сент., 12	1 11 29	Спорадич.	338 31	04 33	60 11	04 13	—5.3	5.3	28	68.6	118.2	94.6	—	—	—	—	—0.206	выходит за
28	окт., 14	1 06 05	Спорадич.	292 59	67 44	136 43	67 58	—2.6	5.3	13	55.4	100.0	88.0	—	—	—	—	0.209	пределы
29	ноябрь 7	22 15 53	Таурид	355 51	15 00	54 37	13 31	—0.4	9.9	33	28.6	92.4	80.5	—	—	—	—	—0.174	кадра
30	ноябрь 10	23 49 40	Спорадич.	296 03	43 34	141 35	43 34	—[illegible].5	3.8	27	69.6	111.3	97.9	—	—	—	—	0.115	Очень слабый
31	ноябрь 11	0 09 58	Спорадич.	58 05	31 42	—	—	—1.4	2.5	60	17.2	94.0	79.0	—	—	—	—	0.605	
32	дек., 8	23 16 33	Спорадич.	330 04	01 38	126 39	01 04	—1.4	6.8	19	55.6	101.3	93.8	—	—	—	—	0.0903	В пункте *A*
33	дек., 9	16 18 53	Спорадич.	138 50	56 09	213 38	54 43	—4.7	17.9	31	42.3	94.4	83.5	84.6	38	83.9	190	0.127	на краю
34	дек., 12	0 19 48	Геминид	03 27	32 38	111 27	32 08	—0.3	2.3	18	35.0	96.8	85.4	—	—	—	—	0.554	кадра

1) No. of the meteor; 2) date in 1958; 3) GMT; 4) shower; 5) visible $t_{1950.0}$; 6) Radiant $\delta_{1950.0}$; 7) corrected radiant; 8) number of shutter breaks; 9) remarks; 10) March; 11) sporadic; 12) very faint; 13) April; 14) faint; 15) August; 16) Perseids; 17) faint at point A; 18) fireball. Off frame at point A; 19) September; 20) sporadic; 21) brighter; 22) October; 23) November; 24) Taurids; 25) very faint; 26) December; 27) at the edge of frame, at point A; 28) Geminids.

TABLE 2

№ точек 1	Относит. момент τ 2	Высота H (км) 3	Скорость v (км/сек) 4	Абсолютная звездная велич. 5^{m}_{100}	Масса M 6	Плотность атмос. $\lg \rho$ 7	Высота однородн. атмосф. H_a (км) 8
			9 Метеор № 14				
1	0	102,8	40,0	—1,1	0,075	—7,12	
2	0.6 Δτ	101,6	.	—1,1	0,065	—7,19	
3	1,2	100,5	.	—0,9	0,049	—7,37	
4	1,6	99,9	.	—1,0	0,034	—7,21	
5	2,6	98,5	.	—1,0	0,025	—7,16	
	Δτ = 0ˢ,0417						
			10 Метеор № 15				
1	0	89,0	34,0	—0,4	0,15	—7,21	
2	1,0 Δτ	89,9	.	—0,3	0,12	—7,18	
	Δτ = 0ˢ,0417						
			11 Метеор № 16				
1	0	98,4	58,8	—2,5	0,57	—8,40	
2	3,0 Δτ	95,5	.	—3,7	0,36	—7,78	
	Δτ = 0ˢ,0434						
			12 Метеор № 17				
1	0	106,3	59,8	—3,4	0,78	—8,04	
2	1,0 Δτ	104,7	.	—3,6	0,71	—7,97	
3	2,0	103,9	.	—3,9	0,62	—7,79	4,53
4	3,0	101,1	.	—3,9	0,50	—7,73	
5	7,0	94,9	.	—3,1	0,38	—7,99	
	Δτ = 0ˢ,0418						
			13 Метеор № 18				
	0	112,3	60,5	—2,6	0,25	—8,18	
2	1,0 Δτ	109,0	.	—3,2	0,20	—8,53	
3	2,0	107,4	.	—3,3	0,14	—8,38	
4	3,0	105,7	.	—2,6	0,09	—8,26	6,08
5	4,0	104,0	.	—2,9	0,05	—8,22	
6	4,5	103,1	.	—3,5	0,02	—8,34	
	Δτ = 0ˢ,0418						
			14 Метеор № 19				
1	0	109,0	59,8	—2,6	0,32	—8,20	
2	1,0 Δτ	107,3	.	—3,2	0,28	—7,94	
3	2,0	105,5	.	—3,2	0,22	—7,86	
4	3,0	103,6	.	—3,5	0,14	—7,62	
5	4,0	101,9	.	—3,7	0,06	—7,26	
	Δτ = 0ˢ,0418						
			15 Метеор № 20				
1	0	110,2	60,5	—2,0	0,086	—8,65	
2	1,0 Δτ	108,9	.	—2,0	0,067	—8,51	
3	2,0	107,6	.	—2,0	0,048	—8,44	
4	3,0	106,3	.	—2,0	0,029	—8,40	
5	4,0	105,0	.	—1,9	0,010	—8,48	
	Δτ = 0ˢ,0428						

TABLE 2 CONTINUED

1 Продолжение табл. 2

№ точек 2	Относит. момент τ 3	Высота H (км) 4	Скорость v (км/сек) 5	Абсолютная звездная велнч. m_{100} 6	Масса M 7	Плотность атмос. $\lg \rho$ 8	Высота однородн. атмосф. H_0 (км) 9
	10 Метеор № 21						
1	0	106,9	60,0	—1,7	1,05	—8,89	
2	1,0 $\Delta\tau$	105,4	.	—1,8	0,91	—8,83	
3	2,0	103,9	.	—1,6	0,74	—8,84	
4	3,0	102,4	.	—2,0	0.59	—8,62	
5	4,0	101,0	.	—1,9	0,42	—8,57	
6	5,0	99,5	.	—2,3	0,22	—8,23	
	$\Delta\tau$ = 0^s,020						
	11 Метеор № 22						
1	0	105,4	58,8	—1,6	0,054	—8,18	
2	0,7 $\Delta\tau$	104,2	.	—1,8	0,022	—7,82	
3	1,0	103,8	.	—1,4	0,012	—7,82	
4	1,4	103,3	.	—1,1	0,009	—7,82	4,76
5	1,6	102,9	.	—1,1	0,005	—7,70	
6	2,0	102,2	.	—1,1	0,003	—7,56	
	$\Delta\tau$ = 0^s,0419						
	12 Метеор № 23						
1	0	110,5	61,9	—4,0	0,23	—7,67	
2	0,5 $\Delta\tau$	109,5	.	—3,4	0,19	—7,83	
3	1,5	107,5	.	—2,9	0,13	—7,93	4,85
4	2,5	105,5	.	—3,2	0,09	—7,68	
5	3,5	103,5	.	—2,9	0,04	—9,57	
	$\Delta\tau$ = 0^s,0418						
	13 Метеор № 24						
	0	111,3	60,4	—3,7	0,52	—7,83	
2	0,5 $\Delta\tau$	110,1	.	—3,4	0,45	—7,91	
3	1,0	109,3	.	—3,7	0,41	—7,77	
4	2,0	107,0	.	—4,0	0,33	—7,59	
5	3,0	104,8	.	—4,0	0,19	—7,46	
6	4,0	102,6	.	—3,0	0,06	—7,47	
	$\Delta\tau$ = 0^s,0417						
	14 Метеор № 25						
1	0	103,6	58,1	—1,3	0,060	—8,15	
2	1,0 $\Delta\tau$	102,1	.	—1,6	0,047	—7,95	
3	1,5	101,4	.	—1,7	0,039	—7,87	
4	2,0	100,7	.	—1,8	0,030	—7,77	
5	3,0	99,3	.	—1,5	0,014	—7,67	
	$\Delta\tau$ = 0^s,0420						
	15 Метеор № 26						
1	0	113,4	66,5	—2,9	2,00	—8,91	
2	0,5 $\Delta\tau$	112,1	.	—3,9	2,00	—8,52	
3	1,0	110,8	.	—5,2	1,95	—8,00	
4	2,0	108,6	.	—6,0	1,74	—7,64	
5	3,0	106,1	.	—5,9	1,18	—7,53	
	$\Delta\tau$ = 0^s,0420						

TABLE 2 CONTINUED

1 Продолжение табл. 2

№ точек 2	Относит. момент τ 3	Высота H (км) 4	Скорость v (км/сек) 5	Абсолютная звездная велич. $6m_{100}$	Масса M 7	Плотность атмос. 8 $\lg \rho$	Высота однородн. атмосф. $9H_0$ (км)
		10 Метеор № 27					
1	0	108,2	68,6	—5,0	1,95	—8,14	
2	1,0 Δτ	106,3	.	—5,1	1,78	—8,09	
3	2,0	104,7	.	—5,1	1,56	—8,02	
4	4,0	100,5	.	—5,2	1,33	—7,97	5,76
5	5,0	98,5	.	—5,2	0,85	—7,82	
6	6,7	95,5	.	—5,3	0,60	—7,70	
	$\Delta\tau = 0^s,0420$						
		11 Метеор № 28					
1	0	100,0	54,7	—2,0	0,17	—8,07	
2	0,5 Δτ	99,1	.	—2,6	0,15	—7,79	
3	1,5	97,3	.	—2,6	0,11	—7,67	
4	2,5	95,1	.	—2,4	0,07	—7,63	4,27
5	3,5	93,8	.	—2,3	0,03	—7,42	
	$\Delta\tau = 0^s,0420$						
		12 Метеор № 29					
1	0	80,5	28,6	0,4	0,23	—7,11	
2	2,0 Δτ	82,3	.	—0,3	0,15	—8,42	
3	3,0	83,3	.	—0,3	0,11	—8,16	
4	4,0	84,3	.	—0,3	0,08	—8,04	
5	5,0	85,3	.	—0,3	0,04	—7,91	
	$\Delta\tau = 0^s,0426$						
		13 Метеор № 30					
1	0	111,3	69,6	—4,6	1,01	—8,00	
2	0,5 Δτ	110,3	.	—4,8	0,90	—7,91	
3	1,0	109,2	.	—5,2	0,81	—7,73	
4	2,0	107,3	.	—5,5	0,69	—7,56	
5	2,5	106,2	.	—5,5	0,38	—7,35	
6	3,0	105,1	.	—5,5	0,19	—7,18	
	$\Delta\tau = 0^s,0421$						
		14 Метеор № 31					
1	0	90,3	17,2	—1,1	8,36	—6.51	
2	3,0 Δτ	88,8	.	—0,6	1,95	—6,32	
3	5,0	87,7	.	—0,6	1,05	—6,12	
4	7,0	86,7	.	—0,4	0,60	—6,05	
5	8,0	86,2	.	—0,3	0,18	—5,73	4,24
	$\Delta\tau = 0^s,0421$						
		15 Метеор № 32					
1	0	101,3	55,6	—1,0	0,05	—8,13	
2	1,0 Δτ	100,0	.	—0,9	0,03	—8,10	
3	2,0	98,6	.	—0,9	0,02	—8,01	
4	3,0	97,2	.	—0,9	0,02	—7,88	
5	4,0	95,8	.	—0,4	0,01	—7,86	5,15
	$\Delta\tau = 0^s,0425$						

TABLE 2 CONTINUED

1 Продолжение табл. 2

№ точек 2	Относит. момент τ 3	Высота H (км) 4	Скорость v (км/сек) 5	Абсолютная звездная велич. m_{100} 6	Масса M 7	Плотность атмосф. lg ρ 8	Высота однородн. атмосф. H_* (км) 9
			10 Метеор № 33				
1	0	94,4	42,3	—4,6	4,33	—7,30	
2	1,0 Δτ	93,5		—4,7	3,48	—7,21	
3	2,0	92,6		—4,4	2,72	—7,88	
4	4,0	91,7		—4,0	1,60	—7,65	4,29
5	6,0 Δτ = 0s,0565	90,9		—3,9	0,70	—7,45	4,17
			11 Метеор № 34				
1	0	96,8	35,0	—0,3	0,16	—7,56	
2	1,0 Δτ	95,4		—0,3	0,14	—7,53	
3	2,0	94,0		—0,3	0,12	—7,48	
4	3,0	92,6		—0,3	0,10	—7,43	4,72
5	5,0	89,8		—0,3	0,08	—7,38	5,56
6	7,0 Δτ = 0s,0421	86,9		—0,2	0,04	—7,19	5,92

1) No. of the point; 2) relative moment τ; 3) altitude H (in kms); 4) velocity v (km/sec); 5) absolute stellar magnitude m_{100}; 6) mass M; 7) atmospheric density log ρ; 8) altitude of homogeneous atmosphere, H_* (kms); 9) meteor No.

various stellar magnitudes. The same adjustments can be applied also to meteors (by taking the difference in velocities into account, of course), since in this methodology a meteor is treated as the sum of starlike objects.

The value of the color index was determined by the Jacchia scale [3]:

m	CI
brighter than $1^m.1$	$-1^m,86$
$1^m.0$ to $-0^m.1$	$-1^m,54$
$0^m.0$ to $+0^m.9$	$-1^m,12$
fainter than $+1^m.0$	$-0^m,96$

Since in the formulas cited above, the color index appears with a small coefficient, it can be said that inaccurate knowledge of its exact value has little bearing on determining the stellar magnitude of the meteor.

The mass of meteor bodies was calculated by this formula:

$$M = \frac{2}{\tau_0} \int_{t_i}^{t_k} \frac{I}{v^2} dt,$$

where $\tau_0 = 10^{-9.07}$, $\log I = 9.84 - 0.4m_{100}$, and $\underline{v}$ is the velocity of the meteor. For determining mass, the graph-adjusted, "smoothed" velocity values were used.

In cases where a definite evaluation of the drag effort for a meteor has been obtained, determination of atmospheric density was made by the formula

$$\rho = -kM^{\frac{1}{3}} \frac{dv}{dt} v^{-2},$$

where $k = 0.863$.

Where the drag factor was unknown or equaled zero, atmospheric density was determined by means of the following formula:

$$\lg \rho = 21{,}23 + \lg I - \frac{2}{3} \lg M - 6 \lg v.$$

The altitude of the homogeneous atmosphere was computed by the method proposed by L.A. Katasyev [4].

The following formula was used:

$$H_* = -3v_i \int_{t_k}^{t_i} \frac{I}{I_i} dt \left[1 - \left(\frac{\int_{t_k}^{t_H} I dt}{\bar{\alpha} \int_{t_k}^{t_i} I dt} \right) \right] \cos z_R.$$

Here, t_H, t_k and t_i are moments corresponding to the appearance and disappearance of meteors and a point having the assigned velocity v_i; $\bar{\alpha}$ is the proportionality coefficient, the value of which is taken to be 1.135.

Table 1 gives some general information about the meteors. Here ℓ^0 is the angular length of the meteor, in degrees; w_1, and w_2 are drag factors at points having an altitude H_1 and H_2; v_∞ is the preatmospheric velocity; m_g is the maximum absolute stellar magnitude of the meteor,

converted to the international visual system; H_H and H_k are the altitudes of appearance and disappearance, and Q is the angle of convergence between the celestial meridians of the meteors.

Table 2 gives information regarding each meteor at several points along its course. Column 2 shows the relative instant in time, in terms of a fraction of one revolution of the obdurator; column 3 gives the mean ve ocity of the meteor in the sector where no visible drag effect exists. The absolute stellar magnitude values are given in accordance with the international visual system.

The altitude of the homogeneous atmosphere is shown only for the points where the value obtained is certain to be correct.

The following took part in obtaining and processing the material contained in this article: I.V. Kozhevnikova, L.M. Kozhevnikov, B.G. Kruchinenko, A.K. Suslov, and Zh.M. Shcherban'.

REFERENCES

1. V.V. Benyukh, A.A. Gavlovskaya, V.P. Konopleva, Yu.N. Krivutsa, V.G. Kruchinenko, Ye.V. Sandakova, A.K. Terent'yeva, Sbornik statey po MGG kievskogo universiteta, vyp. 1, 1960 [Collection of Articles on the IGY from Kiev University, Issue 1, 1960].

2. Ye.V. Sandakova and A.A. Gavlovskaya, Byulleten' komissii po kometam i meteoram AN SSSR [Bulletin of the Commission on Comets and Meteors of the USSR Academy of Sciences], 1960.

3. L. Jacchia, A.J. 62, 20, 1957.

4. L.A. Katasev. A.J. 34, 2, 1959.

THE PHYSICS OF INTERACTION BETWEEN RADIO WAVES AND METEOR TRAINS

(A review)

By: I.V. Bayrachenko

§1. THEORY OF VAPORIZATION AND IONIZATION OF METEORS

The physics of interaction of the body of a meteor and the earth's atmosphere is discussed in detail in the book by B.Yu. Levin [1]. The specific case of a spherical meteor – when the assumption is made that the coefficients of heat transfer and of resistance are equal to 1 – was examined by Herlofson [2].

Let a meteoroid of arbitrary form and a frontal section S enter the atmosphere of the earth with a velocity V_0, at an angle $\underline{x}$ with respect to the zenith. Since the geometric dimensions of meteor particles are very much smaller than the free path run of the air molecules at altitudes at which the meteors appear, the interaction of the molecules and meteors has the character of an elastic or nonelastic mutual collision. As a result of nonelastic collisions, the body of the meteor heats up, then melts, and, finally, vaporizes.

Viewed in reverse, the problem is one of air molecules striking a stationary meteor at geocentric speed. If we assume that, at the altitude at which the meteors appear, the molecular weight of the air $\eta_0 = 29$, then the kinetic energy of the colliding air molecules – for meteor velocities ranging from 10 to 70 km/sec – will be altered by some tens to several hundreds electron-volts. On the other hand, the energy of the atomic bond in the meteor (e.g., in the case of iron atoms) is

on the order of a few unit electron-volts. This means that, given a temperature of vaporization, the colliding air molecule is capable of evaporating up to 100 atoms of the meteoroid, and thus, within a relatively short distance of travel within the earth's atmosphere, can cause the meteor to evaporate almost completely, without experiencing any noticeable drag effect.

The vaporized atoms leave the body of the meteor at velocities slightly higher than that of the meteor body itself (greater by the magnitude of the thermal velocity). As a result of elastic and nonelastic collisions with air molecules, this energy is dissipated in heat, light and ionization. Along the path of the disintegrating meteor, there forms an ionized column, containing free electrons and ions, and capable of scattering the electromagnetic field energy which strikes them and thus give rise to the radiophysical manifestations of meteors.

If, in first approximation, we ignore the factor of drag in the evaporation of a significant part of the body of the meteor, and if we assume that the density of the atmosphere at the altitude of the meteor's appearance, $\rho(H_1)$, is very small as compared with the atmospheric density at the altitude at which the meteor disappears, $\rho(H_2)$, (this approximation is valid for both bright and normal meteors), then the evaporation equation will, [see 1], appear as follows:

$$\frac{dM}{dt} = -\frac{M_0 V_0 \cos\chi}{H^*} \frac{\rho(H)}{\rho(H_M)} \left[1-(1-\mu)\frac{\rho(H)}{\rho(H_M)}\right]^{\frac{\mu}{1-\mu}}, \qquad (1.1)$$

where M_C is the initial mass of the meteoroid, H* is the altitude of the homogeneous atmosphere, μ is the constant in the equation relating the change in mass and change in the frontal section s ($s/s_0 = (M/M_0)\mu$), $\rho(H_M)$ is the atmospheric density at the altitude corresponding to the maximum evaporation rate.

Equation (1.1) can be divided by the mass of η of the individual

meteor atom. Then the number of atoms evaporating per 1 sec will be:

$$n = \frac{M_0 V_0 \cos \chi}{\eta H^*} \frac{\rho(H)}{\rho(H_\infty)} \left[1 - (1-\mu)\frac{\rho(H)}{\rho(H_\infty)}\right]^{\frac{\mu}{1-\mu}}. \qquad (1.2)$$

For a nonrotating body of any shape, which retains it during evaporation, $\mu = 2/3$, while from (1.2) can be deduced the formula obtained by Kaiser [3] on the basis of the work of Whipple and Herlofson:

$$n = (\eta H^*)^{-1} M_0 V_0 \cos \chi \frac{P(H)}{P(H_\infty)} \left[1 - \frac{1}{3}\frac{P(H)}{P(H_\infty)}\right]^2, \qquad (1.3)$$

where P is the atmospheric pressure, associated with atmospheric density by the equation on distance:

$$P = \rho RT/\eta,$$

and

$$P(H_\infty) = \left[\frac{2Qg}{\Lambda V^2 A}\right] M_0^{1/3} \cos \chi. \qquad (1.4)$$

where Q is the energy required for heating and vaporizing 1 gr of meteor matter, g is the acceleration of gravity, Λ is the heat transfer coefficient, which takes into account the insulting action of the evaporated molecules. According to Levin, for bodies giving rise to conventional meteors $\Lambda \approx 0.3$-0.5, while according to Whipple, it is $\Lambda \approx$ ≈ 0.7 and $A = sM_0^{-2/3}$ is the shape factor.

The vaporized atoms of the meteor, colliding with air molecules, convert their kinetic energy into heat, light, and ionization. During the collision of heavy particles, the probability of excitation and ionization is considerably smaller than in the case of a collision between an electron and a heavy particle at comparable energy levels [4]. This difference is due to the difference in mass. It is believed that almost the entire kinetic energy of the meteor is converted into heat, a small part - into light, and only a very small fraction will go into ionization. According to Greenhow and Hawkins [5], the ratio of these

three parts is, for a bright meteor: $10^4:10^2:10$, and for a faint meteor: $10^4:10.10$. The number of free electrons, created per centimeter of the meteor's course, is:

$$\alpha = \beta \frac{n}{V} \frac{\partial A}{c M}, \tag{1.5}$$

where β is the probability of ionization, determined by the equation:

$$\beta = aV^q \tag{1.6}$$

a and q being constants.

According to Eqs. (1.3), (1.4) and (1.5).

$$\alpha = \frac{9}{4} \alpha_M \left(\frac{P}{P_M}\right)\left(1 - \frac{1}{3}\frac{P}{P_M}\right)^2, \tag{1.7}$$

$$\alpha_M = \frac{4}{9} \beta (\mu H^*)^{-1} M_0 \cos \chi. \tag{1.8}$$

From Eq. (1.8), it follows that maximum ionization is proportional to the initial mass and depends on the velocity through the area of probability of ionization.

Weiss [6], showed that the approximation (1.7) yields in the area of the maximum and below it, significant deviations from values obtain from precise formulas applicable to low meteor velocities. He proposed the following expression to determine maximum electron density:

$$\alpha_M = 12 (a V_M^{q-1}/\mu H^*) M_0 F(q)^2 [1 + 2F(q)]^{-2} \cos \chi, \tag{1.9}$$

where

$$V_M^2 = V_0^2 + 12Q \ln (r_M/r_0),$$
$$r_M/r_0 = 2F(q)[1 + 2F(q)]^{-1},$$
$$F(q) = 1 + 3(1 + q) Q/V_0^2,$$

V_m, r_m being the velocity and radius of the body of the meteor at the point of maximum ionization.

Greenhow and Neufeld [7], with the aid of two widely-spaced radar oscillations, investigated experimentally the changes in ionization along the train of faint meteors (with a star-brightness magnitude equivalent of +6 to +8). It developed that the mean ionization curve

is much shorter than would seem to be indicated theoretically, and, specifically, the increase in the maximum el ctron linear density is much steeper.

The question of the dependence of β on velocity has been examined in a number of papers and the results obtained have been extremely contradictory. According to Kaiser [3], the value of β lies in the range of $0.1 \leq \beta \leq 1$. The following values were obtained for $\underline{q}$: by Kaiser: 0 ± 0.6; by Massey and Side [8]: 1.2 to 1.3; by Evans and Hall [9]: 0.5 ± 0.5; by Hawkins [10]: 5.6; and by Fialko, [11]: 0.75 to 1.5. Yu. A. Loshchilov showed that the Hawkins calculations were erroneous, ard he believes that the Massey and Side figures are the correct ones [12, 13].

§2. DISSIPATION OF METEOR TRAINS

When a meteor particle penetrates into the terrestrial atmosphere there is an increase in the concentration of charged particles, which begins immediately within the process of formation to dissipate. The dissipation of the train is a result of the phenomena of diffusion, recombination and adhesion. The most important factor in the dissipation of a meteor train is ambipolar diffusion, which diminishes the volume electron density without affecting the linear density α.

The diffusion equation for the cylindrical distribution of electrons and positive ions without consideration of the terrestrial magnetic field [14, 3]

$$\frac{\partial n_e}{\partial t} = \frac{D_e}{r}\frac{\partial}{\partial r}\left(r\frac{\partial n_e}{\partial r}\right) + \nabla\left(\frac{e\vec{E}n_e}{m\nu_e}\right), \tag{2.1}$$

$$\frac{\partial n_i}{\partial t} = \frac{D_i}{r}\frac{\partial}{\partial r}\left(r\frac{\partial n_i}{\partial r}\right) - \nabla\left(\frac{e\vec{E}n_i}{m_i\nu_i}\right), \tag{2.2}$$

where $\underline{r}$ is the radius of the train, $\underline{t}$ is time, $\underline{m}$ and m_1 are, respective-

ly the mass of the electron and the mass of the ion, ν_e and ν_i are, respectively, the frequency of electron and ion collisions, e is the electron charge, $\vec{E}$ is the electrical field of the charges, and $e\vec{E}/m_i\nu_i$ and $e\vec{E}/m\nu_e$ are, respectively, the drift velocities of the ions and electrons in this field .

If we bear in mind that the difference between the concentrations n_e and n_i is small, having excluded $\vec{E}$ from (2.1) and (2.2), we will obtain

$$\frac{\partial n_e}{\partial t} = \frac{D}{r}\frac{\partial}{\partial r}\left(r\frac{\partial n_e}{\partial r}\right). \tag{2.3}$$

where the coefficient of ambipolar diffusion is given by the approximate expression

$$D = \frac{8}{3}\lambda_i\left(\frac{2kT}{\pi\eta}\right), \lambda_i = \frac{1}{\sqrt{2}\pi n_a \sigma_i}. \tag{2.4}$$

Here k is the Boltzmann constant, T is the temperature of the electrons and ions, n_a is the density of the neutral particles and σ_i is the average classical diameter for the ions and neutral molecules.

In the assumption that the electron line density and the coefficient of diffusion remain constant, the solution for Eq. (2.3) yields

$$n_e = \frac{\alpha}{4\pi Dt}\exp\left[-\frac{r^2}{4Dt}\right]. \tag{2.5}$$

Thus, the radial distribution of electron density is gaussian, and the quantity $(4Dt)^{1/2}$ may be assumed as the radius of the column at the instant t.

In rarefied gases recombination occurs through inelastic collisions of two bodies. Consequently, the number of electron recombinations per 1 cm^3 per unit time will be proportional, all other conditions equal, to the number of encounters between ions and electrons. This number in turn is proportional to the concentrations of electrons

and ions. The drop in the number of electrons per 1 cm^3 per unit time is therefore

$$\frac{dn_e}{dt} = -\alpha_e n_e n_i,$$

where α_e is the coefficient of electron recombination. With $n_e = n_i$, we have

$$\frac{dn_e}{dt} = -\alpha_e n_e^2. \tag{2.6}$$

Having taken the processes of recombination into consideration, we find that (2.3) is written in the following form:

$$\frac{\partial n_e}{\partial t} = \frac{D}{r}\frac{\partial}{\partial r}\left(r\frac{\partial n_e}{\partial r}\right) - \alpha_e n_e^2. \tag{2.7}$$

From (2.7) we have the rate for the change in the electron line density:

$$\frac{d\alpha}{dt} = -2\pi\alpha_e \int_0^\infty r n_e^2 dr. \tag{2.8}$$

If we assume the change in the volume electron density is gaussian with respect to the radius,

$$\alpha^{-1} - \alpha_0^{-1} \simeq \frac{\alpha_e}{8\pi D}\ln\frac{t}{t_0}, \tag{2.9}$$

and the integration of (2.7) yields

$$n_e \simeq \frac{\alpha_0}{t\left[4\pi D + \frac{1}{2}\alpha_0\alpha_e \ln\left(\frac{t}{t_0}\right)\right]}\exp\left[-\frac{r^2}{4Dt}\right], \tag{2.10}$$

where $(4Dt_0)^{1/2}$ and α_0 are, respectively, the initial radius and the initial electron line density.

The adhesion of electrons to neutral gas particles results in the formation of negative ions. The change in ionization as a result of adhesion is given by

$$\frac{dn_e}{dt} = -\beta_e n_e n_m. \tag{2.11}$$

Here β_e is the coefficient of electron adhesion and n_m is the density of the neutral molecules.

When the effect of adhesion is considered, (2.3) assumes the form

$$\frac{\partial n_e}{\partial t} = \frac{D}{r}\frac{\partial}{\partial r}\left(r\frac{\partial n_e}{\partial r}\right) - \beta_e n_e n_m + \text{the term for separation.} \qquad (2.12)$$

If we assume each electron adhering to a neutral molecule as lost, thus enabling us to neglect the term for separation, the integration of (2.12) with respect to the radius yields

$$a = a_0 \exp(-\beta_e n_m t). \qquad (2.13)$$

Since n_e retains the same form as in (2.5),

$$n_e = \frac{a_0}{4\pi D t}\exp\left[-\frac{r^2}{4Dt} - \beta_e n_m t\right]. \qquad (2.14)$$

Let us evaluate the extent to which the above-considered processes affect the dissipation of a meteor train.

From the standpoint of adhesion, of all the components in the upper atmosphere only atomic and molecular oxygen form stable negative ions. From the basis of theoretical calculations [15] the most probable value for the coefficient of electron adhesion for these components is $\beta_e = (10^{-15}\text{-}10^{-}16)$ cm^3/sec, with β a weak function of the temperature. It follows from (2.14) that adhesion can be neglected if $\beta_e n_m t \ll 1$, which is always satisfied for ordinary radiometeors. Indeed, to satisfy this inequality n_m must be smaller than 10^{15} cm^{-3}, which corresponds to an altitude of about 75 km which is less than the height at which radiometeors are observed. The relative order of time within which the effect of adhesion becomes apparent is given by the equation [3]

$$\tau = 1{,}6\cdot 10^{-20}[\lambda V^3/\beta e^2 \cos\chi]^{2/5}. \qquad (2.15)$$

For $\lambda = 4\cdot 10^2$ cm, $V = 4\cdot 10^6$ cm/sec and $\cos\chi \approx 1$, (2.15) yields: for $\beta_e = 10^{-15}$ cm^3/sec, $\tau = 15$ sec; for $\beta_e = 10^{-16}$ cm^3/sec, $\tau = 90$ sec. Parallel photographic and radar observations of meteors [16, 17] for an altitude of 95 km yield a value of $\beta_e \simeq 5\cdot 10^{-15}$ cm^3/sec for the coefficient of adhesion for a radiometeor duration of $\tau = 50$ sec.

Kaiser and Greenhow [18] studied the relative role played by the effect of recombination in meteor trains. They derived $\alpha_e \sim 5 \cdot 10^{-10}$ cm^3/sec, i.e., considerably less than the value of 10^{-8} cm^3/sec obtained for the E layer of the ionosphere. This disparity in the α_e values is explained by the fact that recombination in the E layer is primarily molecular in nature whereas it is atomic in nature in the meteor trains. Greenhow [19], having carried out his investigations on a wavelength of 4.2 meters, demonstrated that the duration of the radioecho during which the effect of recombination becomes apparent must be considerably greater than 60 sec. This contention is borne out by Oepik's calculations [20].

Thus, the effects of recombination and adhesion will become apparent only in the case of extremely long-enduring meteors, and diffusion consequently is the factor responsible for the dissipation of the meteor trains.

§3. INITIAL RADII OF METEOR TRAINS

It follows from Formula (2.5) which gives the ionization density with respect to distance from the axis of the train that at the instant $t = 0$ the ionization density yields an indeterminacy and an initial rad-

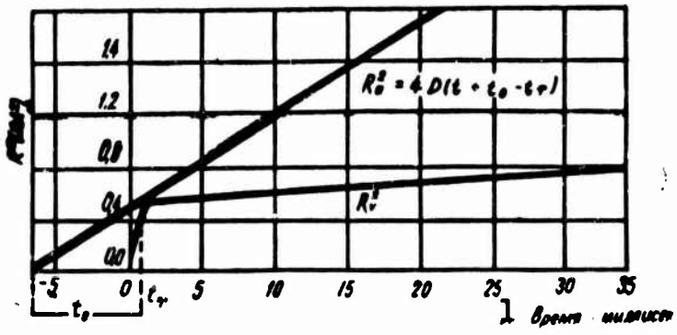

Fig. 1. The square of the train radius as a function of time for $\ell = 5$ cm, $V = 50$ km/sec, and $4D/\ell - 1200$ m/sec. (Manning, 1958). 1) Time, in milliseconds.

ius $r_0 = 0$. To avoid this difficulty, it is assumed [3] that the ini-

tial radius of the train will be of the order of the length of the mean molecular free path of air at the altitudes at which meteoroids become incandescent, i.e., of the order of several centimeters. However, because of the speed of the meteoroid, the vaporizing atoms exhibit great kinetic energy and, consequently, the rate of ionization at the beginning is quite rapid, so that almost instantaneously in the place of a point source we will be dealing with ionization that is spatially distributed [20].

Manning [21] investigated this problem from the standpoint of the kinetic theory of gases and demonstrated that because of the great initial velocity of the meteoric atoms the initial radius from which normal diffusion begins is attained very rapidly, the value of the initial radius in this case being of the order of 14 mean free-path lengths.

Manning considers the ion train from the standpoint that in terms of order of magnitude the number of electrons is comparable with the number of ions in the train. Let us assume that at the initial instant of time the ionization in the train is gaussian in distribution and has an initial radius of r_0. If t_0 is the time within which the radius r_0 is attained, then $r_0^2 = 4Dt_0$ and Formula (2.5) assumes the form

$$n_e = \frac{\alpha}{4\pi Dt + r_0^2} \exp\left[-\frac{r^2}{4Dt + r_0^2}\right]. \qquad (3.1)$$

On colliding with molecules of air the vaporizing atoms of the meteor give up a portion of their energy and as a result the air molecules acquire velocities close to those of the meteor atoms. On the first collision the meteor atom retains 2/3 of its initial velocity on the average, also retaining its initial direction of motion as the most probable. Hence it follows that because of the great initial velocity the meteor atom will cover a path somewhat smaller than three times the mean free path. If the length of the path between collisions is given

L, the atomic and ionic density after M collisions is distributed in the following manner:

$$n = \frac{a}{\pi M} \exp\left[-\frac{3r^2}{4ML^2}\right]. \qquad (3.2)$$

If the radius of the train as a function for the case (3.2) is equated to the radius governed by diffusion at atmospheric temperature, we obtain the following values for the length of the mean free path: $(2)^{1/2}\ell_a$ for atoms; $(2)^{1/2}\ell_1 = (2)^{1/2}\ell_{a/5}$ for ions, where ℓ_a is the length of the mean free path for air molecules at atmcspheric temperature. In Eq. (3.2) L cannot be replaced by $(2)^{1/2}\ell_{a.i}$. This can be done only after several collisions when the meteor atom loses its directivity and when it is possible to apply the kinetic theory to the chaotic motion of the particles. For (3.2) we can therefore write:

$$ML^2 = PM(\sqrt{2}l_{a.i})^2,$$

where P is a constant whose magnitude is a function of the masses of the colliding particles. For the case of meteor atoms whose masses are equal to the masses of the air molecules, Manning derived P = 5.

If the initial velocity of the meteor atom is v_0, becoming V after M collisions, we have

$$V = V_0 \exp[-\psi M],$$

where $\psi = \ln(1/k)$, with k the fraction of the particles retaining meteoric velocity. Generally $2/3 \leq k < 1$. Let us assume $k = (2/3)$, which corresponds to the case of identical masses for the meteor atoms and air particles. In this case $\psi \approx 0.4$.

The time interval between two successive collisions:

$$\frac{\sqrt{2}l_{a.i}}{V} = \frac{\sqrt{2}l_{a.i}}{V_0 \exp[-\psi M]},$$

while the time required for M collisions

$$t = \frac{\sqrt{2}l_{a.l}}{V_0}\int_0^M \exp[\psi M]\,dM = \frac{\sqrt{2}l_{a.l}}{V_0\psi}(e^{\psi M} - 1).$$

Hence the value for M

$$M = \frac{1}{\psi}\ln\left[\frac{\psi V_0 t}{\sqrt{2}l_{a.l}} + 1\right]. \tag{3.3}$$

The radius of the train

$$r = \sqrt{\frac{4pM}{3}}L, \text{where } L = \sqrt{2}l_{a.l}.$$

Consequently, the radius of the train resulting from the high initial velocity of the meteor

$$r_0 = l_{a.l}\left(\frac{8p}{3\psi}\right)^{1/2}\ln^{1/2}\left[\frac{\psi V_0 t}{\sqrt{2}l_{a.l}} + 1\right]. \tag{3.4}$$

For prolonged time intervals r_v should be joined with the radius r_a which is given by the equation

$$r_a^2 = 4D(t + t_a), \tag{3.5}$$

where t_a is the time, taking into consideration the diffusion at the great initial velocities of the diffusing particles.

For altitudes of around 93 km $D_i \approx 3$ m^2/sec, $\ell_i = (1/5)\ \ell_a = 1$ cm [22], and (3.5) assumes the form

$$r_a^2 = \left(\frac{4D_i}{l_i}\right)l_{a.l}(t + t_a) \simeq 1200\,l_{a.l}(t + t_a). \tag{3.5a}$$

Figure 1 shows the curves computed on the basis of Formulas (3.4) and (3.5a), from which we can see that because of the initial velocity the atom train acquires a radius of about 70 cm in a single millisecond, while the ion train acquires this radius within one-fifth of the time.

The value of the initial radius r_0 can be estimated on the basis of the condition that within the time t_0 the curves for r_v and r_a must come into contact, subsequent to which stable diffusion begins. Neglecting the thermal velocities of the air molecules will be compensated somewhat by the drop in the magnitudes of L and p beyond the region of

contact. Let t_t be the time in which $r_v = r_a$. In this case

$$t_t = \frac{\sqrt{2}l_{a.i}}{\psi V_0}\left[\frac{8pV_0}{3\sqrt{2}4D/l_{a.i}} - 1\right] \simeq \frac{8\pi l_{a.i}}{3\psi 4D/l_{a.i}} \simeq \frac{1}{36} l_{a.i}. \qquad (3.6)$$

Having substituted (3.6) into (3.4), we obtain in the place of t a value for the initial radius (the radius at the point of tangency):

$$r_0 = \left(\frac{8p}{3\psi}\right)^{1/2} l_{a.i} \ln^{1/2}\left\{\frac{8pV_0}{[3\sqrt{2}(4D/l_{a.i})]}\right\}. \qquad (3.7)$$

The time t_0

$$t_0 = \frac{r_0^2}{4D} \simeq \frac{0{,}166 l_{a.i}^2}{l_i}. \qquad (3.8)$$

For ions $t_{0i} = 0.277\ \ell_a$ and for atoms $t_{0a} = 0.83\ \ell_a$. Thus the initial radius r_0 of the meteor train is attained within a short period of time, equal approximately to $\ell_i/36 \sim 3 \cdot 10^{-4}$ seconds.

F.I. Peregudov, investigating the effective scattering surface of a meteor train [23], considered the initial radius; it turned out that the theoretical computations are in good agreement with the McKinley experiment [24], if it is assumed that the initial radius $r_0 \simeq 0.4$-0.5 m.

§4. MECHANISM FOR THE REFLECTION OF RADIOWAVES FROM METEOR TRAINS

A meteor train immediately after its formation contains free electrons and positive ions. If an electromagnetic wave of frequency ν impinges on such an ionized column, the charged particles oscillate and this causes a portion of the electromagnetic energy to be absorbed, another portion to be re-emitted. According to field theory [25] the equivalent scattering surface for a particle with mass m and electrical charge e is equal to

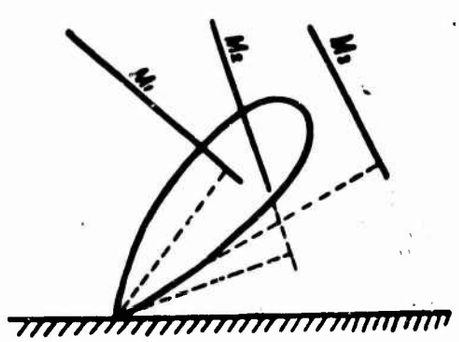

Fig. 2. Only meteor M satisfies the condition of mirror reflection.

$$s_0 = \frac{8}{3}\pi\left(\frac{e^2}{mc^2}\right)^2. \qquad (4.1)$$

where c is the velocity of propagation for the electromagnetic wave.

If we take into consideration that the reflection from the charged particle exhibits a directivity pattern similar to the Hertz dipole pattern and, consequently, exhibits a directivity factor of g = 1.5, the equivalent scattering surface

$$\sigma_0 = 4\pi\left(\frac{e^2}{mc^2}\right)^2. \qquad (4.2)$$

For a singly ionized atom of nitrogen or oxygen

$$e_+ = 4{,}803\cdot 10^{-10}\ CGSE,$$
$$m = 2{,}4\cdot 10^{-23}\ \Gamma,\quad \sigma_0 \simeq 10^{-34}\ \text{cm}^2.$$

For an electron

$$e_- = 4{,}803\cdot 10^{-10}\ CGSE,$$
$$m = 9\cdot 10^{-28}\ \Gamma,\quad \tau_0 \simeq 10^{-25}\ \text{cm}^2.$$

Thus, the scattering surface for electrons is greater by a factor of approximately 10^9 than for ions and it is therefore completely valid to assume that the radio-reflection of radiowaves from meteor trains is governed exclusively by the presence of free electrons.

It is generally assumed that the ionized column of a meteor is long and straight and for this reason the radioecho will be received primarily from the vicinity of a point on the train that is normal to the ray of the antenna directivity pattern (Fig. 2). This assumption is well borne out by the phenomena which take place during the formation of the ionized column by the meteoroid: the time variation in the intensity of the reflected signal coincides in shape with the change in the illumination of the screen in the diffraction of light on a straight edge.

§5. SCATTERING WITHOUT CONSIDERATION OF DIFFUSION

Lovell and Clegg [26] computed the energy reflected from a meteor train containing α electrons per unit length, in the assumption that,

first of all, the diameter of the train is narrow in comparison with the wavelength and, secondly, that the electron density in the train is so small that mutual collisions of electrons under the action of an incidence field can be neglected.

Let us consider a short segment of a train dz long situated at a distance R from a transmitter. This segment contains $N' = \alpha dz$ electrons. Consequently, the total charge and mass of this segment will be equal to $e_\Sigma = e\alpha dz$, and $m_\Sigma = m\alpha dz$, respectively. On the basis of (4.2) the effective scattering surface for electrons

$$\sigma = 4\pi\left(\frac{e^2\alpha dz}{mc^2}\right). \tag{5.1}$$

If emission and reception are accomplished with a single antenna, the power of the reflected signal at the receiver input

$$W = \frac{PG^2\lambda^2}{64\pi^3R^4}\cdot\sigma, \tag{5.2}$$

where P is the power of the transmitter, G is the directivity factor of the emitter and λ is the wavelength.

In the case of radiowave scattering from a cloud of electrons (5.2) assumes the form

$$W' = \frac{PG^2\lambda^2}{16\pi^3R^4}\left(\frac{e^2\alpha dz}{mc^2}\right)^2. \tag{5.3}$$

On the other hand

$$W = \frac{1}{2}\frac{U_m^2}{r}, \tag{5.4}$$

where U_m is the amplitude of the receiver input voltage and $\underline{r}$ is the input resistance of the receiver.

From Eqs. (5.3) and (5.4) we obtain

$$dU_m = \frac{e^2}{mc^2}\frac{G}{4\pi}\frac{(2rp)^{1/2}\lambda}{R^2}\alpha dz. \tag{5.5}$$

The amplitude of the field governed by the scattering of the radiowaves

by the dz element of the meteor train is equal to

$$dA = A_m(R, \alpha)\sin\left(\omega t - \frac{4\pi R}{\lambda}\right)dz. \qquad (5.6)$$

The quantity $A_m(R, \alpha)$ for the given meteor is approximately constant. Let us integrate Eq. (5.6) from the point at which the radioecho z_1 appears to the point z_2 where a constant resulting amplitude is established

$$A = A_m\int_{z_1}^{z_2}\sin\left(\omega t - \frac{4\pi R}{\lambda}\right)dz. \qquad (5.7)$$

From Fig. 3 we see that

$$R = R_0\cos\theta + z\sin\theta \simeq R_0 + \frac{z^2}{R_0}.$$

If we introduce the denotation

$$\varphi = \omega t - \frac{4\pi R_0}{\lambda}$$

and the new variable

$$\frac{\pi x^2}{2} = \frac{2\pi z^2}{R_0\lambda},$$

the amplitude of the signal at point O

$$A = A_m\frac{\sqrt{R_0\lambda}}{2}\int_{x_1}^{x_2}\sin\left(\varphi - \frac{\pi x^2}{2}\right)dx. \qquad (5.8)$$

According to the theory of diffraction

$$\int_{x_1}^{x_2}\sin\left(\varphi - \frac{\pi x^2}{2}\right)dx = C\sin\varphi - S\cos\varphi, \qquad (5.9)$$

where C and S are Fresnel integrals

$$C = \int_{x_1}^{x_2}\cos\frac{\pi x^2}{2}dx,\ S = \int_{x_1}^{x_2}\sin\frac{\pi x^2}{2}dx. \qquad (5.10)$$

As follows from (5.8) and (5.9), the intensity of the reflected wave is ob-

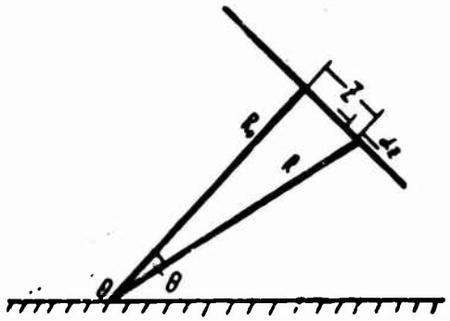

Fig. 3. An illustration of the calculations for signal amplitude. R_0 is the range to the point of mirror reflection.

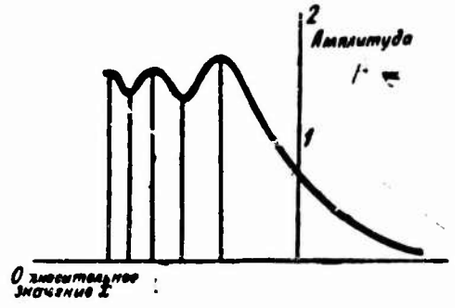

Fig. 4. Theoretical amplitude-time pattern observed when a meteor intersects the perpendicular drawn between the point of observation and the meteor train. A) Amplitude; B) relative value of x.

tained in the following form:

$$I_p = A_0^2 (C^2 + S^2). \tag{5.11}$$

which is identical to the expression for the case of light diffraction on the edge of a straight screen. Figure 4 shows the theoretical amplitude-time pattern which makes it possible to determine the geocentric speed of the meteor:

$$V_g = \frac{0{,}73\sqrt{R\lambda}}{t}. \tag{5.12}$$

Ellyett and Davies [27] were the first to employ this method for the measurement of velocities.

For purposes of determining the resulting signal amplitude we will integrate Eq. (5.8) with respect to the entire train. Since the length of the train is considerably greater than the dimensions of the Fresnel zone, the integration may be accomplished from $-\infty$ to $+\infty$:

$$A = \sqrt{\frac{R_0\lambda}{2}} A_m. \tag{5.13}$$

From Eqs. (5.5) and (5.6)

$$A_m = \frac{e^2}{mc^2} \frac{G}{4\pi} \frac{(2rp)^{1/2}}{R^2} \alpha, \tag{5.14}$$

and

$$A = \frac{e^2}{mc^2} \frac{G}{4\pi} \frac{(2rp)^{1/2}}{\sqrt{2}} \alpha \left(\frac{\lambda}{R_0}\right)^{3/2}. \tag{5.15}$$

From Eq. (5.5)

$$U_m = \frac{e^2}{mc^2} \frac{G}{4\pi} \frac{(2pr)^{1/2}\lambda N}{R^2}. \tag{5.16}$$

From (5.15) and (5.16)

$$N = \alpha \sqrt{\frac{\lambda R_0}{2}}. \tag{5.17}$$

Since the phase delay occurs twice for an incident and a reflected wave, Equation (5.17) defines the number of electrons participating in the reflection. Since the phase delay occurs twice for an incident and a

reflected wave, the size of the first Fresnel zone is equal to $(\lambda R_0/2)^{1/2}$. Thus, with the assumed simplifications only the electrons of the first Fresnel zone take part in the scattering of the electromagnetic energy, while the energy scattered by the electrons of other zones is mutually cancelled.

§6. THE HERLOFSON THEORY OF SCATTERING

The linear distribution of ionization in the column will be disrupted by the effect of ambipolar diffusion. As a result the position of the electrons with respect to each other will change and, consequently, there will also be a change in their relative phase contributions in the scattered signal. In a number of cases the Herlofson theory [28] makes it possible to take into consideration the effect of the ambipolar diffusion.

Herlofson considered the problem of radiowave scattering from meteor trains on the basis of the Maxwell equations of macroscopic electrodynamics which for the case of a meteor train assumed the form:

$$\operatorname{rot}\vec{H} = \frac{4\pi}{c}\vec{i} + j\frac{\omega}{c}\varepsilon_0\vec{E}; \tag{6.1}$$

$$\operatorname{rot}\vec{E} = -j\frac{\omega}{c}\vec{H}; \tag{6.2}$$

$$\operatorname{div}\varepsilon\vec{E} = 0, \tag{6.3}$$

where ω is the angular frequency of the electromagnetic field, ε_0 is the dielectric permeability of free space, $\vec{r}$ is the conduction current, $\vec{H}$ and $\vec{E}$ are, respectively, the magnetic and electrical components of the field.

When a plane electromagnetic wave impinges on an ionized cylinder the displacement current is complemented by the conduction current which is governed by the following phenomena: 1) the motion of electrons under the action of a Lawrence force in the magnetic field of the

earth; 2) the motion of electrons as a result of collisions; 3) the oscillation of electrons owing to the action of the incident field.

The influence of a permanent magnetic field on the propagation of radiowaves is defined by the ratio of gyroscopic frequency ω_H to the radio frequency. The gyroscopic frequency $\omega_H = |e| H_0/mc \simeq 1{,}76 \cdot 10^7 H_0$. In the terrestrial magnetic field which exhibits $H_0 \simeq 0.5$ oersteds at the poles, $\omega_H \simeq 8.82 \cdot 10^6$ cps, which corresponds to a wavelength of $\lambda_H = 214$ m, whereas in the case of radar detection of meteors radiowaves 1-13 meters long are employed. Consequently, the conduction current due to the geomagnetic field need not be taken into consideration.

For the waveband used in the detection of meteors by means of radar the frequency of electron collisions $\nu_c \ll \nu$, and the effect of the collisions can also be neglected. Thus, the conduction current is governed exclusively by the effect of the incident-wave field. It may be maintained that only the electrical component of the incident-wave field affects the electrons, since when $\vec{E} \sim \vec{H}$ the magnetic force $(e/c)[\vec{V}\vec{H}]$ is less than the electrical force $e\vec{E}$ by a factor of approximately 3000, assuming the thermal velocity of the electron as its velocity $\vec{V}$ (it is assumed that $T \sim 300^\circ$).

The equation of motion for the electron

$$m \frac{d\vec{V}}{dt} = e\vec{E}. \tag{6.4}$$

Since the field varies harmonically, velocity must vary in accordance with the same law

$$\vec{V} = \vec{V}_0 e^{j\omega t}. \tag{6.5}$$

On the basis of (6.4) and (6.5)

$$\vec{V} = \frac{e\vec{E}}{j\omega m}. \tag{6.6}$$

The current density

$$\vec{r} = n_e e \vec{V} = \frac{n_e e}{j\omega m} \vec{E}, \tag{6.7}$$

Having used (6.7) and taken into consideration that $\varepsilon_0 = 1$ for free space, we find that Eqs. (6.1) and (6.2) assume the form:

$$\text{rot}\,\vec{H} = jk\varepsilon\vec{E}, \tag{6.8}$$

(6.9)

where $k = 2\pi/\lambda$ is the wave number and

$$\text{rot}\,\vec{E} = -jk\vec{H}, \tag{6.10}$$

If we introduce a rectangular system of coordinates with z along the axis of the ionized column and if we assume that the wave impinges from the direction $x > 0$, on the basis of (6.8), (6.9) and (6.3) we can obtain the following wave equations:

a) for the case of parallel polarization, with $\vec{E} \| z$:

$$\Delta E_z + k^2 \varepsilon E_z = 0; \tag{6.11}$$

b) for the case of transverse polarization, with $\vec{H} \| z$:

$$\Delta H_z - \frac{1}{\varepsilon}\frac{d\varepsilon}{dr}\frac{\partial H_z}{\partial r} + k^2 \varepsilon H_z = 0. \tag{6.12}$$

Thus, to solve the problem of the scattering of radiowaves from a meteor train it is necessary to solve Eqs. (6.11) and (6.12) for certain boundary conditions. Equation (6.11) is presented in the form

$$\Delta E_z + k^2 E_z = 4\pi n_e \rho E_z, \tag{6.13}$$

where $\rho = e^2/mc^2 = 2.8 \cdot 10^{-13}$ cm is the classical radius of an electron.

If the electron density is so small that the right-hand part of (6.13) may be regarded as a small perturbation (a diminished train), the solution of this equation on the basis of the Green theorem is given by

$$E_z' = e^{jkR_0} - 4\pi\rho \int\int\int_v cn_e E_z dv \Big/ \int\int_s \nabla c ds. \tag{6.14}$$

The first term in the right-hand part of the solution represents

the incident wave at the point of observation and the second term represents the scattered wave; $\underline{c}$ is the Green function which is determined from the specific conditions of the problem. We are interested in the scattered wave:

$$E_{\text{рас}} = -4\pi\rho \iiint_{v} c n_0 E_0 dv \Big/ \iint_{s} \Delta c ds. \tag{6.15}$$

The volume integral in the numerator is taken over the entire cross section of the cylinder with a unit train length. The surface integral is taken over the narrow cylinder of unit length about the point of observation. In selecting the Green function let us make use of the condition that the scattered wave at infinity must satisfy the principle of radiation, i.e., it must tend toward zero. This requirement is satisfied by the Hankel function of the second kind, of zero order:

$$c = J_0 - jN_0. \tag{6.16}$$

where J_0 is the Bessel function of zeroth order and N_0 is the Neumann function of zeroth order.

In the volume integral the argument $k|\vec{R}|$ of the Green function is great ($|\vec{R}|$ represents the distance between a point inside the cylinder and the point at which the radiometeor is observed) and therefore we can use the following asymptotic expression for the Hankel function:

$$c \simeq \sqrt{\frac{2j}{\pi k R_0}}\, e^{-jk(R_0 - z)}. \tag{6.17}$$

For the surface integral in Eq. (6.15) let us use the asymptotic expression for the case in which the argument of the Hankel function tends toward zero:

$$c \simeq -\left(\frac{2j}{\pi}\right) \lg |\vec{R}|. \tag{6.18}$$

On the basis of (6.17), (6.18) and (6.15)

$$E_{\text{рас}} = e^{-jkR_0} \sqrt{\frac{2\pi}{jkR_0}}\, \rho \iiint_{v} e^{jk\Delta z} n_0 dv. \tag{6.19}$$

For transverse polarization Eq. (6.12) can be presented in the form

$$\Delta H_z + k^2 H_z = 4\pi\rho\left[n_e H_z + \frac{1}{k^2}(\nabla n_e \times \mathrm{rot}\, H)_z\right]. \tag{6.20}$$

This equation is solved analogously with (6.13) and it develops that

$$E_{\text{рас}} = -H_{\text{рас}}, \tag{6.21}$$

i.e., with low electron density in the column the amplitude of the scattered wave is independent of the polarization of the incident field.

Herlofson introduces the diameter D for scattering energy and this quantity is defined as the width of a strip which exhibits a length such as on absorption and axisymmetric re-emission of all incident power will produce a reflected signal like that from a train:

$$D = 2\pi R_0 |E_{\text{рас}}|^2. \tag{6.22}$$

The amplitude of the scattered wave

$$|E_{\text{рас}}| = \sqrt{\frac{2\pi}{kR_0}}\rho \iiint_V n_e e^{2jks}\, dv, \tag{6.23}$$

and consequently

$$D = \frac{\lambda}{2\pi}\left[2\Delta\rho \iiint_V n_e e^{2jks}\, dv\right]^2. \tag{6.24}$$

Let us consider the effect of diffusion on the amplitude of a radiometeor. If the electron density along the radius exhibits gaussian distribution (2.5), it is not difficult to calculate

$$|E_{\text{рас}}| = \sqrt{\frac{2}{\pi kR_0}}\frac{\pi e^2}{me^2}\alpha e^{-\frac{16\pi^2 Dt}{\lambda^2}}. \tag{6.25}$$

Thus, because of diffusion the amplitude of a weakened radiometeor is damped exponentially. The time during which the amplitude of the signal is diminished by a factor of $\underline{e}$ is given by

$$\tau = \frac{\lambda^2}{16\pi^2 D}. \tag{6.26}$$

Greenhow and Neufeld [29], engaged in an experimental determination of τ, on the basis of (6.26) computed the diffusion factor. The results

are close to the theoretical, as derived by means of Eq. (2.4) (the atmospheric density was determined by means of rocket probes).

If the electron density in the column is sufficiently great, it develops that the amplitude of the reflected signal is a function of the polarization of the incident wave.

In the event of parallel polarization, if the volume electron density is so great that the dielectric permeability of the medium is negative, the field in the medium rapidly attenuates and this is similar to the skin effect in a wire. The depth of penetration at which the field diminishes by a factor of $\underline{e}$ is given by

$$d = \frac{v}{ke}\left(\frac{\pi m}{n_e}\right)^{1/2}. \tag{6.27}$$

The attenuation can be neglected if the cylinder radius a < d. It is a simple matter to prove by means of Eq. (6.27) that this condition is satisfied for meteor trains with a linear electron density $\alpha < 10^{12}$ el/cm. If $\alpha > 10^{12}$ el/cm and, moreover, the depth of penetration is amall in comparison with the radius of the train, the expansion of the train as a result of diffusion results in the expansion of the surface of zero dielectric permeability. The maximum radius of this surface is equal to $3 \cdot 10^2 \alpha^{1/2}/\nu$ cm, and after a period of $6.2\ \alpha/D\nu^2$ this surface is compressed to zero. For meteors with $\alpha \gg 10^{12}$ el/cm the train behaves much like a metallic cylinder and if the radius of the train is small in comparison with the wavelength, the scattering diameter in the case of parallel polarization is given by the formula [22]:

$$D = \frac{2\lambda}{\pi}\left\{1 + \left(\frac{2}{\pi}\ln\frac{\lambda}{5{,}6a}\right)^2\right\}^{-1}. \tag{6.28}$$

In the event of the transverse polarization of the incident field with respect to the axis of the meteor train, the electrons move in the transverse plane of the cylinder, thus bringing about a change in the

surface charge. The theory of radio reflection under consideration here encounters basic difficulties in this connection.

Let us return to Eq. (6.12). In a cylindrical system of coordinates this equation is written in the following manner:

$$\frac{\partial^2 H_z}{\partial r^2}+\left(\frac{1}{r}-\frac{1}{\varepsilon}\frac{d\varepsilon}{dr}\right)\frac{\partial H_z}{\partial r}+\frac{1}{r^2}\frac{\partial^2 H_z}{\partial \varphi}+k^2\varepsilon H_z=0. \tag{6.29}$$

To find the special solution for (6.29) we can make use of the method of separation of the variables:

$$H_z=F(r)\Phi(\varphi). \tag{6.30}$$

This yields the following equations for the functions Φ and F:

$$\Phi''+m^2\Phi=0; \tag{6.31}$$

$$F_m''+\left(\frac{1}{r}-\frac{\varepsilon'}{\varepsilon}\right)F_m'+k^2\varepsilon-\frac{m^2}{r^2}\Big)F_m=0. \tag{6.32}$$

Solution (6.31)

$$\Phi=A\cos m\varphi+B\sin m\varphi. \tag{6.33}$$

Having taken into consideration that the components of the incident-wave field are even functions of the angle φ

$$H_{z\text{пад}}=e^{jkz}=e^{jkr\cos\varphi}, \tag{6.34}$$

let us assume B = 0. Consequently,

$$\Phi=A\cos m\varphi, \tag{6.35}$$

and to eliminate the many values, m must be a whole number. Equation (6.32) represents a differential Bessel equation of the mth order which is difficult to solve because of the fact that it is necessary for the determination of the constants to relate the solutions inside and outside the cylinder in the presence of a singular point for which ε = 0.

Kaiser and Closs [30] proposed the approximate method for the solution of this problem and for this reason we will return to it somewhat later. Herlofson, however, modified Eq. (6.31) to the form of a Riccati-type equation whose integration can be accomplished only for a

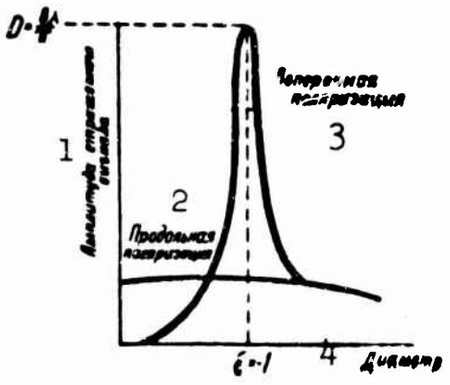

Fig. 5. Theoretical relationship between the variation in the force of the reflected signal and the diameter of the ionized column in the case of a constant number of electrons (Herlofson, 1951). 1) Amplitude of reflected signal; 2) longitudinal polarization; 3) transverse polarization; 4) diameter.

uniform cylinder. As a result it turned out that with $\varepsilon = -1$ resonance takes place and here

$$D_{\text{рез}} = \frac{8}{\pi}\lambda. \tag{6.36}$$

Figure 5 shows graphically the theoretical relationship between the variation in the force of a reflected signal and the diameter of the ionized column for a constant number of electrons.

The physical interpretation of the derived pattern is the following. With a small scattering diameter, i.e., with large negative values for the dielectric constant, $E_{\perp\ \text{ras}} < E_{\parallel\ \text{ras}}$, since the large electrostatic field prevents the shifting of the charges in the plane perpendicular to the axis of the cylinder. With increasing cylinder diameter because of diffusion the dielectric permeability diminishes so that consequently there is a reduction in the electrostatic charge field and the intensity of the signal for $E_{\perp\ \text{ras}}$ at first increases insignificantly, while at $\varepsilon = -1$ there arises distinct resonanct which is associated with the electrical resonance of electrons subject to the effect of regenerative electrostatic forces. With large radii the dielectric permeability becomes positive, tending to unity, and since the train has

been weakened the intensity of the reflected signal is not a function of the polarization of the incident field.

§7. THE KAISER AND CLOSS THEORY OF SCATTERING

Kaiser and Closs [30] used the approximate method of solving the problem on the scattering of radiowaves that is based on the representation of the electrodynamic problem in the form of a problem in statics, assuming that the meteor train is cylindrical in shape and expands gradually as a result of diffusion. A solution is sought for Eq. (6.3):

$$\operatorname{div}(\varepsilon \operatorname{grad} V) = 0, \tag{7.1}$$

where V is the potential of the electrostatic field and the dielectric permeability ε is a function of the radius and, as follows from (6.10), equal to

$$\varepsilon(r) = 1 - \frac{4\pi e^2 n_e(r)}{k^2 m c^2}. \tag{7.2}$$

In a cylindrical system of coordinates, following the separation of the variables, (7.1) is written as follows:

$$\frac{d}{dr}\left(\varepsilon r \frac{dV_m}{dr}\right) = \frac{m^2 \varepsilon V_m}{r}, \tag{7.3}$$

where

$$V(r, \varphi) = \sum_{m=0}^{\infty} V_m(r) \sin m\varphi. \tag{7.4}$$

On the basis of (6.35) we can present Eq. (6.32) in the form

$$\frac{d^2 H_m}{dr^2} + \left[\frac{1}{r} - \varepsilon \frac{d\varepsilon}{dr}\right]\frac{dH_m}{dr} + \left[k^2 \varepsilon - \frac{m^2}{r^2}\right] H_m = 0, \tag{7.5}$$

where

$$H_m(r, \varphi) = \sum_{m=0}^{\infty} H_m(r) \cos m\varphi. \tag{7.6}$$

Equations (7.3) and (7.5) are equivalent if in (7.5) we neglect

the term $k^2 \varepsilon H_m$ which characterizes the phase variations of the field. Let us therefore assume that

$$|\varepsilon (kr)^2| \ll m^2, \tag{7.7}$$

or for the dipole model

$$|\varepsilon (kr)^2| \ll 1. \tag{7.7a}$$

Using the equations

$$\vec{E} = -\operatorname{grad} V, \quad \operatorname{rot} \vec{H} = jk\varepsilon \vec{E}, \tag{7.8}$$

we obtain the relationship between H_m and V_m

$$H_m = j(kr)\varepsilon V'_m/m. \tag{7.9}$$

The solution of Eq. (7.3) for the region outside the cylinder, given that Conditions (7.7) are met, and with consideration of Relationship (7.9), yields

$$H_m(r) = jk\varepsilon (A_m r^m - B_m r^{-m}). \tag{7.10}$$

The constants A_m and B_m can be defined by numerical integration of Eq. (7.3).

Let us expand the plane incident wave of unit amplitude given by Eq. (6.34) into a Fourier series:

$$e^{jkr\cos\varphi} = \sum_{m=0}^{\infty} \varepsilon_m (j)^m J_m(kr) \cos m\varphi. \tag{7.11}$$

Here ε_m is the Neumann factor which for $m = 0$ is equal to $\varepsilon_0 = 1$, while for $m = 1, 2, 3, \ldots \varepsilon_m = 2$, and $J_m(kr)$ is the Bessel function of mth order of the first kind.

For the region outside the train (7.5) assumes the form

$$\frac{d^2 H_m}{dr^2} + \frac{1}{r}\frac{dH_m}{dr} + \left(k^2 - \frac{m^2}{r^2}\right) H_m = 0, \tag{7.12}$$

whose solution

$$H_{psc} = \sum_{m=0}^{\infty} t_m [J_m(kr) - jN_m(kr)] \cos m\varphi. \tag{7.13}$$

where N_m is the Neumann function and t_m is a constant, complex in the

general case.

Let us make use of the asymptotic approximations for the Bessel and Neumann functions [31] for large r

$$J_m(kr) \simeq \sqrt{\frac{2}{\pi kr}} \cos\left[kr - \frac{(2m+1)\pi}{4}\right], \tag{7.14}$$

$$N_m(kr) \simeq \sqrt{\frac{2}{\pi kr}} \sin\left[kr - \frac{(2m+1)\pi}{4}\right], \tag{7.15}$$

and we find

$$H_{\text{рас}} \simeq \sum_{m=0}^{\infty} j^m t_m \left(\frac{2}{\pi kr}\right)^{1/2} e^{-j\left(kr - \frac{\pi}{4}\right)}. \tag{7.16}$$

Since Eq. (7.6) expresses the total external field, according to (7.11), (7.16) and (7.6) we will have

$$\sum_{m=0}^{\infty} H_m \cos m\varphi = \sum_{m=0}^{\infty} \varepsilon_m (j)^m J_m(kr) \cos m\varphi + \sum_{m=0}^{\infty} j^m t_m \left(\frac{2}{\pi kr}\right)^{1/2} e^{-j\left(kr - \frac{\pi}{4}\right)}. \tag{7.17}$$

From Eq. (7.17)

$$\left.\begin{aligned} H_0 &= (1 + t_0) j_0(kr) - j t_0 N_0(kr), \\ H_m &= (2j^m + t_m) J_m(kr) - j t_m N_m(kr). \end{aligned}\right\} \tag{7.18}$$

When (kr) << 1

$$J_m(kr) \simeq \frac{(kr)^m}{2^m m!}, \tag{7.19}$$

$$N_m(kr) \simeq -\frac{2^m (m-1)!}{\pi (kr)^m}, \tag{7.20}$$

where m = 1, 2, 3, ...

Applying Approximations (7.19) and (7.20) and comparing (7.18) with (7.10), we obtain the equations for the determination of the coefficients t_m

$$-\frac{2j^m}{t_m} = 1 + \frac{jm!\,(m-1)!\,4^m}{\pi k^{2m}} \cdot \frac{A_m}{B_m}. \tag{7.21}$$

The coefficient of scattering is determined with the formula

$$g = \sqrt{\frac{\pi kr}{2}}\left(\frac{A_{рас}}{A_{пад}}\right). \tag{7.22}$$

For the case under consideration

$$A_{рас} = H_{рас} = \sum_{m=0}^{\infty} j^m t_m \sqrt{\frac{2}{\pi kr}}, \quad A_{пад} = H_{пад} = 1,$$

and consequently the coefficient of reflection in the case of transverse polarization

$$g_{\perp} \sim \left| \sum_{m=0}^{\infty} j^m t_m \right|. \tag{7.23}$$

In the case of parallel polarization, when $\vec{E} \| z$, we obtain from the wave equation (6.11) in a cylindrical system of coordinates

$$\frac{d^2E_n}{dr^2} + \frac{1}{r}\frac{dE_n}{dr} + \left(k^2\varepsilon - \frac{n^2}{r^2}\right)E_n = 0, \tag{7.24}$$

where

$$E_z = \sum_{n=0}^{\infty} E_n \cos n\varphi. \tag{7.25}$$

Further, the discussion may be continued in a manner similar to the case of transverse polarization with corresponding substitution of notations: $t_m \to \ell_n$, $g_{\perp} \to g_{\|}$; the above-derived formulas are valid here.

If $[\varepsilon(kr)^2] \ll 1$, the basic contribution is made by the term with $n = 0$ and in this case the Lovell-Clegg formula is suitable:

$$g \approx |l_0| = \pi a \frac{e^2}{me^2}. \tag{7.26}$$

Without going into the details of the calculations, let us outline the basic results emanating from the Kaiser and Cless theory.

In the case of a uniform cylinder, when $\varepsilon = \text{const}$ with $r \leq a$ and $\varepsilon = 1$ with $r > a$ with Condition (7.7a) satisfied, it follows from Eq. (7.21) that the coefficient of reflection has its maximum value at $\varepsilon = -1$, in which case the polarization ratio for resonance

$$\left(\frac{g_{\perp}}{g_{\|}}\right)_{рез} = \frac{4}{\pi(ka)^2}. \tag{7.27}$$

The diameter of the scattering in the case of resonance

$$D_{рез} = \frac{8}{\pi}\lambda,$$

which coincides with the result produced by the Herlofson theory.

If $\varepsilon < 0$ and $|\varepsilon(ka)^2| \gg 1$, Formula (7.28) is not valid. In this case the train behaves as a metallic cylinder having a radius a. When $(ka)^2 < 1$ and $\varepsilon \ll -1$

$$g_{\perp} \simeq -\frac{\pi (ka)^2}{2}, \tag{7.28}$$

$$g_{\parallel} \simeq \left|1 - j\left(\frac{2}{\pi}\right)\ln\left(\frac{1{,}781\,ka}{2}\right)\right|^{-1}. \tag{7.29}$$

If, however, $(ka)^2 \gg 1$, on the basis of the laws of geometric optics

$$g_{\perp} = g_{\parallel} = \frac{1}{2}(\pi ka)^{1/2}. \tag{7.30}$$

When diffusion is considered, the electron density in the column exhibits a gaussian distribution and in this case the dielectric permeability on the basis of (7.2) is expressed by the equation

$$\varepsilon(r) = 1 - f\exp\left[-\frac{r}{r_t}\right], \tag{7.31}$$

where

$$f = \frac{4\alpha e^2}{mc^2 (kr_t)^2}.$$

If $(1 - \varepsilon) \ll 1$, the incident wave penetrates the column without distortions and we are confronted with a weakened train. From (7.31) we have the condition of weakness

$$(kr_t)^2 \gg 11{,}24 \cdot 10^{-13}\alpha. \tag{7.32}$$

Since $\varepsilon > 0$ over the entire region of the train, the coefficient of reflection is not a function of the polarization of the incident wave ($g_{\perp} = g_{\parallel}$), and in this case, if $(kr_t)^2 \ll 1$, we obtain the Lovell-Clegg formula (Eq. 7.26). If, however, the train has finite dimensions, the phase differences which were considered in the discussion on the Her-

lofson theory must be taken into consideration.

In the event that the electron density in the column is quite great, but the incident wave nevertheless penetrates all regions of the train, the train in this case is referred to as underdense. The underdense condition is given by $|\varepsilon(kr)^2| \ll 1$, which is equivalent to $\alpha \ll 2.4 \times 10^{12}$ el/cm. For underdense columns the coefficient of reflection is a function of the polarization of the incident wave.

In the case of parallel polarization the Lovell-Clegg formula (7.26) is valid. Until an underdense train weakens because of diffusion, the coefficient of reflection remains constant.

In the case of transverse polarization

$$g_{\perp} \simeq 2\left|1 + \frac{4j}{\pi (kr_t)^2} \cdot \frac{A'}{B'}\right|^{-1}, \tag{7.33}$$

where

$$A_1 = A^1 r_t^{-1}, \quad B_1 = B^1 r_t.$$

From (7.26) and (7.33) the polarization ratio

$$\frac{g_{\perp}}{g_{\parallel}} = \frac{2}{f}\left|\frac{B'}{A'}\right|. \tag{7.34}$$

Hence it follows that $\mathrm{Re}(A') = 0$ is the resonance condition which is found to occur when $f = 2.4$, i.e., when the dielectric constant on the axis has a value of $\varepsilon = -1.4$. Calculations show that because of the scattering boundary the resonance ratio diminishes to 2.

If $\alpha \gg 2.4 \cdot 10^{12}$ el/cm, the incident wave cannot penetrate the central portion of the column and in this case we will be dealing with an overdense train. For the region of the train it is possible to write $\varepsilon < 0$ and $|\varepsilon (kr_t)^2| \gg 1$. For the gaussian distribution Kaiser and Closs assumed that the train behaves as a metallic cylinder whose radius r_e is determined from the equation

$$\varepsilon(r_e)(kr_e)^2 = -1. \tag{7.35}$$

The time during which the dielectric constant on the train axis reaches a value of zero is held to be the duration of the overdense train.

$$\tau = 1{,}124 \cdot 10^{-18} \frac{\lambda^2}{16\pi^2 D} \alpha, \tag{7.36}$$

The maximum coefficient of reflection for an overdense train is independent of the polarization of the incident wave

$$g_M = \frac{1}{2}(\pi k r_0)^{1/2}. \tag{7.36}$$

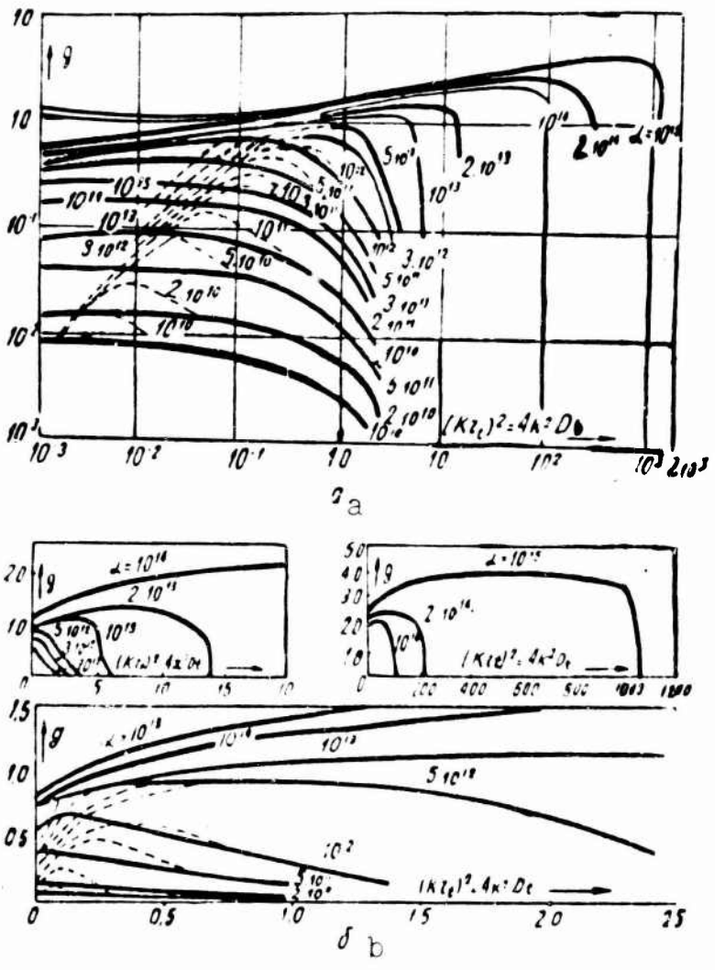

Fig. 6. Coefficient of reflection as a function of $(kr_t)^2 = 4k^2 D_t$: a) For a segment with a logarithmic scale; b) for a segment with a line scale. _____ parallel polarization; - - - - - transverse polarization. (After Kaiser and Closs, 1952).

On the basis of the geometry of reflection Manning [32] computed the power of a radioecho from an overdense column, with consideration of the products of ionization situated beyond the limits of the criti-

cal radius. It developed here that the maximum of signal power was lower by 70% than the quantity predicted by the Kaiser and Closs theory.

Kaiser and Closs smoothly related the solutions for the region of underdense and overdense trains and thus obtained a complete picture of the scattering of radiowaves with varying polarization for gaussian distribution of electrons without restriction of the electron line density and the radius of the train (Fig. 6).

To test the scattering of radiowaves on meteor trains, a number of experimental investigations were conducted [33], [34], [35]. The most correct experiment was carried out by Billam and Browne [35] who studied the polarization effects on a wavelength of $\lambda = 5.45$ meters. Their experimental data are in agreement with the Kaiser and Closs theory for long-enduring signals, and also quantitatively in agreement with the theory of short-duration signals, but in many cases the magnitude of the polarization ratio is greater than predicted by the theory. This is explained by imperfections in the Kaiser and Closs theory, which will be a matter for subsequent consideration.

REFERENCES

1. B.Yu. Levin. Fizicheskaya teoriya meteorov i meteornoye veshchestvo v solnechnoy sisteme [Physical Theory of Meteors and Meteoric Matter in the Solar System], Izd. AN SSSR, [USSR Acad. Sci. Press], 1956.
2. N. Herlofson, Phys. Soc. Rep. Prog. Phys., 1948, 11, 444.
3. T.R. Kaiser, Phil. Mag. Suppl., 1953, 2, No. 8, 495.
4. G. Messi and Ye. Barkhop, Elektronnyye i ionnyye stolknoveniya [Electron and Ion Collisions], IL [Foreign Literature Press, 1958.
5. J.S. Greenhow, G.S. Hawkins, Nature, 1952, 170, 365.

6. A.A. Weiss, Austral. J. Phys., 1958, 11, No. 4, 591.

7. G.S. Greenhow, E.L. Neufeld, Mon. Not. Roy. Astr. Soc., 1957, 117, 359.

8. H.S. Massey, D.W. Side, Phil. Mag., 1955, 46, No. 373, 190.

9. S. Evans, Dzh. E. Kholl. Meteory [Meteors], Collection of Articles, 1959.

10. G.S. Hawkins, Astrophys. J., 1956, 124, page 311.

11. Ye.Y. Fialko, Astr. zhurn., [Astronomy Journal], 1959, 36, Issue 3.

12. Yu.A. Loshchilov, Izv. O.A.O. [Bulletin of the O.A.O.], 1959, 5, Issue 1, 34.

13. Yu.A. Loshchilov, Izv. O.A.O., 1959, 5, Issue 1, 35.

14. L.G.H. Huxley. Austr. J. Sci. Res., 1952, A., 5, 10.

15. D.R. Bates, R.A. Buckingham, H.S. Massey, J.J. Unwin, Proc. Phys. Soc., 1950, 63, 129.

16. J. Davis, J.S. Greenhow, J.E. Hall. Proc. Roy. Soc. A., 1959, 253, 121.

17. J. Davis, J.S. Greenhow, J.E. Hall, Proc. Roy. Soc. A, 1959, 253, 130.

18. T.R. Kaiser, G.S. Greenhow. Proc. Phys. Soc. B., 66, 150, 1953.

19. G.S. Greenhow. Proc. Phys. Soc., B., 1952, 65, 169.

20. E.J. Öpik, Irish. astr. J., 1955, 3, No. 6, 165.

21. L.A. Manning, J. Geoph. Res., 1958, 63, No. 1, 181.

22. Dzh. L. Pozi, R.N. Breysuell. Radioastronomiya [Radioastronomy], IL, 1958.

23. F.I. Peregudov, Astr zhurn., 1957, 34, vyp. 4.

24. D.W.R. McKinley, Can. J. Phys. 1951, 29, No. 5, 403.

25. L.D. Landau, Ye.M. Lifshits, Teoriya polya, [Field Theory],

Fizmat, [Physics-Mathematics Press], 1960.

26. A.C.R. Lovell, J.A. Clegg. Proc. Phys. Soc. 1948, 60, 491.

27. J.G. Davies, C.D. Ellyett. Phil. Mag. ser. 7, 1949, 40, Nos. 305, 615.

28. N. Herlofson. Arkiv f. Fysik [Physics Archives], 1951, 3, 247.

29. G.S. Greenhow, E.L. Neufeld, J. Atmos. Terr. Phys., 1955, 6, 133.

30. T.R. Kaiser, R.L. Closs, Phil. Mag., Ser. 7, 1952, 43, No. 336, 1.

31. G.N. Vatson, Teoriya besselevykh funktsiy [Theory of Bessel Functions], IL, 1949.

32. L.A. Manning, J. Atmosp. Terr. Phys. 1953, 4, page 219.

33. D.W.R. McKinley, Canad. J. Phys., 1951, 29, No. 5, 403.

34. R.L. Closs, J.A. Clegg, T.R. Kaiser. Phil Mag. 1953, 44, Nos. 350, 313.

35. E.R. Billam, J.C. Browne, Proc. Phys. Soc. Sec. B. 1956, 69, No. 433B, 98.

Manuscript Page No.	[Transliterated Symbols]
12	м = m = maksimal'nyy = maximum
32	рас = ras = rasseyaniye = scattering
34	пад = pad = padayushchiy = incident
34	рез = rez = rezonans = resonance

7.

THE SCATTERING OF RADIOWAVES FROM UNDERDENSE METEOR TRAINS

I.V. Bayrachenko

According to theoretical and experimental investigations into the scattering of radiowaves from meteor trains, the nature and power of the reflected signal are significant functions of the magnitude of the electron line density in the column. In the general case, when the same antenna is used both for reception and transmission, the power of the radioecho with consideration of the sphericity of the electromagnetic wave can be presented in the form [1]

$$P_{np} = \frac{P_n G^2 \lambda^3}{32\pi^4 R^3} g^2, \tag{1}$$

where P_{pr} is the power at the receiver input; P_p is the power emitted by the transmitter; G is the directivity factor for the antenna with respect to an isotropic emitter; λ is the wavelength; R is the slant range; g is the reflection factor determined by the equation

$$g = \sqrt{\frac{\pi k R}{2}} \left(\frac{A_{рас}}{A_{пад}} \right). \tag{2}$$

Here $k = 2\pi/\lambda$ is the wave number; A_{ras} is the amplitude of the scattered wave at the point of observation; A_{pad} is the amplitude of the incident wave in the region of the meteor train.

If we assume the meteor train to represent a cylinder whose radius is considerably smaller than the wavelength, the coefficient of reflection for faint trains ($\alpha << 10^{12}$ el/cm) regardless of the polarization of the incident wave is equal to

$$g = \pi\alpha \left(\frac{e^2}{mc^2} \right). \tag{3}$$

where e^2/mc^2 is the classical radius of the electron.

In the case of underdense trains ($\alpha < 10^{12}$ el/cm) the coefficient of reflection is a function of the polarization of the incident wave: in the case of longitudinal polarization it is defined by Eq. (3), while for transverse polarization it is given by the expression

$$g_{\perp} = \sum_{0}^{\infty} f^m t_m, \tag{4}$$

where

$$t_m = -\frac{2f^m}{1 + j\dfrac{m!(m-1)!\,4^m}{\pi k^{2m}} \cdot \dfrac{A_m}{B_m}}.$$

Here A_m and B_m are constants whose ratio is a function of the distribution of electron density in the column.

Only the dipole form of the oscillation (m = 1) makes a significant contribution to the reflection and therefore

$$g_{\perp} \simeq \frac{2}{1 + j\dfrac{4}{\pi k^2} \cdot \dfrac{A_1}{B_1}}. \tag{5}$$

In the case of overdense columns ($\alpha \gg 10^{12}$ el/cm) the meteor train behaves much as a metallic cylinder whose maximum coefficient of reflection, excluding the case in which $g_{\parallel}$ exceeds $g_{\perp}$, regardless of the polarization of the incident wave, is equal to

$$g_{max} = 7{,}1 \cdot 10^{-4}\alpha^{1/4}. \tag{6}$$

In experimental investigations the antenna system is generally positioned so that the plane of polarization is parallel to the plane of the earth. However, meteoroids penetrate into the terrestrial atmosphere from all directions. Therefore, with the scattering of radiowaves from meteor trains the electrical vector of the electromagnetic field will be oriented through a variable angle with respect to the axis of the meteor train. In the case of faint and overdense columns, as can be seen from Eqs. (3) and (6), this plays no part. However, one

must take this fact into consideration in the case of underdense trains, since the coefficient of reflection in the case of transverse polarization may exceed the coefficient of reflection in the case of longitudinal polarization severalfold (resonance in plasma). Consequently, in analyzing individual radiometeors of known streams consideration must be given to the spatial position of the meteor train and the electrical vector of the electromagnetic field.

The present paper considers the question of the magnitude of signal power during the scattering of radiowaves from underdense meteor trains in the case of varying polarization of the incident electromagnetic wave with respect to the axis of the meteor train. We consider the influence exerted by the distribution of electron density in the column on the magnitude of the resulting coefficient of reflection.

Let an electromagnetic wave be propagated in the $X < 0$ direction with the Z axis coincident with the axis of the meteor train (Fig. 1). If β is the angle between the electrical vector of the incident wave and the axis of the train, it is not difficult to see from the figure that

$$g_{\perp} \sim \sin\beta,$$
$$g_{\parallel} \sim \cos\beta,$$

therefore

$$g_{\parallel} = \pi a \frac{e^2}{mc^2} \cos\beta, \tag{7}$$

$$g_{\perp} = \frac{2}{1 + j\frac{4}{\pi k^3} \cdot \frac{A_1}{B_1}} \sin\beta. \tag{8}$$

In the general case the coefficient of reflection may be represented as a complex number

$$g = ge^{i\varphi}. \tag{9}$$

In this case Eq. (1) is written as follows [3]:

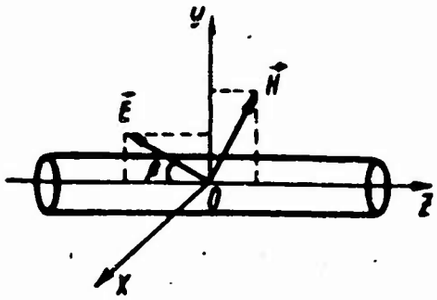

Fig. 1. Orientation of electromagnetic wave with respect to the axis of the meteor train.

$$P_{np} = \frac{P_n G^2 \lambda^2}{32\pi^4 R^4} gg^*, \tag{10}$$

where g* is the magnitude of the complex conjugate g.

Let

$$g_\parallel = g_\parallel e^{j\Phi}, \tag{11}$$

$$g_\perp = g_\perp e^{j\psi}; \tag{12}$$

in which case

$$g = g_\parallel + g_\perp = g_\parallel e^{j\Phi} + g_\perp e^{j\psi} = g_\parallel \cos\Phi + g_\perp \cos\psi + j(g_\parallel \sin\Phi + g_\perp \sin\psi),$$

and

$$gg^* = (g_\parallel \cos\Phi + g_\perp \cos\psi)^2 + (g_\parallel \sin\Phi + g_\perp \sin\psi)^2.$$

As follows from Eq. (7), in the event of longitudinal polarization the coefficient of reflection is a real number and therefore

$$gg^* = g_\parallel^2 + g_\perp^2 + 2g_\parallel g_\perp \cos\psi. \tag{13}$$

Let us expand the content of this equation with respect to various special cases.

For a uniform cylinder (ε = const when $r \leq a$ and $\varepsilon = 1$ when $r > a$, where ε is the dielectric permeability and a is the cylinder radius) [1]:

$$\frac{A_1}{B_1} = \frac{1+\varepsilon}{1-\varepsilon} a^{-2}.$$

Let us substitute the ratio of the quantities A_1 and B_1 into Eq. (8)

$$g_\perp = \frac{2\sin\beta}{1 + j\frac{4}{\pi(ka)^2}\cdot\frac{1+\varepsilon}{1-\varepsilon}}.$$

Hence the modulus and phase of the coefficient of reflection

$$g_\perp = g_\perp e^{j\psi} = \frac{2\sin\beta}{\sqrt{l^2+1}} e^{j\psi}, \tag{14}$$

where

$$l = \frac{4c^2 m}{\pi^2 a^2 e^2 n} - \frac{4c^2}{\pi a^2 \omega^2},$$

$$\psi = \operatorname{arctg} l,$$

ω is the angular frequency of the incident electromagnetic wave, n is the electron volume density in the train.

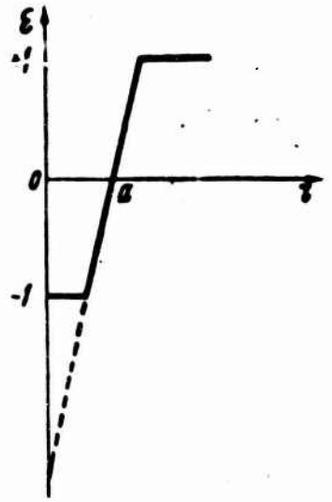

Fig. 2. Distribution of electron density in column after the Herlofson model.

On the basis of Eqs. (10), (13) and (14) the power of the received signal

$$P_{пр} = \frac{P_0 G^2 \lambda^2}{32\pi^4 R^2}\left[\pi^2 a^2\left(\frac{e^2}{mc^2}\right)^2 \cos^2\beta + \frac{4\sin^2\beta}{l^2+1} + \frac{4\pi a e^2 \cos\beta \sin\beta}{mc^2\sqrt{l^2+1}}\cos\psi\right]. \quad (15)$$

Because of the effect of ambipolar diffusion the power of the received signal will exhibit a time variation. In the case of longitudinal polarization [2]

$$g_1 = \pi a \frac{e^2}{mc^2} e^{-(kr_t)^2},$$

where

$$r_t^2 = r_0^2 + 4Dt,$$

r_0 is the initial radius of the meteor train; D is the coefficient of ambipolar diffusion.

Until an underdense train because of diffusion becomes a faint train the coefficient of reflection $g_{\parallel}$ will be virtually constant. This is associated with the fact that for $(kr_t)^2 \ll 1$

$$e^{-(kr_t)^2} \sim 1.$$

In the case of transverse polarization $g_{\perp}$ initially increases attaining a maximum and then diminishes. For a uniform cylinder resonance appears at $\varepsilon = 1$ and with variable polarization of the incident wave

$$\left(\frac{g_{\perp}}{g_1}\right)_{рез} = \frac{4\operatorname{tg}\beta}{\pi(ka)^2}. \quad (16)$$

In the Herlofson model case [2] the column is nonhomogeneous in the region r = a (Fig. 2), and here, as follows from the work of Kaiser and Closs,

$$\frac{A'}{B'} = \frac{(1+\varepsilon) + \varepsilon/a\varepsilon'(a)(j\pi - \ln|\varepsilon|)}{(1-\varepsilon) + \varepsilon/a\varepsilon'(a)(j\pi - \ln|\varepsilon|)}. \tag{17}$$

Here $A' = A_1 a$ and $B' = B_1 a^{-1}$.

If the dielectric permeability is presented in the form [1]

$$\varepsilon(r) = 1 - f \exp\left[-\left(\frac{r}{r_0}\right)^s\right], \tag{18}$$

where

$$f = \frac{4\pi}{(kr_0)^3} \cdot \frac{e^2}{mc^2},$$

in which case for the Herlofson model we must assume $s \gg 1$.

In the case of resonance $\varepsilon \sim -1$, $f = 2$ and

$$a\varepsilon'(a) = s \ln f. \tag{19}$$

Through Eqs. (8), (17) and (19), we will obtain

$$g_\perp \simeq \frac{a\pi e^2 \sin\beta}{m^2} (0{,}44.s - j), \tag{20}$$

whence the modulus and phase of the coefficient of reflection

$$g_\perp = \frac{a\pi e^2 \sin\beta}{mc^2} \sqrt{(0{,}44.s)^2 + 1}, \quad \psi = \operatorname{arctg}(0{,}44.s)^{-1}. \tag{21}$$

On the basis of (10), (13) and (21) the power of the received signal

$$P_{пр} = \frac{P_n G^2 \lambda^2}{32\pi^4 R^2}\left[\pi a \frac{e^2}{mc^2}\right]^2 [\cos^2\beta + \sin^2\beta\{(0{,}44.s)^2 + 1\} + 2\sqrt{(0{,}44.s)^2 + 1}.\ \sin\beta\cos\beta\cos\psi]. \tag{22}$$

The ratio of the coefficients of reflection in the case of resonance

$$\left(\frac{g_\perp}{g_\parallel}\right)_{рез} \simeq \sqrt{(0{,}44.s)^2 + 1}\ \operatorname{tg}\beta. \tag{23}$$

For the most interesting case – the gaussian distribution of electron density in the column, when $s = 2$ in Eq. (18) – the constants A_1 and B_1 from Eq. (8) cannot be determined analytically; therefore, we must resort to the numerical integration of the original differential equation which is presented in the form

$$\frac{d}{d\rho}\left(\rho\varepsilon\frac{dv}{d\rho}\right)=\frac{\varepsilon v}{\rho}. \tag{24}$$

where $\rho = r/r_t$ and V is the potential associated with the electrical field by the equation $E = -\text{grad } \underline{v}$.

The solution for (24) for the region outside of the train, where $\varepsilon = 1$, is given by

$$v = A'\rho + B'\rho^{-1}.$$

If $\rho \ll 1$, $\varepsilon = \text{const}$, and the solution for (24) is

$$v \simeq \rho.$$

Hence, if $\rho = 0$, then $V = 0$, and in this case

$$\frac{\varepsilon v}{\rho} = \varepsilon(0).$$

The integration of (24) in this approximation yields

$$\rho\varepsilon v' = \int_0^\rho \frac{\varepsilon v}{\rho}\,d\rho, \quad v = \int_0^\rho v'\,d\rho. \tag{25}$$

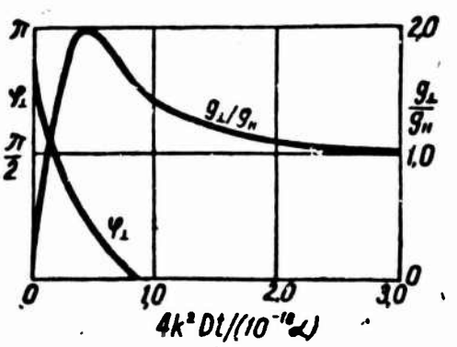

Fig. 3. Magnitude and phase angle of coefficient of reflection for transverse scattering from underdense train with gaussian distribution of electron density (after Kaiser, 1955).

On the basis of the method of successive approximations, making use of (25), we can compute V from point to point and thus determine the constants A' and B'. In this case

$$g_\perp = \frac{2\sin\beta}{1+\frac{4}{\pi(kr_t)^2}\cdot\frac{-B+AC}{1+C^2}+j\frac{4}{\pi(kr_t)^2}\cdot\frac{A+BC}{1+C^2}}, \tag{26}$$

where $A = \frac{A'_P}{B'_R}$, $B = \frac{A'_I}{B'_R}$, $C = \frac{B'_I}{B'_R}$ are determined graphically as a function of f [1].

In practical calculations it is convenient to use the curves obtained by Kaiser [3] (Fig. 3). Since $g_\perp/g_\parallel \sim \tan\beta$ and the coefficient of reflection in the case of longitudinal polarization is given by the simple Expression (3), it is not difficult with the curves shown in Fig. 3 to find the modulus and phase of the coefficient of retraction for transverse polarization and on the basis of Eqs. (10) and (13) to compute the power of the reflected signal.

From the analysis presented above we can see that the magnitude of the resulting coefficient of reflection is a function both of the distribution of the electron density in the column as well as of the spatial orientation of the meteor train. If we take into consideration that the experimental investigations of resonance effects [4], as a rule, yield observed values of polarization ratios systematically higher than the theoretical, the need to consider the resonance effect brought about by the transverse components of the electrical field of the incident wave becomes quite obvious in the study of the scattering of radiowaves from underdense meteor trains in the case of variable polarization of the incident electromagnetic wave with respect to the axis of the meteor train.

REFERENCES

1. T.R. Kaiser, R.L. Closs, Phil. Mag., Vol. 43, No. 336, 1952.
2. N. Herlofson, Arkiv für Fysik [Archives of Physics], Bd. 3, No. 15, 1951.
3. T.R. Kaiser. "Meteors," Ed. by T.R. Kaiser, 1955, page 55.
4. E.R. Billam, I.C. Browne, Proc. Phys. Soc. Ser. B. Vol. 69, No. 433, 1956.

Manuscript Page No.	[Transliterated Symbols]
46	пр = pr = pryemnoye ustroystvo = receiver
46	п = p = peredatchik = transmitter
46	рас = ras = rasseyaniye = scattering
46	пад = pad = padayushchaya volna = incident wave
47	макс = maks = maksimum = maximum
51	рез = rez = rezonans = resonance

THE EFFECT OF THE ANTENNA DIRECTIVITY PATTERN ON THE OBSERVED DISTRIBUTION OF METEOROIDS WITH RESPECT TO MASS

R.I. Moysya, V.G. Kruchinenko, I.V. Bayrachenko

We presently have several methods available to us for the determination of the exponent s in the meteoroid-mass distribution function when we make use of radar data. One of the most common is the method involving the use of the experimentally measured distribution of radiometeor durations. In the selection of this method a number of assumptions were necessary. First of all, the derived theoretical expressions for the number of meteors recorded by radar are valid only in the case of signal reception from a narrow sector of the directivity pattern. In an actual case reception is always accomplished over the entire area of the pattern and the antenna gain is a function of direction. It is clear even from general considerations that the meteor-mass distribution established by radar under conditions in which antenna gain varies as a function of direction must differ from the actual case. In this connection there is some interest in a study of the influence exerted by the directivity pattern of an antenna on the distribution by mass of the recorded meteors.

The present paper represents an attempt to evaluate the influence of the antenna directivity pattern in the vertical plane on the results provided by meteor radio techniques.

CERTAIN PROBLEMS PERTAINING TO THE THEORY OF RADIOWAVE SCATTERING FROM METEOR TRAINS. SELECTION OF THE ELECTRON DENSITY AND MASS INTERVAL

According to the present theory of radiowave scattering from me-

teor trains [1, 2] there are three characteristic types of radio echoes. If in the train the electron line density $\alpha \ll 10^{12}$ el/cm (faint train), as was demonstrated by Herlofson, the amplitude of a radiometeor is not a function of the polarization of the incident wave and diminishes exponentially with time

$$A = A_0 e^{-\frac{16\pi^2 Dt}{\lambda^2}}, \qquad (1)$$

where

$$A_0 = \frac{P^{1/2} G_1^{1/2} G_2^{1/2} \lambda^{3/2}}{(4\pi)^{3/2} R^{3/2}} (2\pi)^{1/2} \left(\frac{e^2}{mc^2}\right) \alpha;$$

here A_0 is the magnitude of the reflected signal at the initial instant of time $t = 0$; D is the coefficient of diffusion in the region of the meteor zone; λ is the wavelength; P is the transmitter power; G_1 and G_2 are the directivity factors of the transmitter and receiver antennas, respectively; R is the slant range; e^2/mc^2 is the classical electron radius.

Kaiser and Closs [2], depending on the magnitude of α, distinguish between underdense and overdense trains. If $\alpha < 2.4 \cdot 10^{12}$ el/cm, the amplitude of a radiometeor, defined by Eq. (1), is a strong function of the polarization of the incident wave. The time for the recording of these reflections for this case [3]

$$T_p < \frac{\lambda^2}{16\pi^2 D} \ln \left[0{,}55 \frac{r_e^2 (P_t G_1 G_2)^{1/2}}{R^{3/2} (\xi^2 \varepsilon_{min} \lambda)^{1/2}} e^{-(kr_e)^2} \right], \qquad (2)$$

where $\xi^2 \varepsilon_{min}$ is the level of discrimination; ε_{min} is the magnitude of the threshold signal; r_e is the equivalent initial train radius; $\underline{k}$ is the wave number.

As follows from Eq. (2), the boundary value for the recording time is a function of the radar-station parameters, as well as of the height and distance at which the meteor appears.

If $\alpha \gg 2.4 \cdot 10^{12}$ el/cm, the meteor train is regarded as a metallic

cylinder whose radius is defined by the equation

$$\varepsilon(r_c (kr_c)^3 = -1,$$

where ε is the dielectric constant of the cylinder.

The amplitude of a signal from a stable train

$$A = A_1 \frac{P_i^{1/2} G \lambda^{3/2}}{R^{3/2}} \alpha^{1/4}, \tag{3}$$

where

$$A_1 = \left(\frac{1}{64\pi^3}\right)^{1/2} e^{-\frac{1}{4}} \left(\frac{e^2}{me^2}\right)^{1/4}.$$

The duration of the reflection in the case of stable trains [2]

$$\tau = 7{,}1 \cdot 10^{-15} \frac{\alpha\lambda^2}{D}. \tag{4}$$

The result obtained for underdense and overdense trains have been extended by Kaiser and Closs to the transitional region for which $\alpha \sim 10^{12}$ el/cm. Investigations have shown [4] that the derived experimental polarization ratios for short-duration echoes are systematically higher than those obtained theoretically, and for the transitional region the theory is totally incapable of explaining the observed phenomena. However, if we take into consideration that for the transitional region plasma resonance takes place, we have a strong basis for using the theoretical results obtained for the region of unstable trains. It follows from the experimental data that the overwhelming part of the radiometeors on a wavelength of $\lambda = 4$ m corresponds to trains of the transitional type. Indeed, on the basis of Eq. (4), assuming $\alpha \approx 10^{12}$ el/cm and $D = 3 \cdot 10^4$ cm^2/sec, we will obtain $\tau = 4.2 \cdot 10^{-14}\ \alpha$.

The majority of the meteors recorded by the radar station on a wavelength of $\lambda = 4$ meters, as demonstrated by experience, exhibits a duration in the interval $0.05 < \tau < 5$ sec, which corresponds to the interval of electron densities of $10^{11} < \alpha < 10^{13}$ el/cm.

Let us evaluate the stellar magnitude of meteors with electron

densities for the trains in the interval from $10^{11} < \alpha < 10^{13}$ el/cm. For this we will use the relationship [5]

$$M = -2{,}5 \lg \alpha_m + 35. \qquad (5)$$

Here M is the absolute stellar magnitude. The result of this evaluation is presented in Table 1.

TABLE 1

α	10^{11}	10^{12}	10^{13}	10^{14}
τ	$4{,}2 \cdot 10^{-3}$	$4{,}2 \cdot 10^{-3}$	$4{,}2 \cdot 10^{-1}$	4,2
M	$7^m.5$	$5^m.0$	$2^m.5$	$0^m.0$

As we can see, trains with a density of 10^{14} el/cm (persistent trains) are formed by meteors of zero magnitude, whose relative number on the basis of visual observational data is very small. As follows from radar observations, more than 90% of all radiometeors (for a wavelength of $\lambda = 4$ meters) form trains of the transitional type (with α in the interval from 10^{11}-10^{13} el/cm).

On the other hand, according to [3] there exists no definite value for the duration separating the reflection from trains of the persistent and unstable types. We may therefore make use of Eq. (4) for the transitional region and hold that

$$\tau \sim \alpha.$$

The number of free electrons per centimeter of meteor path is given by the expression [6]

$$\alpha = \beta \frac{n}{V} \text{ el/cm}, \qquad (6)$$

where β is the probability of ionization; V is the velocity of the meteoroid; $\underline{n}$ is the number of atoms vaporized within a single second.

For a nonrotating body of arbitrary shape, retaining this shape on vaporization [5]

$$n = (\eta H^*)^{-1} m V \cos\chi \left(\frac{P}{P_{max}}\right)\left(1 - \frac{1}{3}\frac{P}{P_{max}}\right)^2, \qquad (7)$$

where $P_{max} = \left(\frac{2Qg}{\Lambda^{1/3}A}\right) m^{1/3} \cos\chi$ is the atmospheric pressure at the point of maximum vaporization; Λ is the coefficient of heat transfer; Q is the energy required for the heating and vaporizing of 1 gram of meteoroid matter; H* is the height of the homogeneous atmosphere; η is the mass of an individual meteor atom; g is the acceleration of the force of gravity.

On the basis of (6) and (7) we draw the conclusion that

$$\alpha \sim m. \qquad (8)$$

Consequently,

$$\tau \sim m. \qquad (9)$$

Thus, having considered the distribution of radiometeors with respect to duration for the transitional region, we can investigate the influence of the equipment parameters and, in particular, the antenna directivity patterns for the experimental distribution of meteoroids by mass.

Derivation of Basic Relationships and the Method for Evaluation of Data

In the derivation of the basic relationships we employed a number of assumptions. It should first of all be stressed that we are examining the influence of only the directivity patterns in the vertical plane on the observational results or, in other words, we are investigating only the function of the angle Θ (Θ is the angle in the plane of the echo, from the line of intersection between the echo plane and the horizontal plane to the directional line to the reflecting point of the meteor). All remaining factors such as, for example, the parameters of the radar, atmospheric parameters, etc., are regarded as constant (throughout the experiment they do not change significantly). The case in which we consider the influence of the antenna directivity pattern

in the horizontal plane will be treated separately.

Let us assume that the majority of meteors are formed in some thin layer of altitudes h_2-h_1 with an average altitude of h_{sr}. For our case we will assume the average height to be equal to 90 km [7] and we will hold this height to be constant.

The distribution function for meteoroids by mass is generally given in the form

$$p(m) = \frac{b}{m^s} \tag{10}$$

or in integral form

$$N(m > m_0) = \frac{b}{(s-1)m_0^{s-1}}, \tag{11}$$

where: b is a constant; s is the parameter characterizing the distribution of the meteoroids by mass.

The number of meteoroids with masses in the interval m-m + Δm passing in time Δt through area ΔS, perpendicular to the direction of the stream [5, 8], is

$$\Delta N = \frac{b \cdot \Delta t \ \Delta m \cdot \Delta S}{m^s}. \tag{12}$$

The area element ΔS (Fig. 1) is equal to

$$\Delta S = R \Delta R \Delta \theta. \tag{13}$$

The number of meteors recorded in a narrow sector with an angle of taper $\Delta\theta$ in the slant range interval R_1-R_2

$$\Delta N_c = b \Delta t \Delta \theta \int_{R_1}^{R_2} \frac{dm R dR}{m^s}. \tag{14}$$

In addition, it is generally held that if the parameters of the radar do not change, the total number of meteors recorded in a narrow sector is equal to [8]

$$N_{c.общ} = \frac{b \cdot h_{ср} \Delta \vartheta \Delta h}{(s-1) \sin^2 \chi \cdot \sin^2 \theta \cdot m_{min}^{s-1}}; \tag{15}$$

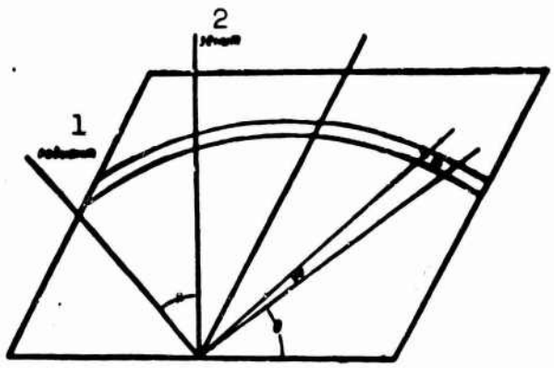

Fig. 1. Echo plane. Determination of area element ΔS. 1) Radiant; 2) zenith.

Here χ is the zenith distance of the radiant; θ is the elevation; m_{min} is the minimum mass of the meteor which can be recorded by radar.

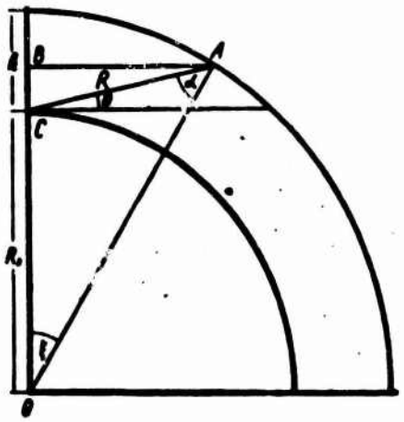

Fig. 2. Derivation of analytical expression for the function $f(\xi\Theta)$.

Hence we can draw the conclusion that for recorded meteors the integral law governing the distribution by mass is the following:

$$N_{\text{общ}} = \frac{A}{m^{s-1}}, \qquad (16)$$

i.e., coincides with the actual conditions in space (11). As was indicated above, Formula (15) fails completely to take into consideration the fact that under actual conditions reception is accomplished not from the narrow sector but from the entire plane of the antenna directivity pattern.

In Formula (14) let us turn from the slant ranges to the heights h. Let us take note of the fact that in this transition it is absolutely necessary to take into consideration the curvature of the earth's surface. In the opposite case the formulas would yield a greater error for smaller values of the angle θ.

Let us consider Fig. 2. Here O is the center of the earth; C is the point at which the radar unit is located; A is the reflecting point; h

is the height of the reflecting point above the terrestrial surface; R_3 is the radius of the terrestrial globe.

From the triangle AOC

$$(R_3 + h)^2 = R_3^2 + R^2 + 2R_3 R \sin\theta. \tag{17}$$

Let us rewrite (17) to the form

$$\frac{h}{R} = \frac{R + 2R_3 \sin\theta}{2R_3 + h}. \tag{18}$$

Since $2R_3 \gg h$, $\underline{h}$ in the denominator of the right-hand part in Eq. (18) can be neglected.

Now we will have

$$\frac{h}{R} = \frac{R}{2R_3} + \sin\theta. \tag{19}$$

Having differentiated (19) with respect to R and $\underline{h}$, after modification we obtain:

$$R_3 dh = \left(1 + \frac{R_3}{R}\sin\theta\right) R dR. \tag{20}$$

R_3/R is defined in terms of the angles θ and ξ (Fig. 2). From Δ ABO

$$\operatorname{tg}\xi = \frac{\frac{AB}{BC}}{1 + \frac{R_3}{BC}}. \tag{21}$$

From Δ ABC

$$\frac{AB}{BC} = \operatorname{ctg}\theta; \quad BC = R\sin\theta.$$

Expression (21) is rewritten in the form

$$\operatorname{tg}\xi = \frac{R\cos\theta}{R\sin\theta + R_3};$$

or

$$\operatorname{ctg}\xi = \operatorname{tg}\theta + \frac{R_3}{R}\frac{1}{\cos\theta}.$$

Hence

$$\frac{R_3}{R} = (\operatorname{ctg}\xi - \operatorname{tg}\theta)\cos\theta. \tag{22}$$

Angle ξ is a function of the angle θ and associated with the last equa-

tion in the following manner:

$$\xi = 90^\circ - \alpha - \theta,$$

where α is defined in terms of θ as

$$\sin\alpha = \frac{R_3}{R_3 + h}\cos\theta.$$

With consideration of (22) we obtain the expression for RdR

$$RdR = R_3 \frac{\operatorname{tg}\xi\,(1 + \operatorname{tg}^2\theta)\cdot dh}{(\operatorname{tg}\theta + \operatorname{tg}\xi)} = R_3 f(\xi, \theta)\,dh. \tag{23}$$

Having substituted (23) into (14), we obtain

$$\Delta N_e = \frac{b\cdot R_3\cdot \Delta t\cdot f(\xi,\theta)(h_2 - h_1)\,\Delta m}{m^s}. \tag{24}$$

The total number of meteors recorded in the narrow sector having an angle of taper $\Delta\theta$

$$N_e = bR_3\Delta t f(\xi,\theta)\,\Delta\theta \int_{m_{min}}^{\infty} \frac{dm}{m^s} = \frac{Bf(\xi,\theta)\,\Delta\theta}{m_{min}^{s-1}}, \tag{25}$$

where

$$B = \frac{bR_3\Delta t}{(s-1)}.$$

The number of meteors with masses in the interval m_{min}-m_1, recorded in the sector $\Delta\theta$, is equal to

$$N_{e.\Delta m} = Bf(\xi,\theta)\,d\theta\left(\frac{1}{m_{min}^{s-1}} - \frac{1}{m_1^{s-1}}\right). \tag{26}$$

As has been demonstrated in a number of works, the minimum mass of a meteor which can be established by means of radar can be represented in the form

$$m_{min} = A'\left(\frac{\varepsilon_n R^3}{P_i G^2 \lambda^3}\right)^{\frac{1}{2}}, \tag{27}$$

where A' in our case is a certain constant; ε_n is the power of the threshold signal; R is the slant range; P_i is the pulse power of the transmitter; G is the field antenna directivity pattern; λ is the wavelength.

Since we are considering the relationship only to the angle θ, having denoted

$$P(\theta) = \frac{G}{R^{3/2}}, \tag{28}$$

we can present m_{min} as

$$m_{min} = \frac{m_0}{P(\theta)} \tag{29}$$

$$m^*_{min} = \frac{m_0}{P(\theta)_{max}}. \tag{30}$$

Function $P(\theta)$ expresses the relationship of the minimum recorded meteoroid mass and the angle θ. Meteors with the least mass m^*_{min} may be recorded only at such an angle θ at which $P(\theta)$ takes on the maximum value.

Let us substitute (29) into (25):

$$N_0 = B' f(\xi, \theta) P(\theta)^{s-1} d\theta, \tag{31}$$

where

$$B' = \frac{B}{m_0^{s-1}}.$$

Let us select the mass interval m_{min}-m_i in such a manner as to have the mass m_i exceed the least mass m^*_{min} by a factor of n

$$m_i = m^*_{min} \cdot n = n \frac{m_0}{P(\theta)_{max}}. \tag{32}$$

It is clear that m_i is not a function of θ since $P(\theta_{max})$ simply represent a number.

Let us substitute (29) and (32) into (26)

$$N_{s,\Delta m} = B' f(\xi, \theta) \left(P(\theta)^{s-1} - \frac{1}{n^{s-1}} P(\theta)^{s-1}_{max} \right) d\theta. \tag{33}$$

The total number of meteors recorded by radar over the entire plane of the antenna directivity pattern

$$N^* = B' \int_0^{90} P(\theta)^{s-1} f(\xi, \theta)\, d\theta. \tag{34}$$

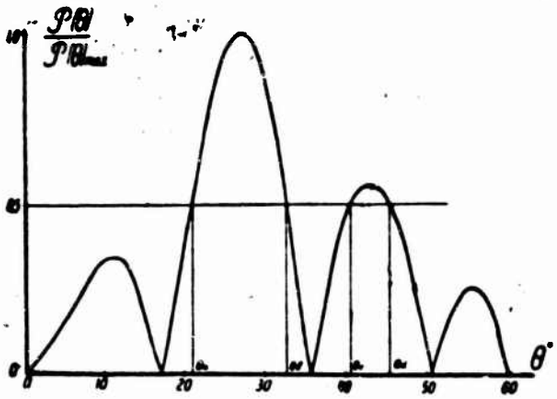

Fig. 3. The form of the function $P(\theta)$ for an antenna of the wave-channel type. The determination of the integration limits in the case in which $\frac{m_i}{m^*_{min}}=2$ is shown.

The number of meteors with masses in the interval from m_{min} to m_i, recorded over the entire plane of the directivity pattern

$$N^*_{\Delta m}=B'\left[\int_{\theta_1}^{\theta_2}P(\theta)^{s-1}f(\xi,\theta)\,d\theta-\frac{P(\theta)^{s-1}_{max}}{n^{s-1}}\int_{\theta_1}^{\theta_4}f(\xi,\theta)\,d\theta\right]. \qquad (35)$$

We obtain the integration limit on the basis of the following considerations. We have to find the number of meteors with masses in the interval m_{min}-m_i. Since the minimum mass recorded by radar is a function of θ, the radar can establish meteors of the given minimum mass only at angles θ for which the function $P(\theta)$ exceeds a certain value. For example, if the mass m_i is set equal to two least masses m^*_{min} ($n = 2$), the integration should be accomplished with respect to the region in which $P(\theta)$ exceeds half its maximum magnitude. It is not difficult to see that $\frac{P(\theta)_{max}}{P(\theta)}=n$. Figure 3 shows the function $P(\theta)$ for a nine-element antenna of the wave-channel type and shows the determination of the integration limits for the case $n = 2$. The function $P(\theta)$ exceeds half its value in the intervals θ_a-θ_b and θ_c-θ_d. These values of the angles θ_a-θ_b and θ_c-θ_d should be chosen as the integration limit for the determination of $N^*_{\Delta m}$.

The integral law of distribution by mass for recorded meteors (the

number of meteors with masses greater than the given) with consideration of the influence of the antenna directivity pattern is obtained in the form

$$N^* - N^*_{\delta m} = B' \int_0^{90} P(\theta)^{s-1} f(\xi, \theta)\, d\theta - B' \left[\int_{\theta_1}^{\theta_2} P(\theta)^{s-1} f(\xi, \theta)\, d\theta - \frac{P(\theta)^{s-1}_{max}}{n^{s-1}} \int_{\theta_1}^{\theta_2} f(\xi, \theta)\, d\theta \right]. \tag{36}$$

The normed distribution law

$$N(m > m_1) = \frac{N^* - N^*_{\delta m}}{N^*} = 1 - \frac{\int_{\theta_1}^{\theta_2} P'(\theta)^{s-1} \cdot f(\xi, \theta)\, d\theta - \frac{1}{n^{s-1}} \int_{\theta_1}^{\theta_2} f(\xi, \theta)\, d\theta}{\int_0^{90} P'(\theta)^{s-1} \cdot f(\xi, \theta)\, d\theta}, \tag{37}$$

where $P'(\theta) = \frac{P(\theta)}{P(\theta)_{max}}$

Discussion of Results

A comparison of the results for various antennas with patterns differing from one another by shape and degree of directivity is of great interest. We considered three cases:

a) an undirected antenna – a half-wave dipole located at a height $\lambda/3$ above the earth's surface, with a pattern of the form

$$G(\theta) = \sin\left(\frac{2}{3}\pi \sin\theta\right); \tag{38}$$

b) a slightly directed antenna – an active dipole-reflector system positioned at a height $\lambda/2$ above the earth's surface, with a pattern of the form

$$G(\theta) = \sin(\pi \sin\theta) \cdot \cos\left[\frac{\pi}{4}(\sin\theta - 1)\right]; \tag{39}$$

c) an acutely directed antenna – "a wave channel," with nine elements, located at a height of 1.7λ above the earth's surface, with a pattern of the form (Fig. 4)

$$G(\theta) = \frac{\sin\left[\frac{n+2}{\lambda}\pi d\,(1-\cos\theta)\right]}{\sin\left[\frac{\pi d}{\lambda}(1-\cos\theta)\right]}\sin\left(\frac{2\pi}{\lambda}h\sin\theta\right), \qquad (40)$$

where d is the average distance between the dipoles and n is the number of dipoles.

However, Expression (37) for the general form of the mass-distribution law, with consideration of the influence exerted by the antenna directivity pattern, proved to be so complex that even for simple cases of slightly directed antennas it was impossible to carry out the integration and obtain a result in elementary functions. As an example let us cite the form of the integrand expression in the denominator of Eq. (37) for the case of a dipole-reflector antenna system:

$$P(\theta)^{s-1} f(\xi,\theta) = \frac{(1+\mathrm{tg}^2\theta)(1-\mathrm{tg}\xi\cdot\mathrm{tg}\theta)^{3/2(s-1)}\cdot\sin^{s-1}(\pi\sin\theta)\cdot\cos^{s-1}\left[\frac{\pi}{4}(\sin\theta-1)\right]}{(\mathrm{tg}\,\theta+\mathrm{tg}\,\xi)\cdot\cos^{3/2(s-1)}\theta\ \ \mathrm{tg}^{3/2(s-5/3)}\xi}. \qquad (41)$$

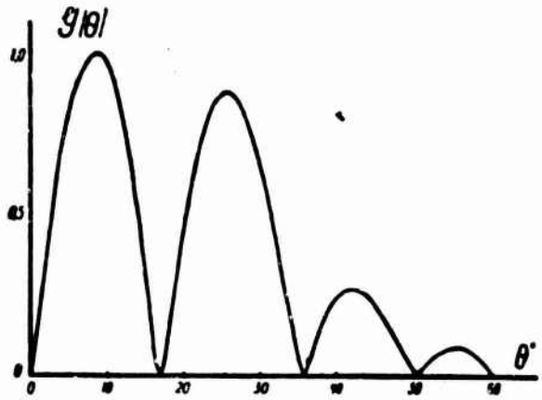

Fig. 4. Directivity pattern in vertical plane of a "wave channel" type antenna (nine-element antenna located 7 meters above the ground, λ = = 4 meters).

Here the expression $P(\theta)=\frac{G}{R^{3/2}}$ has been transformed with consideration of (39) and (22). Since it was impossible to obtain a result in analytical form, the integration was carried out graphically.

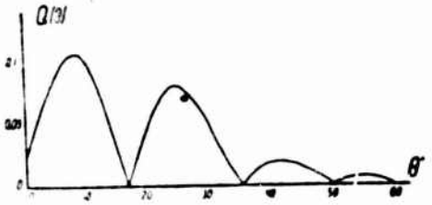

Fig. 5. Integrand function $Q(\theta) = P(\theta)^{s-1}$, $f(\xi,\theta)$ for a "wave channel" type antenna for $s = 2$.

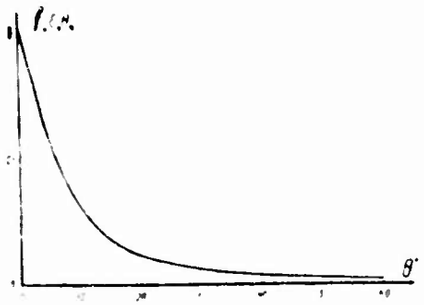

Fig. 6. Function $f(\xi, \theta)$ expressing the area ΔS as a function of the angle θ with consideration of the earth's curvature.

The form of the integrand function $Q(\theta)=P(\theta)^{s-1}\cdot f(\xi,\theta)$ for the case of a "wave channel" type antenna with $s = 2$ is given in Fig. 5. The integration limits in the right-hand part of Eq. (37) were determined in accordance with the above-described method (Fig. 3). Function $f(\xi, \theta)$, expressing the change in area ΔS with angle θ is given in Fig. 6. The results of the integration for cases a), b) and c) are presented, respectively, in Figs. 7, 8 and 9. Distribution laws were found to account for the influence of the antenna directivity pattern for three values of s: $s_1 = 1.5$; $s_2 = 2.0$; $s_3 = 2.5$. For purposes of comparison Figs. 7-9 also show curves of the $1/m^{s-1}$ type for the same values of s.

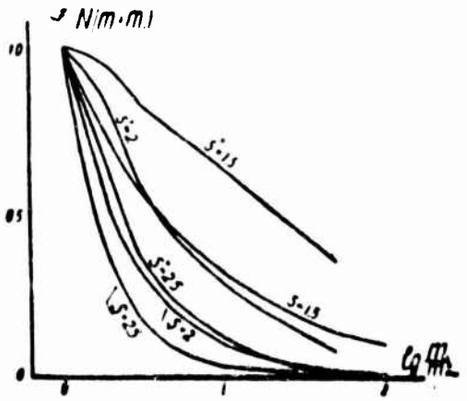

Fig. 7. Integral mass-distribution law for the case of an undirected antenna with a (half-wave) dipole situated at a height $\lambda/3$ above the earth/s surface). The curves for which the exponent in the law of distribution is denoted with s* have been plotted with consideration of the influence exerted by the directivity pattern. For comparison curves of the $1/m^{s-1}$ type have been included (these are marked with s).

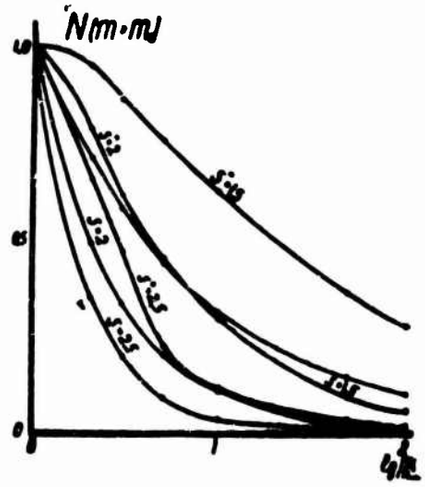

Fig. 8. Integral distribution law with respect to masses in the case of a slightly directed antenna (an active dipole-reflector system, situated at a height $\lambda/2$ above the earth's surface).

The observed distribution of radiometeors by mass is presented in Fig. 10 in logarithmic scale for various antennas had identical values for the exponent s

$$\lg N(m \geqslant m_i) = f\left(\lg \frac{m_i}{m_{min}}\right) \tag{42}$$

A study of the derived data leads to the following conclusions.

1. Distribution by mass of the observed meteors with consideration of the influence of the directivity pattern differs from the distribution function which actually exists in space. The difference is particularly marked in the region of small masses.

2. Influence of the directivity pattern state is comparatively small. It also appears primarily in the region of small masses.

3. Curve (42) shows a break, whereas the law $1/m^{s-1}$ in logarithmic scale results in a straight line.

4. In determining s from the slope of Curve (42), the result that is closest to the theoretical is obtained through use of the region of great durations (Fig. 10). However, it is also necessary in this case to introduce a number of correction factors.

The results are, in our opinion, explained as follows.

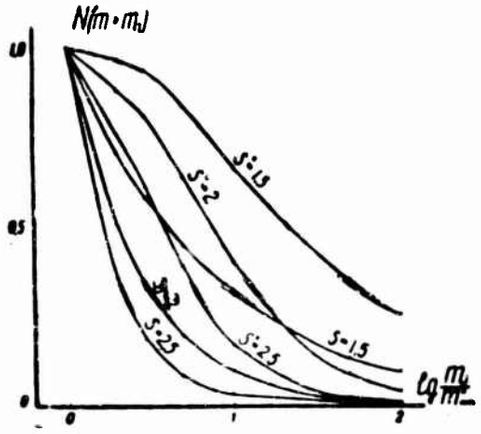

Fig. 9. Integral mass-distribution law in the case of an acutely directed antenna (wave channel, nine-element, situated at a height 1.7λ above the earth's surface).

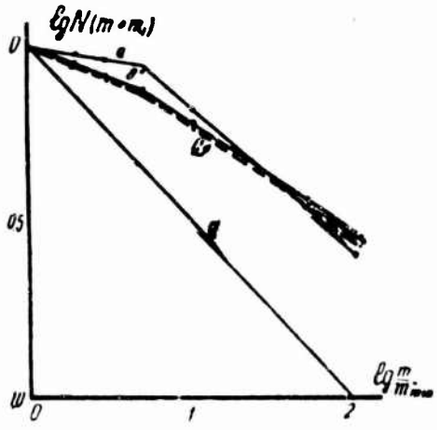

Fig. 10. Integral mass-distribution law for the case of various antennas with a value s = 1.5. a) Wave channel antenna type; b) dipole-reflector system; c) half-wave dipole; d) theoretical curve $1/m^{s-1}$ without consideration of the directivity pattern effect.

Let us consider Fig. 10. The curve segment in the region of small masses will be known as the first region and the curve segment corresponding to the large masses will be known as the second region. We will investigate the behavior of the curve in each of the regions separately.

The second region. Let us rewrite Eq. (37) in the form

$$N(m \geqslant m_i) = 1 - \frac{\int_0^{\theta_0} P(\theta)^{s-1} f(\xi, \theta)\, d\theta}{\int_0^{\pi} P(\theta)^{s-1} f(\xi, \theta)\, d\theta} +$$

$$+\frac{1}{n^{s-1}}\frac{\int_{\theta_1}^{\theta_2} f(\xi,\theta)\,d\theta}{\int_0^{90} P'(\theta)^{s-1} f(\xi,\theta)\,d\theta}. \tag{43}$$

In (43) the numerator and denominator of the second term in the right-hand part differ only by the integration limits which are functions of the magnitude of the subject minimum mass m_1. It is clear that with some sufficiently great magnitude for m_1 virtually the entire pattern will sense masses greater than m_1. In this case the integration limits for the numerator will differ little from the integration limits of the denominator, i.e., with sufficiently large m_1

$$\frac{\int_{\theta_1}^{\theta_2} P'(\theta)^{s-1} f(\xi,\theta)\,d\theta}{\int_0^{90} P'(\theta)^{s-1} f(\xi,\theta)\,d\theta} \approx 1.$$

On the other hand, the numerator $\int_{\theta_1}^{\theta_2} f(\xi,\theta)d\theta = \text{const}$ of the third term of the right-hand part of the equation may be considered constant. Consequently, for values of masses exceeding a certain magnitude m_1, the mass-distribution law is expressed as

$$N(m \geqslant m_1) = \frac{C}{n^{s-1}}, \tag{44}$$

where

$$C = \frac{\int_{\theta_1}^{\theta_2} f(\xi,\theta)\,d\theta}{\int_0^{90} P'(\theta)^{s-1} \cdot f(\xi,\theta)\,d\theta}.$$

Thus, in this region the distribution law coincides with that actually existing in space. This serves to explain the fact that the slope of Curve (42) in the second region is close to the slope of the curve of the $1/m^{s-1}$ type. It may be held that in this region the shape of the directivity pattern plays no significant role.

The first region. In this region the minimum mass of a meteor depends on the selected direction (more exactly, the minimum mass is the function $P(\theta) = G/R^{3/2}$). The second term of Eq. (43) is a variable in this case and the nature of its change is governed by the shape of the directivity pattern.

As a criterion for the influence of the directivity pattern we have the behavior of the function

$$P(\theta) = \frac{G}{R^{3/2}}.$$

In this case, if the function $P(\theta)$ is a smooth curve and its magnitude changes little over the greater part of the interval of change in the angle θ (i.e., the minimum mass of the meteor is a weak function of direction), the influence of the directivity pattern is comparatively small, the bend in Curve (42) is slight and the slopes of the segments of Curve (42) in regions I and II differ little from one another. Such a case is attained through the use of an acutely directed antenna with a single narrow lobe or when a slightly directed antenna exhibits a pattern such that $G \sim R^{3/2}$ over the greater portion of the range of variations in the angles θ.

If the magnitude of the function $P(\theta)$ differs markedly as a function of θ in a wide range of angles ϑ (i.e., the minimum mass is a strong function of direction), the directivity pattern exerts greater influence on the distribution of recorded meteors by mass. This is possible in the case of a multilobe directivity pattern, or when $P(\theta)$ is such that it exhibits a shape close to that of a triangle.

Consequently, it is not so much the width of the directivity pattern lobe as its shape which affects the magnitude of the bend and slope of the curve in the first region.

Until now we have been considering the mass distribution of ob-

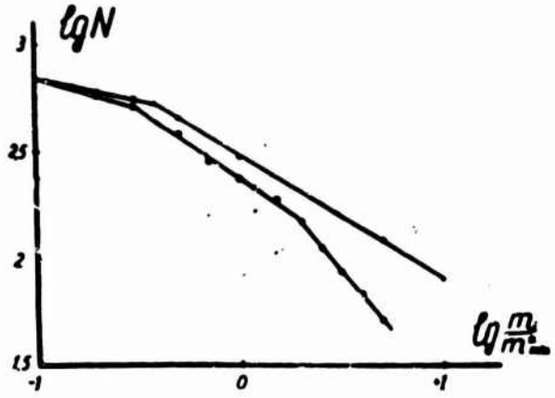

Fig. 11. Integral mass-distribution function.) Experimental mass-distribution curve (duration-distribution) for the Geminid stream of 8-14 December 1960;) theoretical curve with consideration of directivity pattern for s = 1.5.

served meteors. However, it is impossible to measure the mass of a meteor directly. The mass distribution is generally obtained indirectly -- measuring the duration of radiometeors. If we hold that for the transitional region between the mass of a meteor and the duration of the radio reflection there exists a relationship of the type shown in (9), a direct comparison of the experimental results with the conclusions drawn above becomes possible.

Figure 11 shows the derived experimental curve $\log N = f(\log \tau)$ for the 1960 Geminid stream. The observations were carried out with wave-channel type antennas with nine elements, situated 7 meters above the ground. The operating wavelength of the radar unit was 4.12 meters. For purposes of comparison, Fig. 11 shows the theoretical curve $\log N = f(\log m)$ with consideration of the directivity pattern for a value of s equal to 1.5.

As can be seen from the figure, the experimental curve for the Geminids exhibits two discontinuities - in the region of small and great durations. The nature of the discontinuity in the region of great durations was considered in Reference [9] where it is demonstrated that this discontinuity is a result of the influence of adhesion and recom-

bination in persistent trains.

With regard to the nature of the discontinuity in the region of small and intermediate durations, which is encountered in the majority of experiments [10], no unified viewpoint exists at the present time. Some investigators tend to regard the structure of the actual meteor stream as responsible for the discontinuity [11]. Ye.I. Fialko assumes that the discontinuity is a result of the varying nature of the radio-wave reflection from the meteor train within various mass ranges for meteor particles.

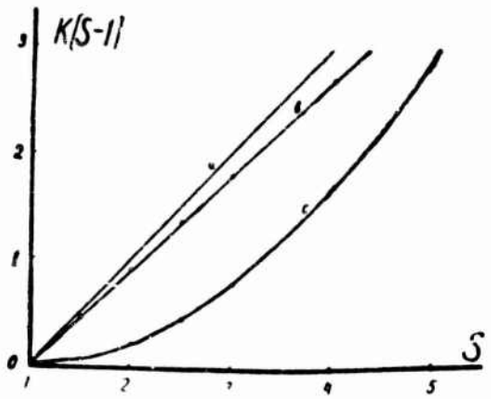

Fig. 12. Graph showing the slope of the curve log N = f(log m) as a function of the true value of the parameter s. a) Theoretical curve without consideration of directivity pattern effect; b) relationship for 11th segment of the curve log N = f(log m) in the case of a wave-channel type antenna; c) relationship for the 1st curve segment in the case of a wave-channel type antenna.

As follows from Fig. 11, excellent agreement is found between the observed and theoretical curves in regions I and II (the slight divergence between the curves is a result, in all probability, that $s \simeq 1.7$ for the Geminids, whereas the theoretical curve has been constructed for $s = 1.5$). It is indicative that the discontinuities of the theoretical and experimental curves are encountered for virtually identical mass values (duration values). Let us recall that in the construction of the theoretical curve no assumptions with respect to change in the structure of the stream or with respect to the varying nature of radio-

wave reflection in various regions were made. Only the influence of the antenna directivity pattern in the vertical plane was taken into consideration.

In this connection, we can assume that the appearance of a discontinuity in the experimental curves $\log N = f(\log \tau)$ is a result of the influence exerted by the directivity pattern, i.e., purely an equipment effect. It goes without saying that for a definitive clarification of the nature of the discontinuity in the curve $\log N = f(\log \tau)$ in the region of small durations a number of special experiments must be carried out.

In the general case, with consideration of the antenna directivity pattern, the law for meteoroid distribution by mass can be presented in the form

$$N(m > m_i) = \frac{C_1}{m_i^{k(s-1)}},$$

where the coefficient $\underline{k}$ is a function of $\underline{s}$ and the type of the antenna under consideration. The value of $\underline{k}$ varies from region I to II.

Figure 12 shows the empirically derived curves which make it possible on the basis of the slope of the observed curve $\log N(\tau \geq \tau_0) = f(\log \tau_0)$ to obtain the true value of $\underline{s}$ for the meteor stream through the use of a wave-channel antenna. For the Geminid stream the value of $\underline{s}$, determined by means of the indicated curves in Fig. 12, is equal to 1.64.

CONCLUSIONS

1. The break in the curve $\log N(\tau \geq \tau_0) = f(\log \tau_0)$ in the region of small and intermediate durations may be brought about by the influence of the antenna directivity pattern.

2. The magnitude of the break and the slope of the curve $\log N(\tau \geq \tau_0) = f(\log \tau_0)$ in the region of small durations is determined by the

shape and number of directivity pattern lobes.

3. The shape of the distribution function for the observed radiometeors by duration in the region of intermediate and large durations is close to the state for the actual meteoroid distribution function by mass.

REFERENCES

1. N. Herlofson, Arkiv f. Fysik [Archive of Physics] 1951, 3, 247.
2. T.R. Kaiser, R.L. Closs, Phil. Mag., ser, 7, 1952, 43, No. 336, 1.
3. F.I. Peregudov, Astr. zh. [Astronomy Journal], 1960, 37, Issue 3.
4. E.R. Billam, G.C. Browne, Proc. Phys. Soc. B., 1956, 69, No. 433, 98.
5. T.R. Kaiser, Phil. Mag. Suppl., 1953, 2, No. 8, 495.
6. N. Herlofson, Phys. Soc. Rep. Prog. Phys. 1948, 11, 444.
7. S. Evans, M.N. 1954, 114, Ni, 63.
8. Ye.I. Fialko, Astr zh., 1959, 36, vyp. 4.
9. J. Davies, J.S. Greenhow, J.E. Hall, Proc. Roy. Soc., A, 1959, 253, 130.
10. V.C. Kruchinenko, R.I. Moyseya, I.V. Bayrachenko. Radiolokatsionnyye nablyudeniya meteornykh potokov [Radar Observations of Meteor Streams], Collection of works in connection with the International Geophysical Year, Issue 1, Izd-vo KGU [Kiev State University Press], 1961.
11. B.L. Kashcheyev, V.N. Lebedinets, Astr. zh., 1959, 36, vyp. 4.

Manuscript Page No.	[Transliterated Symbols]
56	р = r = registratsiya = recording
56	э = e = ekvivalentnyy = equivalent
60	общ = obshch = obshcheye chislo = total number

THE PROBLEM OF CLASSIFYING THE SPECTRA OF POLAR AURORAE

V.I. Ivanchuk, Ye.S. Kurochka

1. During the period of the International Geophysical Year and the International Geophysical Cooperation massive spectrographic studies of the emissions of the upper atmosphere were carried out at various geographic locations, both within the zone of the polar aurorae, and outside of this zone. Unlike the visual, photographic and radar studies, the spectral studies were conducted without a unified and clearly defined program adapted by all of the investigators. This situation is attributed to the specific nature of spectral investigations. Limited surface brightness and rapid changes in polar aurorae results in extensive averaging of the spectral characteristics of high-atmosphere luminescence. The spectrograph exposure time Δt considerably exceeds the characteristic time τ (on the order of several seconds) during which the physical conditions in some volume of polar aurora luminescence may be regarded as homogeneous. In addition, there is virtually always spatial averaging since the dimensions of the homogeneous volumes — ℓ (on the order of several kilometers) are considerably smaller than the volume which is cut by the spectrograph having an angle of taper $\Delta\varphi$ by several tens of degrees.

The photoelectric and spectrometric method introduced in recent times to study emissions of the upper atmosphere makes it possible considerably to narrow the limits of Δt and $\Delta\varphi$. However, installations of this type suffer from a large number of drawbacks which are not present in conventional spectrographs of the SP-48 type. These include the low

resolving power of the spectrometers (~20 Angstrom units) and of the electrophotometers with interference filters whose transmission bands are ~100 Angstrom units, as well as the comparatively great spectral scanning time (in the spectrometer). This latter situation, strictly speaking, results in having the various recorded emissions characterizing physical processes which vary as to time. Therefore, a comparison of line and band intensities when using the spectroelectrophotometric method is frequently unsatisfactory. These remarks, of course do not reduce the advantages and prospects for the application of photoelectronic methods in the study of emissions from the upper atmosphere.

The variety and volume of observations resulting from the use of conventional spectrographs can, in our opinion, to a certain extent offset their primary drawback, i.e., the low space-time "resolution" and facilitate the bringing to light not only of general but of "local" features of polar aurorae. These features, because of the method by which they are obtained, will be more general, i.e., those which are necessary to understand the essence of the process without excessive detail.

The results of the spectrometric observations point to the great complexity and confusion in the behavior of various polar auroral emissions. In part this may be a result of the above-mentioned instrumental factors. At the same time, we know from a study of ordinary spectra obtained spectrographically that the majority of polar auroral emissions exhibits simple linear relationships [1, 2]. This "linearity," apparently must be referred to the most general quantitative relationships or to first approximation, whereas the deviations recorded with photoelectrical installations must be referred to the second approximation characterizing special cases and details of the physical processes taking place in polar aurorae.

A study of spectra at Tiksi Bay in accordance with the program of the IGY in 1958-1959 confirmed the validity of these thoughts [3]. All of the spectra, and more than 100 were processed for the region between 4700 and 6100 Angstrom units, fall within a certain continuous sequence in which it is possible to isolate as many as 10 groups. It developed that the position of the spectrum in a given sequence is best characterized by the ratio of the intensities of two adjacent lines:

$$s = \frac{I_{\lambda 5200 [NI]}}{I_{\lambda 5238 N_2^+}}.$$

The quantity s is a unique spectral indicator which is easily determined with the naked eye without a detailed photometric processing of the spectrum. Discussions regarding the quantitative relationships governing the sequence which, to some extent, is analogous to the sequence of stellar spectra, led to the conclusion that it may be based on a parameter such as the effective height of luminescence.

It would be a good idea to check and carry out mass comparisons and a classification based on spectral materials from other stations. Various differential features of emission luminescence connected with polar aurorae might easily result, and these would be related to geographical or geomagnetic coordinates of the points of the points of observation for other conditions.

From the works of Ya.I. Fel'dshteyn [4] it might be assumed that polar aurorae above the polar auroral zone (i.e., at points where $\Phi \geq \geq 70^{\circ}$) take place on the average at a considerably greater height than within the limits of the actual zone. This hypothesis could easily be verified by mass spectral studies at one of the stations above the polar auroral zone.

2. From the investigations of Stoermer and his coworkers [5] it follows that the lower the luminescence, the brighter it is on the aver-

age. Thus, if our conclusion as to the altitude relationship of the spectral sequence is valid, a unique spectrum-brightness relationship must exist for the polar aurorae. The hypothetical form of this relationship is presented in [3]. The present paper presents quantitative estimates of the mean effective brightness (I_{sr}) for a large number of spectra based on materials from observation logs in connection with polar aurorae at Tiksi Bay. The spectra on the basis of which the spectrum-brightness relationship was checked out satisfy the following requirements:

a) normal or slight darkening on emulsion;

b) obtained in excellent transparency conditions or on moonless nights;

c) the "cleanest," i.e., obtained with a minimum number of guided polar auroral forms.

A brightness curve I = I(t) was plotted for each spectrum, within the limits of the accuracy provided by observer records. The mean effective brightness of the guided forms was computed in the following manner

$$I_{cp} = \frac{\int I dt}{\Delta t_1},$$

where $\Delta t_1 \leq \Delta t$ is the exposure time which was determined from the curve showing the experimentally derived normal blackening in the guiding of some averaged form with brightness I as a function of the exposure time for the film D_N being employed (Fig. 1). Through the use of this graph it would be possible to eliminate the fainter aurorae from the curve I = I(t), where these could have made no contribution to the blackening in the given exposure. As a result the very brightest aurorae exerted the greatest influence on the magnitude of I_{sr}, and this is actually the case. The resulting diagram (Fig. 2) would experience no signifi-

cant change without elimination of the faint auroras; the entire diagram would only shift downward into the region of lesser brightnesses.

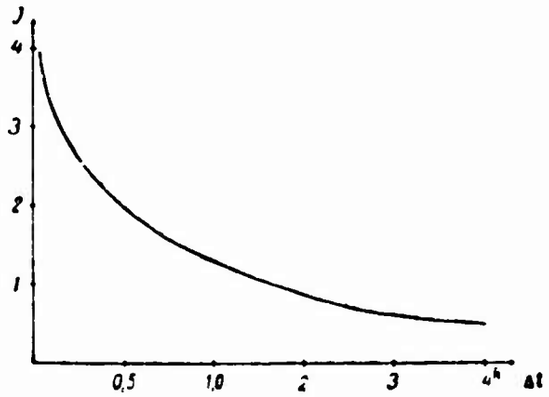

Fig. 1

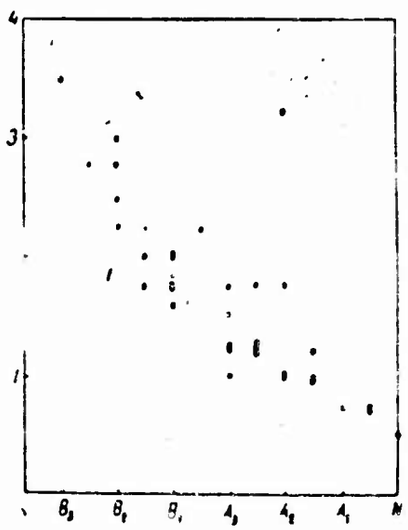

Fig. 2.

Table 1 presents brief excerpts from the observation log for each of the investigated spectra and the results of our determinations of the spectral type S on the basis of the classification proposed in [3], and the average brightness I_{sr}. In addition, the beginning of exposure and the corresponding times of observation of the most characteristic auroral forms are noted, as well as their intensity on a 4-point scale which is accurate to half a point. A total of 36 spectra were processed in this manner. The forms and color of the auroras are indicated in accordance with classifications recommended by NIZMIK [6]:

св = sv = svecheniye = luminescence

дп = dp = diffuznyye pyatna = diffuse spots

пп = pp = pul'siruyushchiye pyatna = pulsating spots

од = od = odnorodnyye dugi = homogeneous arcs

пд = pd = pul'siruyushchiye dugi = pulsating arcs

лд = ld = luchistyye dugi = rayed arcs

ол = ol = otdel'nyye luchi = individual rays

рс = ps = plamennyye siyaniya = flaming aurorae

н.н. = n.n. = nochnoye nebo = night sky

к = k = vse siyaniye krasnoye = entire aurora red

нк = nk = nizhniy kray krasnyy = lower edge red

вк = vk = siyaniye krasnoye vverkhu = aurora red at top

з. и ф. = z. & f. = sootvetstvenno zelenyy i fioletovyy tsvet p.s. = green and violet polar auroral color, respectively

TABLE 1

Дата наблюдения 1	Δt	2 Время наблюдения. Описание гидируемых форм п. с.	s	$I_{ср}$
3.XII 1958 г.	2^h30^m	21 03 — 22 10 н.н. 22 30 од и лд до 1 23 00 н.н. 3	A_1+N	0,7
8.XII 1958	9 30	17 55 — 03 24 н.н.	N	0,5
13.XII 1958	65	21 27 од 1 22 15 — 22 17 лд 3—4 к	A_2	3,3
13.XII 1958	2 30	$22^h33^m-22^h55^m$ лд (корона) 2 4 гид. точка схождения лучей 23 00 — 00 30 н.н. 00 30 — лд (корона) 2 5	A_2+N	1,8
14.XII 1968	6^h	18 12 — 18 45 сл 1 19 30 — 22 47 н.н. 23 00 лд 3—4 очень подвижна и драпри 3—4 гидируется нижний край 6 00 05 драпри 2—3 7	B_2+N	3,0
16.XII 1968	72	21 00 од 1 21 30 од 1	A_{2-1}	1,0
16.XII 1968	4	01 40 — 02 20 од 1 02 40 лд 1 03 00 — 05 50 н.н.	A_1+N	0,7
5.I. 1959	2	21 39 — 22 03 од 1 23 15 — 23 39 од и лд 1—2	B_1+N	1,7
28.I 1959	30	21 00 од 1 21 12 н.н. 22 00 од 1	A_1	0,7

TABLE 1 CONTINUED

29.I 1959	90	21 00 од и лд 1—2 21 40 — 22 00 од 2 22 15 сд 2—3 22 20 эд 2—1	B_1	2,0
29.I 1959	1 45	22 32 од 1—2 22 45 — 23 15 од 2 22 20 од 1—2	B_1	1,8
31.I 1959	3	23 55 од № и св 1 00 30 од 1—2 многоярусная 8 01 45 лд (драпри) 2—3 02 00 лд, ол, дп, св все 1 9	B_1	2,0
1. II 1959	2 10	19 00 св 1, ол 1 21 10 св 1, дп 1 и н.н.	$A_{2-1}+N$	0,9
1.II 1959	42	22 00 од 1—2 10 22 20 од 1—2 быстро меняющиеся 22 30 лп превращается в лд 2—3 (драпри) 11	B_{2-1}	2,3
3.II 1959	65	20 45 од 1—2 20 50 од и ол 2 21 00 — 21 50 св 1—1.5 и н.н.	B_1	1,6
3.II 1959	55	22 15 лд (корона) 2—3 гид. яркие образования 12 22 37 лд превращается в св 13 22 47 лд (корона) 2—3 14	B_{3-2}	2,8
4.II 1959	32	19 22 од и лд 1 19 49 сд распадается на ол и лп 15 19 54 корона 1 14	A_3	1,0
4.II 1959	3h20m	19 55 св 1 20 00 — 21 05 од 1—1.5, лд и ол 1 22 20 лд и св 1	A_{3-1}	1,2
1.III 1959	20	19 25 лд 2—3 и пд нк 19 35 лд 1—5 — 2 нк гидрируется нижний край 16	B_3	2,3
1.III 1959	45	19 50 лд и лп до 2, лучи к. почти до зенита, внизу з., гид нижний край 17 19 57 лд до 3 20 10 лд уменьшается до 1 18 20 10 слабое св 19	A_{3-2}	1,8
1.III 1959	2	21 15 лд 1 и дп 1 21 17 гп и пд до 1, лп 1 22 10 — 22 50 лп и од 1 23 00 — 23 06 лд 1.5—1	A_{2-1}	1,2
1.III 1959	25	23 23 — 23 30 лд (драпри) 3 нижний край к — ф 20 23 30 лд (драпри) до 2 21	B_3	2,5
1.III 1959	40	23 50 лд, пд (корона) 2—3 вк 14 00 00 лд 1—1.5 (пульсирующая корона) 22 00 20 пп и пд 1	A_3	1,7
1.III 1959	2 30	00 30 — 01 10 пд и лд 1—2 (корона) 01 40 н.н 01 50 — 03 00 корона, пульсации большого периода 23	A_3+N	1,3
2.III 1959	15	21 43 лд 3—4 (драпри), превращаются в полыхающие драпри, по 24 2—3—4 нф	B_3	3,5

TABLE 1 CONTINUED

		21 50 лд 3—4 полых. корона (пс) 25 21 58 пс уменьшается до 2 26		
4.III 1959	40	20 12 лд 2—3 спиралеобразная и лп 2 27 20 52 лд и лп 2 гид. нижний край 28	B_1-A_1	2,3
4.III 1959	37	20 56 лд 2 (многоярусная) гид. нижний край 29 21 00 лд 2 с движущимися волнами 30	B_{2-1}	2,0
4.III 1959	2	21 34 лд 1—2, св 1 23 20 дп 1	A_{3-2}	1,2
4. III. 1959	1.15	23.42 лп. 1.5 спиралеобразн. дп и св 1 н. н. 31	A_3	1,0
4.III 1959	55	02 00 лп и лд 2 02 35 лд превращается в пс с бегущим «лидером» 32 02 50 св 1	B_1	1,8
5.III 1959	40	22 50 лд 2—3 (многоярусная) 33 23 00 лд 1—2 рассеивается 23 30 од 1, св 1 34	B_{2-1}	1,7
5.III 1959	1h25m	23 36 диффузные полосы 1.5 35 00 25 лд (полосы) 1 н н.н. 36 00 50 лд 1.5 (волокнистая) 37	A_3+N	1,3
5.III 1959	3	01 00 лд 1.5 (волокнистая) 37 св 1, лп 1—2 и лд 1.5 03 00 н м. 03 30 св (волокнистое) 1—2 по всему небу 38	A_3+N	1,5
9.III 1959	40	00 03 ол и оп до 2 в зените 39 20 лд 2 25 лд в корону 3—4 нк — з гид. нижний край 40 28 корона до 1—2 14 37 корона с бегущими волнами 2—3 41	B_3	2,7
9.III 1959	90	00 50 св 1 01 05 лд и лп 1—1.5 02 10 оп превращается в корону 1—1.5 42 02 25 лд и од 1 03 20 од 1	A_{3-2}	1,3
9.III 1959		03 25 лп 1 04 08 од 1 04 30 лп и св 1	A_3	1,0

1) Data of observation; 2) observation time. Description of guided polar auroral forms; 3) 22:30 od & ld to 1; 4) 22:33-22:55 ld (corona) 2 guided point of ray convergence; 5) 00:30 ld (corona) 2; 6) 23:00 ld 3-4 extremely mobile and draperies 3-4 lower edge guided; 7) 00:05 draperies 2-3; 8) 00:30 od 1-2 multilevel; 9) 01:45 ld (draperies) 2-3; 10) 22:20 od 1-2 rapidly changing; 11) 22:30 lp turns into ld 2-3 (draperies); 12) 22:15 ld (corona) 2-3 bright formations guided; 13) 22:37 ld turns into sv; 14) 22:47 ld (corona) 2-3; 15) 19:49 od decays into ol and lp; 16) 19:35 ld 1-5-2 nk lower edge guided; 17) 19:50 ld and lp to 2, rays k virtually to zenith, underneath z, lower edge guided; 18) 20:10 ld reduces to 1; 19) 20:10 faint sv; 20) 23:23-23:30 ld (draperies) 3 lower edge k-f; 21) 23:30 ld (draperies) to 2; 22) 00:00 ld 1-1.5 (pulsating corona); 23) 01:50-03:00 corona, with pulsation of large period; 24) 21:43 ld 3-4 (draperies), turning into flaming draperies,

ps 2-3-4 nf; 25) 21:50 ld 3-4 flaming corona (ps); 26) 21:58 ps reduces to 2; 27) 20:12 ld 2-3 spiral & lp 2; 28) 20:52 ld & lp 2, lower border guided; 29) 20:56 ld 2 (multilevel), lower border guided; 30) 21:00 ld 2 with waves in motion; 31) 23:42 lp 1.5 spiral dp & sv 1 n.n.; 32) 02:35 ld turns into ps with a running "leader"; 33) 22-50; ld 2-3 (multilevel); 34) 23:00 ld 1-2 scatters; 35) 23:36 diffuse bands 1.5; 36) 00:25 ld (bands) 1 and n.n.; 37) 00:50 ld 1.5 (fibrous); 38) 03:30 sv (fibrous) 1-2 over the entire sky; 39) 00:03 ol and op up to 2 at zenith; 40) 00:25 ld into corona 3-4 nk - z, lower border guided; 41) 00:37 corona with traveling waves 2-3; 42) 02:10 op turns into corona 1-1.5.

As can be seen from the tables and Fig. 2, the assumption as to the existence of a relationship between spectral type and polar auroral brightness is confirmed. The spectra of the type B low-altitude polar aurora exhibit great brightnesses 2-3-4. The high-altitude aurorae of type A on the average diminish in brightness to the N of the night sky which we assume to be 0.5. For type A aurorae there exists a branch into a region of greater brightness 2-3. All these aurorae were recorded by observers as being red on the top (vk). These are noted in the figure with solid circles.

For a further refinement of the form of the spectrum-brightness diagram not only are mass investigations at various points around the terrestrial globe required, expansion of the classification for other spectral regions, but also a recording of brightness or polar auroral luminosity in parallel with the survey by means of more objective photographic or photoelectric methods.

REFERENCES

1. Yu.I. Gal'perin. Spektral'nyye elektrofotometricheskiye i radiolokatsionnyye issledovaniya polyarnykh siyaniy i svecheniya nochnogo neba [Spectral Electrophotometric and Radar Investigations of Polar Aurorae and Night-sky Luminosity] No. 1, 7, 1959.

2. V.S. Prokudina, Ibid., No. 2, 68, 1960.

3. V.I. Ivanchuk. Sbornik rabot KGU po MGG [Collection of Works from Kiev State University on the IGY], No. 1.

4. Ya.I. Fel'dshteyn. Issledovaniya polyarnykh siyaniy [Investigations of Polar Aurorae], No. 4, 61, 1960.

5. C. Stoermer, The Polar Aurorae, 1955.

6. Informatsionnyy sbornik MGG [Informational Bulletin on the IGY], No. 3, 74, 1957.

ON THE POSSIBILITIES OF ELEMENTARY MOLECULAR AND ATOMIC IONIZATION AND DISSOCIATION PROCESSES IN POLAR AURORAE OWING TO HYDROGEN AND HELIUM IONS FROM THE SUN

V.I. Cherednichenko

As has been demonstrated in recent experimental works [1] and [2], the effectiveness of oxygen and nitrogen molecular ionization and dissociation processes due to protons and the heavier ions is considerably greater than the effectiveness of the identical processes under conditions of electron bombardment. It is therefore of definite interest to examine the elementary processes of interaction between heavy solar corpuscles and the molecules and atoms present in the terrestrial atmosphere. The presence of hydrogen ions in the solar corpuscular streams is now a solidly established fact. With regard to the presence of helium ions in the corpuscular streams, we have but a comparatively limited number of data available. For the moment there is the single direct observed emission of neutral helium in the polar aurorae. In the spectrum of a powerful polar aurora observed in February 1958 at Zvenigorod there were found the intense infrared lines of helium He I $\lambda = 10830$ Angstrom units [3] and of ionized atomic nitrogen N II $\lambda = 5004$ and 5680 Angstrom units. The last lines were also observed by Meinel [5] [6] in bombardment of air at a pressure $P = 10^{-4}$ mm Hg with helium ions HeIII. D. Bates [7] and I.S. Shklovskiy [8] suggested the possible presence of helium emission in the polar aurorae. In the opinion of Professor V.I. Krasovskiy [4], the absence of hydrogen emission in some polar aurorae points to the penetration of corpuscular streams consisting of

helium ions into the terrestrial atmosphere.

There was considerable interest in the determination of the probability of various processes converting the molecules N_2, O_2, H_2O and their decay products on bombardment with hydrogen and helium ions He^+ and He^{++} from the corpuscular streams.

The maximum effective cross sections for these processes were computed on the basis of the following empirical formulas [9, 10]:

1. For the process of molecular dissociation by ion impact without formation of ionized products of decay:

$$\sigma_k = \sigma_r \frac{2u_a}{|u_a - u_0|} \exp\left(\frac{u_a}{|u_a - u_0|}\right) (\text{cm}^2), \qquad (1)$$

where σ_g is the gaskinetic cross section of the dissociated molecule; u_a is the excitation energy of the electron level of the dissociated molecule closest to the boundary of dissociation; u_0 is the dissociation energy. The difference $u_a - u_0$ in Formula (1) is taken as an absolute quantity.

2. For the process of molecular dissociation by ion impact with formation of ionized decay products:

$$\sigma_k = z \cdot \left(\frac{2u_0}{|u_0 - u_1|}\right)^{1/2} \cdot \exp\left(-\frac{2u_0}{|u_0 - u_1|}\right) \cdot 10^{-16} (\text{cm}^2), \qquad (2)$$

where $\underline{z}$ is the number of electrons in the ionized decay products; u_1 is the ionization energy of the ionized decay product in neutral state; u_0 is the dissociation energy of the molecule.

However, if the ionized molecule is subjected to a dissociation process, $\underline{z}$ represents the number of electrons of the dissociated molecule (in the neutral state); u_1 is the ionization energy of the dissociated molecule in the neutral state; u_0 is the minimum energy required for the given process.

In the case of a singly ionized molecule or atom by means of ion

impact z represents the number of electrons of the ionized molecule (or atom); u_0 gives the ionization energy; $u_1 = 0$.

For a process of double ionization z represents the number of electrons in the ionized molecule; $u_0 - u_1 = u_1$ is the potential of single ionization; u_0 is the potential of double ionization.

3. For the process of molecular charge transfer with simultaneous molecular dissociation:

$$\sigma_k = \frac{5{,}3 \cdot 10^{-13}}{u_i^2 \cdot [1 + 1{,}4 \cdot \Delta w \cdot (9 - z_1)]}, \qquad (3)$$

where u_i is the molecular dissociation energy; Δw is the difference between the energy of ion neutralization (in electronvolts) and the dissociation energy; z_1 is the number of molecular valence electrons.

For the process of nonresonant charge transfer the effective section may also be found with Formula (3). However, in this case u_i is the ionization energy for the atom or molecule subject to charge transfer; Δw is the difference between the ionization energy for the molecule or atom and the energy of ion neutralization; z_1 is the number of valence electrons for the atoms or molecules subject to charge transfer.

The values of σ_k computed with Formulas (1), (2) and (3) are the maximum values for the effective sections of the corresponding processes at ion energies of the order of 1-10 kev [9].

Relationships (1), (2) and (3) are empirical. They were derived by the author in 1955 [9], [10] on the basis of qualitatively theoretical positions regarding the processes of ionization, dissociation and charge transfer [11], [12], and an analysis of extensive experimental material pertaining to these processes [9]. In the majority of cases the divergence between the experimental value and that computed for the ion energies of 1-10 kev did not exceed $\pm 10\%$ of the measured magnitude [9].

In recent years the Leningrad Physics and Engineering Institute

has been doing work on measuring the effective sections of ionization and dissociation charge transfers for nitrogen and oxygen molecules at an air pressure in a collision chamber of $1.5 \cdot 10^{-4}$ mm Hg and an energy of 1-5 kev for the colliding ions [1, 2, 13, 14]. The measurement areas amounted to no more than $\pm 12\%$ of the measured magnitude. It is interesting to note that the effective cross sections derived on the basis of Relationships (1-3) were in good agreement with experimental data [1, 2, 13, 14].

Is it possible for heavy particles of the corpuscular stream to penetrate the polar auroral zone? As we know, 95% of the polar aurorae occur at heights between 110 and 120 km, where the particle concentration is $n = 5 \cdot 10^{12}$ cm^{-3}, and the height of the homogeneous atmosphere is $H = 10^6$ cm. Thus it would seem that protons from the corpuscular stream moving at a velocity $v = 10^8$ cm/sec and consequently exhibiting an energy of $E = 5$ kev could not possibly penetrate the polar auroral zone. However, I.S. Shklovskiy indicated an extremely effective mechanism for the penetration of protons into the polar auroral zone as far back as 1951 [15]. This is the mechanism of charge transfer between protons and oxygen atoms:

$$H^+ + O \rightarrow H + O^+ - 0{,}02 \text{ ev}$$

Because of the low energy of this process $\Delta E = 0.02$ ev is virtually resonant. The effective cross section of this process for the proton energy of $E = 5$ kev amounts to $\sigma = 10^{-15}$ cm. In this case the proton, in its motion through the polar auroral zone, loses energy $E_1 = H \cdot n\sigma\Delta E = 100$ ev $= 0.1$ kev, i.e., a negligibly small portion of its total energy. From this example we see that the protons of the corpuscular streams can reach the polar auroral zones.

It is also characteristic that the corpuscular mechanisms for the excitation of polar aurorae make it possible in individual cases to ex-

plain the intensities of the majority of polar auroral emissions [16].

There are also arguments in favor of the contention that the reactions computed in Tables 1-9 proceed under the action of direct corpuscular solar radiation. It has been observed that when a small quantity of hydrogen is introduced into a discharge tube containing oxygen at a pressure of 1 mm Hg, a noticeable intensification of the green oxygen line λ 5577 Angstrom units is noted in the spectrum of the discharge simultaneously with an intensification of the H_α and H_β hydrogen lines [17]. In a number of cases this correlation is found in polar aurorae [18]. In the same discharge tube containing nitrogen with an admixture of helium at a pressure of 0.01 mm Hg, the discharge spectrum showed infrared Meinel bands $A^2\Pi - X^2\Sigma_g^+$ of the N_2^+ ion and the first positive system of $B^3\Pi - A^3\Sigma_u^+$ bands of an N_2 molecule with an intensity distribution similar to the distribution of intensities in the spectrum of the polar aurorae [19]. In the opinion of the well-known polar-aurorae investigator – Bates [20] – the N_2 and N_2^+ bands in the polar aurorae can be effectively excited by impact of solar protons. Thus there is a strong basis for the contention that the heavy particles of the corpuscular streams are responsible for the excitation of the primary polar auroral emissions.

The various processes for the conversion of O_2, N_2 and H_2O molecules when bombarded with heavy corpuscular-stream particles were examined on the basis of Relationships (1-3). The results of these calculations are presented in Tables 1-9.

The following diagrams of the most probable molecular conversions for nitrogen, oxygen and the water in the terrestrial atmosphere were constructed on the basis of these tables for the interaction between these and the hydrogen and helium ions of the corpuscular streams (Fig. 1-5).

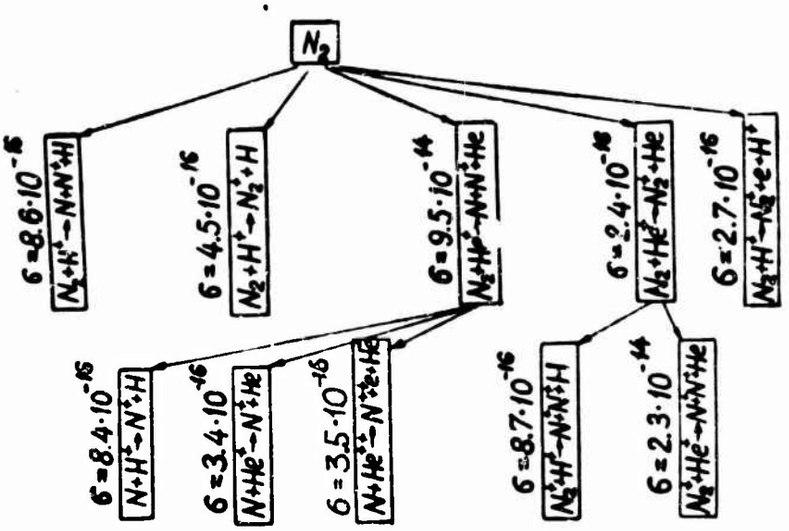

Fig. 1. Diagram snowing the most probable conversions of nitrogen molecules under the action of hydrogen and helium ions from solar corpuscular streams.

TABLE 1

Processes of Nitrogen-Molecule Conversion Under the Action of the Hydrogen Ions from Corpuscular Streams

№ процессов 1	2 Схема процесса	3 Эффективное сечение σ_{max} ($см^2$.)
1	$N_2 + H^+ \rightarrow N^+ + N + e + H^+ - 24{,}3$ эв	$1{,}1 \cdot 10^{-17}$
2	$N_2 + H^+ \rightarrow N + N^+ + H - 10{,}7$ эв	$8{,}6 \cdot 10^{-16}$
3	$N_2 + H^+ \rightarrow N_2^+ + e + H^+ - 15{,}6$ эв	$2{,}7 \cdot 10^{-16}$
4	$N_2 + H^+ \rightarrow N_2^{++} + 2e + H^+ - 49{,}5$ эв	$6{,}8 \cdot 10^{-18}$
5	$N_2 + H^+ \rightarrow N_2^+ + H$	$4{,}5 \cdot 10^{-16}$
6	$N_2 + H^+ \rightarrow N + N + H^+ - 9{,}76$ эв	$1{,}1 \cdot 10^{-17}$
7	$N_2 + H^+ \rightarrow N_2^{++} + e + H - 36$ эв	$8{,}2 \cdot 10^{-17}$
8	$N_2^+ + H^+ \rightarrow N + N^+ + H^+ - 8{,}72$ эв	$1{,}8 \cdot 10^{-16}$
9	$N_2^+ + H^+ \rightarrow N^+ + N^+ + e + H^+ - 23{,}3$ эв	$8{,}1 \cdot 10^{-18}$
10	$N_2^+ + H^+ \rightarrow N^+ + N^+ + H - 9{,}7$ эв	$8{,}7 \cdot 10^{-16}$
11	$N + H^+ \rightarrow N^{++} + 2e + H^+ - 43{,}9$ эв	$4{,}1 \cdot 10^{-18}$
12	$N + H^+ \rightarrow N^{++} + e + H - 30{,}4$ эв	$5{,}7 \cdot 10^{-17}$
13	$N + H^+ \rightarrow N^+ + H$	$8{,}4 \cdot 10^{-16}$
14	$N + H^+ \rightarrow N^+ + e + H^+ - 14{,}5$ эв	$1{,}3 \cdot 10^{-16}$

1) Process number; 2) process reactions; 3) effective cross section, σ_{max} (cm^2). эв = ev = electron-volt.

An examination of the processes of interaction between solar corpuscles and the molecules of the terrestrial atmosphere shows that the

TABLE 2

Processes of Nitrogen-Molecule Conversion Under the Action of Helium Ions He^+ from Corpuscular Streams

№ процессов	Схема процесса	Эффективное сечение σ_{max} ($см^2$)
15	$N_2 + He^+ \rightarrow N^+ + N + e + He^+ - 24{,}3$ эв	$1{,}1 \cdot 10^{-17}$
16	$N_2 + He^+ \rightarrow N + N^+ + He + 0{,}2$ эв	$9{,}5 \cdot 10^{-14}$
17	$N_2 + He^+ \rightarrow N_2^+ + e + He^+ - 15{,}6$ эв	$2{,}7 \cdot 10^{-16}$
18	$N_2 + He^+ \rightarrow N_2^+ + He$	$2{,}4 \cdot 10^{-16}$
19	$N_2 + He^+ \rightarrow N_2^{+\,+} + e + He - 25$ эв	$2{,}9 \cdot 10^{-16}$
20	$N_2^+ + He^+ \rightarrow N^+ + N^+ + He - 1{,}3$ эв	$2{,}3 \cdot 10^{-14}$
21	$N + He^+ \rightarrow N^+ + He$	$3{,}4 \cdot 10^{-16}$

1) Process number; 2) process reactions; 3) effective cross section, σ_{max} (cm^2). эв = ev = electron-volt.

TABLE 3

Processes of Conversion for Nitrogen Molecules Under the Action of Helium Ions He^{++} from Corpuscular Streams

№ процессов	Схема процесса	Эффективное сечение σ_{max} ($см^2$)
22	$N_2 + He^{+\,+} \rightarrow N + N^+ + He^+ + 29{,}9$ эв	$3{,}4 \cdot 10^{-17}$
23	$N_2 + He^{+\,+} \rightarrow N^+ + N^+ + He + 29{,}9$ эв	$1{,}9 \cdot 10^{-17}$
24	$N_2 + He^{+\,+} \rightarrow N_2^{+\,+} + He + 29{,}2$ эв	$1{,}1 \cdot 10^{-17}$
25	$N_2 + He^{+\,+} \rightarrow N_2^+ + He^+ + 38$ эв	$3{,}1 \cdot 10^{-17}$
26	$N_2 + He^{+\,+} \rightarrow N_2^{+\,+} + e + He^+ + 20{,}3$ эв	$7{,}9 \cdot 10^{-17}$
27	$N_2 + He^{+\,+} \rightarrow N^+ + N^+ + He^+ + 31{,}0$ эв	$3{,}8 \cdot 10^{-17}$
28	$N_2 + He^{+\,+} \rightarrow N_2^+ + He^+ + 59{,}7$ эв	$2{,}8 \cdot 10^{-17}$
29	$N + He^{+\,+} \rightarrow N^{+\,+} + e + He^+ + 10{,}3$ эв	$3{,}5 \cdot 10^{-16}$
30	$N + He^{+\,+} \rightarrow N^{+\,+} + He + 34{,}8$ эв	$3{,}1 \cdot 10^{-17}$

1) Process number; 2) process reactions; 3) effective cross section, σ_{max} (cm^2). эв = ev = electron-volt.

following processes are the most probable: charge transfer; charge transfer with dissociation; and charge transfer with ionization. This fact was confirmed experimentally in the works of Il'in [2, 3].

Despite the fact that the helium ions He^+ and He^{++}, apparently, are present in the corpuscular streams in considerably smaller quantity than hydrogen ions (3) in a number of processes, for He^+ and He^{++}, as

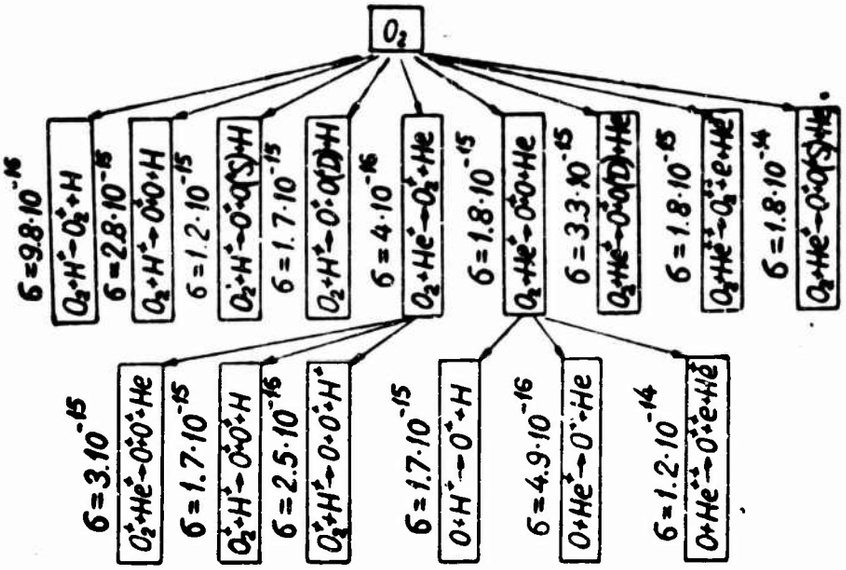

Fig. 2. Diagram showing most probable conversions of oxygen molecules under the action of hydrogen and helium ions from solar corpuscular streams.

TABLE 4

Molecular Conversion Processes for Oxygen Under the Action of Hydrogen Ions from Corpuscular Streams

№ процессов	Схема процесса	Эффективное сечение σ_{max} ($см^2$)
31	$O_2 + H^+ \rightarrow O + O + H^+ - 5{,}08$ эв	$1{,}2 \cdot 10^{-18}$
32	$O_2 + H^+ \rightarrow O + O(^1D) + H^+ - 7{,}04$ эв	$7{,}1 \cdot 10^{-18}$
33	$O_2 + H^+ \rightarrow O_2^+ + e + H^+ - 12{,}2$ эв	$3{,}1 \cdot 10^{-16}$
34	$O_2 + H^+ \rightarrow O_2^+ + H$	$9{,}8 \cdot 10^{-16}$
35	$O_2 + H^+ \rightarrow O^+ + O + e + H^+ - 19{,}2$ эв	$2{,}2 \cdot 10^{-18}$
36	$O_2 + H^+ \rightarrow O^+ + O + H - 5{,}2$ эв	$2{,}8 \cdot 10^{-15}$
37	$O_2 + H^+ \rightarrow O^+ + O(^1S) + H - 9{,}24$ эв	$1{,}2 \cdot 10^{-15}$
38	$O_2 + H^+ \rightarrow O^+ + O(^1D) + H - 7{,}04$ эв	$1{,}6 \cdot 10^{-15}$
39	$O_2^+ + H^+ \rightarrow O^+ + O^+ + H - 6{,}58$ эв	$1{,}7 \cdot 10^{-15}$
40	$O_2^+ + H^+ \rightarrow O + O^+ + H^+ - 6{,}48$ эв	$2{,}5 \cdot 10^{-16}$
41	$O_2 + H^+ \rightarrow O_2^{++} + 2e + H^+ - 50$ эв	$1{,}3 \cdot 10^{-18}$
42	$O_2 + H^+ \rightarrow O_2^{++} + e + H - 36{,}5$ эв	$3{,}4 \cdot 10^{-17}$
43	$O_2 + H^+ \rightarrow O^+ + O^+ + 2e + H^+ - 32{,}3$ эв	$1{,}3 \cdot 10^{-19}$
44	$O_2^+ + H^+ \rightarrow O_2^{++} + H - 24{,}3$ эв	$3{,}1 \cdot 10^{-17}$
45	$O + H^+ \rightarrow O^+ + H$	$1{,}7 \cdot 10^{-15}$
46	$O + H^+ \rightarrow O^+ + e + H^+ - 13{,}6$ эв	$1{,}5 \cdot 10^{-16}$
47	$O + H^+ \rightarrow O_2^{++} + e + H - 34{,}9$ эв	$3{,}8 \cdot 10^{-17}$
48	$O + H^+ \rightarrow O^{++} + 2e + H^+ - 48{,}4$ эв	$1{,}3 \cdot 10^{-18}$

1) Process number; 2) process reactions; 3) effective cross section, σ_{max} (cm^2). эВ = ev = electron-volt.

TABLE 5

Molecular Conversion Processes for Oxygen Under the Action of Helium Ions He^+ from Corpuscular Streams

№ процессов [1]	[2] Схема процесса	[3] Эффективное сечение σ_{max} ($см^2$)
49	$O_2 + He^+ \rightarrow O_2^+ + He + 12{,}3$ эв	$4 \cdot 10^{-16}$
50	$O_2 + He^+ \rightarrow O^+ + O + He + 5{,}3$ эв	$1{,}8 \cdot 10^{-15}$
51	$O_2 + He^+ \rightarrow O^+ + O(^1D) + He + 3{,}8$ эв	$3{,}3 \cdot 10^{-15}$
52	$O_2 + He^+ \rightarrow O^+ + O(^1S) + He + 1{,}6$ эв	$1{,}8 \cdot 10^{-14}$
53	$O_2 + He^+ \rightarrow O_2^{++} + e + He - 25{,}5$ эв	$2{,}5 \cdot 10^{-16}$
54	$O_2 + He^+ \rightarrow O^+ + O^+ + He + 4$ эв	$3 \cdot 10^{-15}$
55	$O + He^+ \rightarrow O^+ + He + 10{,}9$ эв	$4{,}9 \cdot 10^{-16}$
56	$O + He^+ \rightarrow O^{++} + e + He - 23{,}9$ эв	$3{,}4 \cdot 10^{-16}$

1) Process number; 2) process reactions; 3) effective cross section, σ_{max} (cm^2). эв = ev = electron-volt.

TABLE 6

Molecular Conversion Processes for Oxygen Under the Action of Helium Ions He^{++} from Corpuscular Streams

№ процессов [1]	[2] Схема процесса	[3] Эффективное сечение σ_{max} ($см^2$)
57	$O_2 + He^{++} \rightarrow O_2^{++} + He + 28{,}7$ эв	$1{,}6 \cdot 10^{-17}$
58	$O_2 + He^{++} \rightarrow O_2^+ + He^+ + 42{,}0$ эв	$6{,}4 \cdot 10^{-16}$
59	$O_2 + He^{++} \rightarrow O^+ + O + He^+ + 35{,}0$ эв	$4{,}0 \cdot 10^{-17}$
60	$O_2 + He^{++} \rightarrow O^+ + O(^1S) + He^+ + 31{,}3$ эв	$4{,}6 \cdot 10^{-17}$
61	$O_2 + He^{++} \rightarrow O^+ + O(^1D) + He^+ + 33{,}3$ эв	$4{,}2 \cdot 10^{-17}$
62	$O_2 + He^{++} \rightarrow O_2^{++} + e + He^+ + 4{,}2$ эв	$1{,}8 \cdot 10^{-15}$
63	$O_2^+ + He^{++} \rightarrow O^+ + O^+ + He^+ + 34{,}1$ эв	$3{,}8 \cdot 10^{-17}$
64	$O_2^+ + He^{++} \rightarrow O_2^{++} + He^+ + 10{,}4$ эв	$1{,}2 \cdot 10^{-16}$
65	$O + He^{++} \rightarrow O^{++} + He + 30{,}3$ эв	$4{,}5 \cdot 10^{-17}$
66	$O + He^{++} \rightarrow O^+ + He^+ + 30{,}3$ эв	$4{,}4 \cdot 10^{-17}$
67	$O + He^{++} \rightarrow O^{++} + e + He^+ + 5{,}8$ эв	$1{,}2 \cdot 10^{-14}$

1) Process number; 2) process reactions; 3) effective cross section, σ_{max} (cm^2). эв = ev = electron-volt.

Indicated by the conversion diagrams, the effective cross sections exceed the gaskinetic cross sections by one, two and in certain cases three orders of magnitude. Therefore, the helium ions He^+ and He^{++} together with the hydrogen ions H^+ in the corpuscular streams may play an important role in the dissociation of the nitrogen, oxygen and water

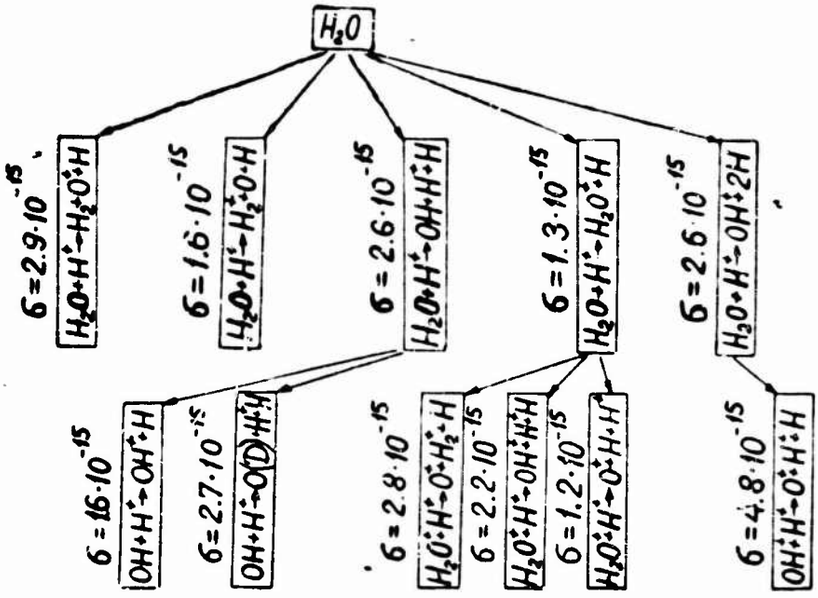

Fig. 3. Diagram of most probable conversions for H_2O molecules under the action of hydrogen ions H^+ from solar corpuscular streams.

TABLE 7

Molecular Conversion Processes for H_2O Under the Action of Hydrogen Ions from Corpuscular Streams

№ 1 процессов	2 Схема процесса	Эффективное сечение 3 σ_{max} ($см^2$)
68	$H_2O + H^+ \rightarrow H_2O^+ + H$	$1{,}3 \cdot 10^{-15}$
69	$H_2O + H^+ \rightarrow H_2 + O^+ + e + H^+ - 18{,}5$ эв	$1{,}2 \cdot 10^{-17}$
70	$H_2O + H^+ \rightarrow OH + H^+ + e + H^+ - 18{,}9$ эв	$2{,}4 \cdot 10^{-18}$
71	$H_2O + H^+ \rightarrow OH^+ + H + e + H^+ - 18{,}9$ эв	$1{,}5 \cdot 10^{-18}$
72	$H_2O + H^+ \rightarrow OH + H - 9$ эв	$9{,}1 \cdot 10^{-17}$
73	$H_2O + H^+ \rightarrow H_2 + O^+ + H - 5{,}1$ эв	$2{,}9 \cdot 10^{-18}$
74	$H_2O + H^+ \rightarrow H_2^+ + O + H - 7{,}3$ эв	$1{,}6 \cdot 10^{-17}$
75	$H_2O + H^+ \rightarrow H + H^+ + O(^1D) - 25$ эв	$1{,}1 \cdot 10^{-16}$
76	$H_2O + H^+ \rightarrow H + H^+ + O(S) - 27$ эв	$7{,}5 \cdot 10^{-17}$
77	$H_2O + H^+ \rightarrow OH + H^+ + H - 5{,}4$ эв	$2{,}6 \cdot 10^{-15}$
78	$H_2O + H^+ \rightarrow O + H^+ + 2H - 5{,}4$ эв	$2{,}6 \cdot 10^{-15}$
79	$H_2O^+ + H^+ \rightarrow O^+ + H_2 + H^+ - 6$ эв	$2{,}2 \cdot 10^{-15}$
80	$H_2O^+ + H^+ \rightarrow O^+ + H_2^+ + H - 8{,}3$ эв	$2{,}8 \cdot 10^{-15}$
81	$H_2O^+ + H^+ \rightarrow O + H_2^+ + H^+ - 8{,}2$ эв	$4{,}6 \cdot 10^{-17}$
82	$H_2O^+ + H^+ \rightarrow OH^+ + H + H^+ - 6{,}3$ эв	$1{,}9 \cdot 10^{-15}$
83	$H_2O^+ + H^+ \rightarrow OH^+ + H^+ + H - 6{,}3$ эв	$2{,}2 \cdot 10^{-15}$
84	$H_2O^+ + H^+ \rightarrow OH + H^+ + H^+ - 6$ эв	$2{,}2 \cdot 10^{-16}$
85	$H_2O^+ + H^+ \rightarrow O^+ + H + H^+ + H - 10{,}5$ эв	$1{,}2 \cdot 10^{-15}$
86	$OH + H^+ \rightarrow OH^+ + e + H^+ - 13{,}8$ эв	$1{,}7 \cdot 10^{-16}$

87	$OH + H^+ \rightarrow OH^+ + H$	$1{,}6 \cdot 10^{-15}$
88	$OH + H^+ \rightarrow O(^1D) + H^+ + H - 6{,}4$ эв	$2{,}7 \cdot 10^{-15}$
89	$OH + H^+ \rightarrow O^+ + H + e + H^+ - 18$ эв	$6{,}4 \cdot 10^{-19}$
90	$OH + H^+ \rightarrow O^+ + H + H - 18{,}1$ эв	$4{,}1 \cdot 10^{-16}$
91	$OH^+ + H^+ \rightarrow O^+ + H^+ + H - 4{,}2$ эв	$4{,}8 \cdot 10^{-15}$

1) Process number; 2) process reactions; 3) effective cross section, σ_{max} (cm^2). эв = ev = electron-volt.

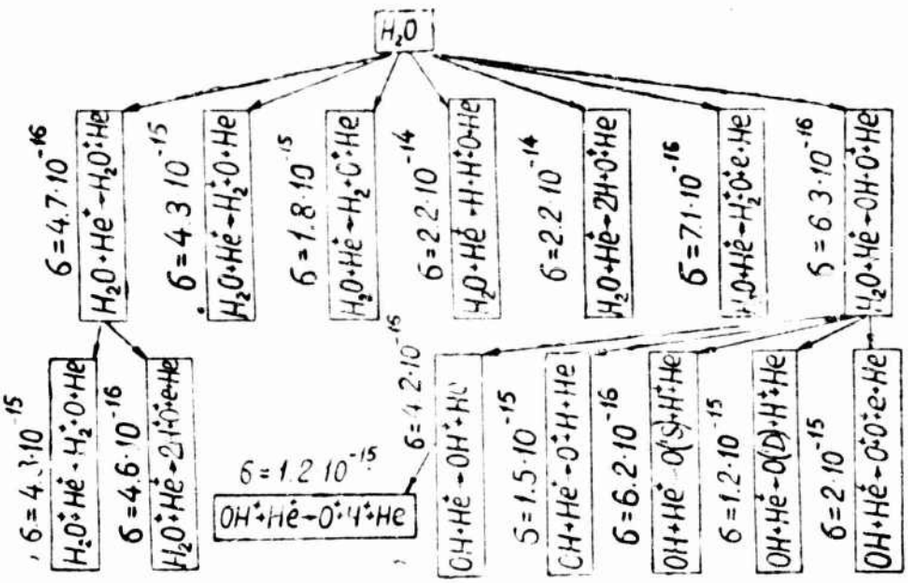

Fig. 4. Diagram of most probable molecular conversions for H_2O under the action of helium ions He^+ from solar corpuscular streams.

TABLE 8

Molecular Conversion Processes for H_2O Under the Action of Helium Ions He^+ from Corpuscular Streams

№ процессов 1	Схема процесса 2	Эффективное сечение 3 σ_{max} ($см^2$)
92	$H_2O + He^+ \rightarrow H_2O^+ + He + 11{,}9$ эв	$4{,}7 \cdot 10^{-16}$
93	$H_2O + He^+ \rightarrow H_2^+ + O + He + 3{,}7$ эв	$4{,}3 \cdot 10^{-15}$
94	$H_2O + He^+ \rightarrow H_2 + O^+ + He + 5{,}9$ эв	$1{,}8 \cdot 10^{-15}$
95	$H_2O + He^+ \rightarrow H + H^+ + O + He + 1{,}5$ эв	$2{,}2 \cdot 10^{-14}$
96	$H_2O + He^+ \rightarrow 2H + O^+ + He + 1{,}6$ эв	$2{,}2 \cdot 10^{-14}$
97	$H_2O^+ + He^+ \rightarrow H_2^+ + O^+ + He + 2{,}7$ эв	$7{,}0 \cdot 10^{-16}$
98	$H_2O + He^+ \rightarrow H_2^+ + O^+ + e + He - 9{,}9$ эв	$7{,}1 \cdot 10^{-16}$
99	$H_2O^+ + He^+ \rightarrow H_2^+ + H + O + He - 3{,}5$ эв	$4{,}3 \cdot 10^{-15}$
100	$OH + He^+ \rightarrow OH^+ + He + 10{,}7$ эв	$4{,}2 \cdot 10^{-16}$
101	$OH + He^+ \rightarrow O^+ + H + He + 6{,}5$ эв	$1{,}5 \cdot 10^{-15}$
102	$OH + He^+ \rightarrow O + H^+ + He + 6{,}6$ эв	$3{,}7 \cdot 10^{-15}$
103	$OH + He^+ \rightarrow O(^1S) + H^+ + He + 10{,}8$ эв	$6{,}2 \cdot 10^{-16}$
104	$OH + He^+ \rightarrow O(^1D) + H^+ + He + 8{,}8$ эв	$1{,}2 \cdot 10^{-15}$
105	$OH^+ + He^+ \rightarrow O^+ + H^+ + He + 6{,}8$ эв	$1{,}2 \cdot 10^{-15}$

106	$H_2O^+ + He^+ \rightarrow H^+ + H^+ + O^+ + e + He - 13$ эв	$4{,}6 \cdot 10^{-16}$
107	$OH + He^+ \rightarrow O^+ + H^+ + e + He - 7{,}0$ эв	$2{,}0 \cdot 10^{-15}$
108	$H_2O + He^+ \rightarrow OH + O^+ + He - 8{,}1$ эв	$6{,}3 \cdot 10^{-16}$

1) Process number; 2) process reactions; 3) effective cross section, σ_{max} (cm^2). эв = ev = electron-volt.

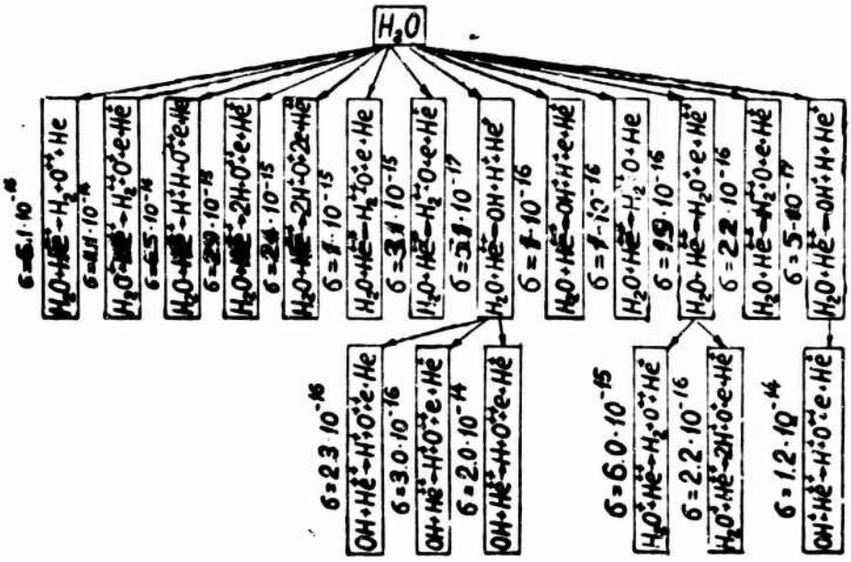

Fig. 5. Diagram of most probable conversions of H_2O molecules under the action of helium ions He^{++} from solar corpuscular streams.

TABLE 9

Molecular Conversion Processes for H_2O Under the Action of Helium Ions He^{++} from Corpuscular Streams

1 № процессов	2 Схема процесса	3 Эффективное сечение σ_{max} ($см^2$)
109	$H_2O + He^{++} \rightarrow H_2 + O^{++} + He - 25{,}3$ эв	$6{,}1 \cdot 10^{-16}$
110	$H_2O + He^{++} \rightarrow H_2^+ + O^+ + He + 44{,}3$ эв	$2{,}4 \cdot 10^{-17}$
111	$H_2O^+ + He^{++} \rightarrow H_2 + O^{++} + He^+ - 2{,}4$ эв	$6{,}0 \cdot 10^{-15}$
112	$OH + He^{++} \rightarrow H + O^{++} + He + 25{,}9$ эв	$5{,}8 \cdot 10^{-17}$
113	$OH^+ + He^{++} \rightarrow H + O^{++} + He^+ - 15{,}2$ эв	$1{,}7 \cdot 10^{-16}$
114	$H_2O^+ + He^{++} \rightarrow H_2^{++} + O + He^+ + 11{,}8$ эв	$2{,}7 \cdot 10^{-16}$
115	$H_2O^+ + He^{++} \rightarrow H_2^{++} + O^+ + He + 22{,}7$ эв	$6{,}5 \cdot 10^{-17}$
116	$H_2O^+ + He^{++} \rightarrow H_2^{++} + O^+ + e + He^+ - 1{,}8$ эв	$1{,}1 \cdot 10^{-14}$
117	$H_2O + He^{++} \rightarrow H^+ + H + O^{++} + e + He - 7{,}3$ эв	$6{,}5 \cdot 10^{-16}$
118	$H_2O + He^{++} \rightarrow H_2 + O^+ + He^+ + 35{,}7$ эв	$4{,}9 \cdot 10^{-17}$
119	$H_2O + He^{++} \rightarrow OH + H^+ + He^+ + 35{,}6$ эв	$5{,}1 \cdot 10^{-17}$
120	$H_2O + He^{++} \rightarrow OH^+ + H + He^+ + 35{,}3$ эв	$5 \cdot 10^{-17}$
121	$H_2O + He^{++} \rightarrow OH^+ + H^+ + e + He^+ + 21{,}8$ эв	$1 \cdot 10^{-16}$
122	$H_2O + He^{++} \rightarrow 2H + O^{++} + e + He^+ - 3{,}7$ эв	$2{,}9 \cdot 10^{-15}$
123	$H_2O + He^{++} \rightarrow H^+ + H + O^{++} + e + He^+ + 17{,}2$ эв	$1{,}6 \cdot 10^{-16}$
124	$H_2O + He^{++} \rightarrow 2H^+ + O^+ + 2e + He^+ + 4{,}1$ эв	$2{,}4 \cdot 10^{-15}$

125	$H_2O + He^{++} \rightarrow H_2^{++} + O + e + He^+ - 5{,}3$ эв	$3{,}4 \cdot 10^{-15}$
126	$H_2O + He^{++} \rightarrow H_2^{++} + O + He + 19{,}2$ эв	$1 \cdot 10^{-16}$
127	$H_2O + He^{++} \rightarrow H_2^{++} + O^+ + e + He + 5{,}7$ эв	$1 \cdot 10^{-15}$
128	$H_2O + He^{++} \rightarrow H_2O^+ + e + He^{++} - 12{,}6$ эв	$1{,}9 \cdot 10^{-16}$
129	$H_2O^+ + He^{++} \rightarrow 2H^+ + O^+ + e + He^+ + 16{,}7$ эв	$2{,}2 \cdot 10^{-16}$
130	$OH + He^{++} \rightarrow H^+ + O^{++} + e + He + 12{,}4$ эв	$2{,}3 \cdot 10^{-16}$
131	$OH + He^{++} \rightarrow H^+ + O^{++} + 2e + He^+ - 12{,}1$ эв	$3{,}0 \cdot 10^{-16}$
132	$OH^+ + He^{++} \rightarrow H^+ + O^{++} + e + He^+ + 1{,}7$ эв	$1{,}2 \cdot 10^{-14}$
133	$H_2O + He^{++} \rightarrow H_2O^+ + e + He^{++} - 12{,}6$ эв	$1{,}9 \cdot 10^{-16}$
134	$OH + He^{++} \rightarrow H + O^{++} + e + He^+ + 1{,}4$ эв	$2{,}0 \cdot 10^{-14}$

1) Process number; 2) process reactions; 3) effective cross section, σ_{max} (cm^2). эв = ev = electron-volt.

molecules in the formation of O^+, O^{++}, N^+, N^{++}, OH^+, H_2^+ ions and also in the excited oxygen atoms $O(^1S)$ and $O(^1D)$.

REFERENCES

1. R.N. Il'in, Ionizatsiya, zakhvat elektronov i dissotsiatsiya pri stolknoveniyakh ionov vodoroda kiloelektronovol'tnykh energiy s atomami i molekulami gazov [Ionization, Electron Capture and Dissociation in Collisions of Hydrogen Ions of Kiloelectronvolt Energies with Atoms and Molecules of Gases], Author's Abstract of Dissertation, Leningrad, 1959.
2. R.N. Il'in, V.V. Afrosimov, N.V. Fedorenko. ZhTF [Journal of Technical Physics], 36, Issue 1, 41, 1959.
3. V.I. Ivanchuk, P.Ya. Sukholvanenko. Astr. Tsirk [Astronomical Circular], 196, 9, 1958.
4. V.I. Kranovskiy. Astr. zhurn [Astronomy Journal], 35, 222, 1958.
5. C.I. Fan, A.B. Meinel, Ap. J., 118, 205, 1953.
6. C.I. Fan. Ap. J. 122, 390, 1955.
7. D.R Bates. IAGA Bulletin, No. 15 b, 135, 1956.
8. I.S. Shklovskiy. Izv. Krym. Astr. obs [Bulletin of the Crime-

an Astronomical Observatory], 8, 51, 1952.

9. V.I. Cherednichenko. Byull. Komiss. po kometam i meteoram [Bulletin of the Commission on Comets and Meteors], Astr. Sove ta AN SSSR [Astronomy Council of the USSR Academy of Sciences], No. 2, 10, 1958.

10. V.I. Cherednichenko. Astr. zhurn., 36, 256, 1959.

11. V.N. Kondrat'yev. Elementarnyye khimicheskiye protsessy [Elementary Chemical Processes], ONTI, Khimteoret [Joint Scientific and Technical Publishing Houses, Publishing House for Theoretical Literature in Chemistry], Moscow-Leningrad, 1936.

12. V.L. Granovskiy. Elektricheskiy tok v gaze [Electrical Current in Gas], Vol. I, GITTL [State Publishing House of Technical and Theoretical Literature], Moscow-Leningrad, 1952.

13. N.V. Fedorenko, V.V. Afrosimov, R.N. Il'in, D.M. Kaminker. ZhETF [Journal of Experimental and Theoretical Physics], 36, 385, 1959.

14. D.M. Kaminker and N.V. Fedorenko, ZhETF, 25, 2239, 1954.

15. I.S. Shklovskiy. DAN SSSR [Proceedings of the USSR Academy of Sciences], 81, 525, 1951.

16. V.I. Cherednichenko. Informatsionnyy byulleten' MGG po Ukraine [Informational Bulletin on the IGY for the Ukraine], Issue 4, 1961.

17. M. Miyanishi and K. Watadani, J. Phys. Soc. Jap., 7, 69, 1952.

18. S.K. Mitra. Verkhiyaya atmosfera [The Upper Atmosphere] IL [Foreign Literature Press], Moscow, 1955.

19. D.T. Stewart. P.W.F. Gribbona. K.G. Emelens, Proc. Phys. Soc. 67, 188, 1954.

20. D.R. Bates, Ann. Geophys., 11, 253, 1955.

Manu-
script
Page
No.

[Transliterated Symbols]

89 г = g = gazokineticheskiy = gaskinetic

CORPUSCULAR MECHANISMS FOR THE EXCITATION OF ULTRAVIOLET EMISSIONS IN POLAR AURORAE

V.I. Cherednichenko

1. Emissions of the molecular ion N_2^+ (the negative band system 1NG), a nitrogen atom [NI] and a nitrogen molecule N_2 (the second positive band system 2PG) predominate in the ultraviolet section of the polar auroral spectrum [1, 2, 3]. The ultraviolet line 3466.5 Angstrom units is the most characteristic of the [NI] emissions for polar aurorae of all types. It has been established that the intensity I_{3466} increases with the height of the polar aurora and the more intense lines [N] are encountered in the low-latitude polar aurorae which are found at great altitudes [1]. Studies of high-altitude polar auroral spectra have shown that they apparently result from direct collisions between solar corpuscles H^+ and He^+ and are accompanied by the emission of hydrogen H_α [3, 4, 5].

It would be of great interest from this standpoint to examine the possibility of exciting ultraviolet polar auroral emissions through the action of solar corpuscular radiation on the atoms and molecules of the terrestrial atmosphere.

2. In 1957-1958, at Roshchino (geomagnetic latitude $\varphi = 60^\circ$), spectroscopic observations of polar aurorae were carried out (dispersion 80 Angstrom units/mm) and five spectrograms were obtained with H_α emission during aurorae of the Ha, R, F and RP types [3]. F.K. Shuyska measured the wavelengths of several auroral spectra in the near ultraviolet region, performed the supposed identification and evaluated the

relative intensity in fractions of the intensity for the line [NI] at λ 3466 A [3].

The measurement results are presented in Table 1. The third column shows the emission intensities in conditional units ($I_{3466} = 1$) and the last column gives the absolute emission intensities in kiloRayleighs (kR). The method for determining the absolute emission values is indicated below.

3. We demonstrated the important role of corpuscular radiation in the processes of the dissociation and ionization of N_2 molecules and N atoms in Reference [6]. The presence in the majority of the above-mentioned spectrograms of the hydrogen emission H_α in which the shift of the maximum corresponded to a velocity of 360 km/sec for the hydrogen atoms [3] gave rise to the idea that hydrogen atoms and ions of solar origin may be responsible for the observed intensity of the bands $N_2$2PG, N_2^+ 1NG, N_2VK and the lines [N I]. This was also indicated by the high kinetic temperature of the polar auroras, reaching in a number of cases to the order of 2500°K [3]. The most effective processes for the excitation of N_2, N_2^+ and N in collisions with H and H^+ may be the processes of charge transfer with excitation and dissociative charge transfer with excitation [6, 7]:

$$N_2 + H^+ \rightarrow N^* + N^+ + H^* - U_1, \quad (1)$$

$$N_2 + H^+ \rightarrow (N_2^+)^* + H - U_2, \quad (2)$$

$$N_2^+ + H \rightarrow N_2^* + H^+ - U_3. \quad (3)$$

The asterisk denotes excited products of reaction, while U_1, U_2 and U_3 denote the energy of the reactions. Reaction (1) may yield excited metastable atoms $N(^2P)$, producing emission at λ 3466 A. As a result of Reaction (2) the molecular ions $N_2^+(B'^2\Sigma_u^+)$ appear and these are the initial ions for emission at λ = 3914 A of the negative system of bands 1NG of the N_2 molecule. Excited N_2 molecules appear as a result of Reac-

tion (3) in the $C^3\Pi_u$ and $B^3\Pi g$ states, providing the beginning for the emissions of the second positive system of bands 2PG of the N_2 molecule and the Vegard-Kaplan VK bands of the N_2 molecule. The great probability of Processes (1), (2) and (3) wa proved experimentally at the Leningrad Physics and Engineering Institute [8].

TABLE 1

λ (Å)	Отождествление	I	I (%)
3997	N_2 2PG (1,4)	2,2	0,4
3943	N_2 2PG (2,5)	0,35	0,07
3914	N_2^+ 1NG (0,0)	24,	4,8
3882	N_2^+ 1NG (1,6)	3,8	0,7
3857	N_2^+ 1NG (2,2)	0,57	0,1
3832	N_2^+ 1NG (3,3)	0,32	0,06
3804	N_2 2PG (0,2)	4,5	0,9
3756	N_2 2PG (1,3)	2,9	0,6
3707	N_2 2PG (2,4)	1,6	0,3
3684	N_2 VK (1,11)	0,06	0,012
3582	N_2^+ 1NG (1,0)	2,2	0,4
3576	N_2 2PG (0,1)	8,9	1,8
3535	N_2 2PG (1,2)	4,3	0,9
3466	$N^+ 2P^3\ ^4S - 2p^3\ ^2P$	1,0	0,2
3500	N_2 2PG (2,3)	1,4	0,3
3425	N_2 VK (1,10)	1,5	0,3
3371	N_2 2PG (0,0)	11	2,2
3341	N_2 2PG (1,1)	0,95	0,19
3285	N_2 2PG (2,2)	0,94	0,18
3270	N_2 2PG (3,3)	1,2	0,2
3160	N_2 2PG (1,0)	2,5	0,5
3134	N_2 2PG (2,1)	0,92	0,1

1) Identification.

We obtain the following empirical formula in Reference [7] for purposes of calculating the effective cross sections of Processes (1), (2) and (3):

$$\sigma = \frac{5{,}3 \cdot 10^{-13}}{U_i [1 + \sqrt{\Delta W}\,(9 - z)]}. \qquad (4)$$

For processes of dissociative charge transfer with excitation: U_1 is the process energy (U_1); ΔW is the difference between the energies of the ion neutralization and the energy of dissociation (in terms of absolute magnitude); $\underline{z}$ is the number of valence electrons of the dissociating molecule.

For the charge-transfer processes (2) and (3):

U_1 is the difference between the energy of the electron state of the neutral particle prior to and after charge transfer; ΔW is the energy of the process (U_2, U_3); n is the number of valence electrons of the neutral particle.

Formula (4) makes it possible to compute the effective cross section at the maximum of the function of charge transfer with excitation and corresponds to the energy of the incident particles $U \geq 1$ kev [9, 10]. The theoretical values of σ, obtained from this formula, are in good agreement with experimental values [6, 8].

4. In order to compute theoretically the intensity of the ultraviolet emissions in the polar aurorae, it is not enough to know only the effective cross section of Processes (1), (2) and (3).

According to the relationship

$$I^0 = 10^{-6} \cdot H \cdot n_0 \cdot n_{H^+} \cdot v_{H^+} \cdot \sigma, \qquad (5)$$

where H is the height of the homogeneous atmosphere above the lower border of the polar aurora; n_0 is the concentration of N_2 molecules and O atoms at the lower border of the polar aurorae. (As shown by measurements carried out with geophysical rockets [1, 2], the atmosphere above 100 km consists primarily of N_2 and O); n_H^+ and v_H^+ are, respectively, the concentration and velocity of the polar protons at the lower border of the polar aurorae; I^0 is the intensity of emission in kiloRayleighs (kR). For a theoretical calculation of the ultraviolet emissions I^0, with the exception of σ, it is also necessary to know the quantities H, n_0, n_H^+ and v_H^+. In addition, in order to compare I^0 with the observed I the latter must be expressed in absolute units.

5. The intensity of the emissions presented in Table 1 can be expressed in absolute units (kR), proceeding from the following considerations. Of two hundred electrophotometric measurements in the polar auroral zone, carried out by Dzhordzhio at the Loparskaya station (φ =

$= 69^{\circ}$) and at Zvenigorod ($\varphi = 56^{\circ}$), it has been established that on the average the intensity of the green oxygen line ^1S at λ 5577 A amounts to 20 kR for aurorae greenish-white in color [3]. The ratio of the intensity of the negative band at λ 4278 A of the molecular ion N_2^+ to the intensity of the green oxygen line ^1S for polar aurorae of the indicated type is

$$\frac{I_{4278N_2^+}}{I_{5577[OI]}} = 0{,}26. \qquad (6)$$

Hence, since $I_{5577[OI]} = 20$kR, $I_{4278N_2^+} = 0.26 \cdot 20 = 5.2$ kR.

The distribution of energy in the spectrum of a polar aurora on the basis of numerous auroral observations in the Soviet Union [3, 11] and abroad [2] yields for the ratio of the intensity of the negative bands at λ 3914 A and λ 4278 A for the N_2^+ ion

$$\frac{I_{3914N_2^+}}{I_{4278N_2^+}} = 2. \qquad (7)$$

From Relationship (7) it follows that $I_{3914N_2^+} = 2 \cdot 5{,}2 = 10{,}4$ kR. In Table 1 $I_{3914N_2^+} = 24$ conditional units, i.e., one conditional unit of intensity is equal to 0.433 kR. From this we obtain the values of the absolute intensities presented in the fourth column in Table 1.

6. No determinations have been made of the height of the lower polar auroral border at Roshchino. The magnitude of the concentration n_0 was found indirectly – on the basis of the lifespan of the metastable state ^2P of an atom of nitrogen. At the height at which the extinction of luminescence at λ 3466 A becomes noticeable, it is necessary to satisfy the condition

$$\tau = \frac{\bar{\lambda}}{\bar{v}}, \qquad (8)$$

where τ is the lifespan of the metastable state ^2P of an N atom; $\bar{\lambda}$ is the length of the free path; $\bar{v}$ is the mean-arithmetic velocity of the N atoms. However,

$$\lambda = \frac{1}{4\sqrt{2}\cdot\sigma\cdot n}, \tag{9}$$

where σ is the effective cross section of the de-exciting collisions.

From (8) and (9) we have:

$$n = \frac{1}{4\sqrt{2}\cdot\sigma\cdot v\cdot\tau}. \tag{10}$$

7. The process of de-excitation (extinction) of excited nitrogen atoms $N(^2P)$ may be a result of collisions of the second kind with ionization, charge transfer, transfer of excitation to an O atom or N_2 molecule and the transfer of excitation to an electron. Let us examine in order the efficiency of all of these possibilities in the extinction of the luminescence at λ 3466 Å [NI].

1) The processes of de-excitation of $N(^2P)$ atoms with ionization may be as follows:

$$N(^2P) + N_2 \rightarrow N + N_2^+ + e, \tag{11}$$

$$N(^2P) + O \rightarrow N + O^+ + e, \tag{12}$$

$$N(^2P) + N \rightarrow N + N^+ + e. \tag{13}$$

The effective cross sections of these processes are very small, since the ionization potentials for N_2 (15.6 ev), O (13.6 ev) and N (14.5 ev) considerably exceed the excitation potential of the metastable level ^2P (3.56 ev) [9].

2) Extinction with charge transfer:

$$N_2^+ + N(^2P) \rightarrow N^+ + N_2 - 4{,}6 \text{ ev}, \tag{14}$$

$$O^+ + N(^2P) \rightarrow N^+ + O - 2{,}6 \text{ ev}. \tag{15}$$

The effective cross sections for these processes, calculated in accordance with Formula (4), are, respectively, equal to $4.45\cdot10^{-16}$ cm^2 and $5.25\cdot10^{-16}$ cm^2, i.e., rather substantial.

3) The transfer of excitation from the metastable atom $N(^2P)$ to the neutral atom O or molecule N_2

$$N(^2P) + O \rightarrow N + O(^1S) + 1{,}6 \text{ ev}, \tag{16}$$

$$N(^2P) + N_2(v' = 10) \rightarrow N + N^2(v'' = 9) + 0{,}0312 \text{ ev}. \qquad (17)$$

According to experimental data the probability of electron excitation between colliding systems will reach its maximum if the difference between the energies of the electron states of both systems is equal to zero. The probability of the transfer of excitation depends in great measure on the difference ΔE between the energies of the electron states on the velocity $\underline{v}$ of the colliding particles and on whether or not the transitions of the given state to the ground level are allowed or forbidden [10, 12].

The effective cross section for the transfer of excitation, associated with the electron transitions, is described by the following relationship [10, 12]:

$$\sigma_s = \pi \left(\frac{p_1 \cdot p_2}{\Delta E}\right)^{2/s} \cdot f\left(\Delta E^{\frac{s-1}{s}} \cdot (p_1 p_2)^{1/s} \cdot \bar{v}^{-1} \cdot \bar{h}^{-1}\right), \qquad (18)$$

where $f(x) \approx (8\pi/s)$ for $x \ll 1$,

$$f(x) \approx 32 \cdot x^{s-1} \cdot e^{-2x} \text{ for } x \gg 1;$$

$\underline{s}$ is the order of the multipolarity of the electrical moment of the electron transition (if the electron transitions in both colliding systems are allowed, $s = 3$; if the transition in one system is allowed, while forbidden in the other, $s = 4$; if, however, both transitions are forbidden, $s = 5$ [10, 12, 13]); p_1 and p_2 are the electrical moments of the electron transitions. For the allowed transition $p_1 = e \cdot a$ ($\underline{e}$ is the electron charge; $\underline{a}$ is the order of magnitude for the gaskinetic radius of the atom or molecule); for the forbidden transition $p = ea^2$ (the quadrupole moment); $\bar{h} = (h/2\pi)$, with $\underline{h}$ the Planck constant.

For process (16) both transitions are forbidden, $\underline{s}$ is large and equal to 5; $\Delta E = 1.6$ ev is also large. In this case $x = 100$ and $f(x) \approx \approx 0$, i.e., Process (16) is virtually impossible.

For Process (17) the transition for a nitrogen atom is forbidden,

while allowed for a nitrogen molecule and $s = 4$, with the product of the quadrupole and dipole electrical moments $p_1 p_2 = (ea_1^2)\cdot(ea_2)$ ($a_1 = 0.75\cdot10^{-8}$ cm, $a_2 = 1.55\cdot10^{-8}$ cm – respectively, the gaskinetic radii of the atom N and the molecule N_2).

Having substituted these values into Formula (18) and having made use of the value of $\bar{v} = 1.94\cdot10^5$ cm/sec which corresponds to T = 2500°K, for Process (17) we obtain:

$$\sigma_\tau = 1{,}3\cdot10^{-15}\ \text{cm}^2.$$

The great probability of de-exciting collisions for (17) also follows from the fact that for this process the following condition is not satisfied [10, 12]:

$$\frac{a\cdot\Delta E}{h\bar{v}} \gg 1. \qquad (19)$$

When this condition is satisfied σ_τ must be considerably smaller than the gaskinetic cross section. In our case a = 1.55:10^{-8} cm; $\Delta E = 5\cdot10^{-12}$ ergs and $(a\cdot\Delta E)/h\bar{v} = 0.92 \approx 1$ and Condition (19) is not satisfied, i.e., σ_τ must be substantial.

4. The extension of luminosity as a result of electron impact. The effective cross section for de-exciting electron collisions for the process

$$N(^2P) + e \rightarrow N(^4S) + e$$

is defined by the relationship [9]:

$$\sigma_{n0}(U) = 2{,}72\,\frac{\Sigma g_0}{\Sigma g_n}\cdot\sigma_{on}(U_m)\cdot\frac{U-U_a}{U_m-U_a}\cdot\exp\left(-\frac{U}{U_m-U_a}\right). \qquad (20)$$

where $\Sigma g_0 = 4$ and $\Sigma g_n = 6$ are, respectively, the sum of the statistical weights of the ground and excited states of the atom N; σ_{n0} is the effective excitation cross section of the level ^2P; $U_a = 3.58$ ev is the excitation potential of the level ^2P; U_m is the electron energy corresponding to the maximum of the excitation function; U is the electron

TABLE 2

	Длина волны эмиссий Å λ 1	Отождествление 2	3 Схема процесса	$\sigma \times 10^{-16}$ см^2	I (kR)	I° (kR)	$\frac{I^\circ}{I}$
1	3997	N_2 2PG (1,4)	$N_2^+ + H \rightarrow N_2 (B^3\Pi g) (1,4) + H^+ - 8,4$ эв	3,16	0,34	0,468	0,5
2	3943	» (2,5)	$N_2^+ + H \rightarrow N_2 (B^3\Pi g) (2,5) + H^+ - 8,44$ эв	3,15	0,152	0,465	3,0
3	3804	» (0,2)	$N_2^+ + H \rightarrow N_2 (B^3\Pi g) (0,2) + H^+ - 8,56$ эв	3,14	1,95	0,465	2,1
4	3756	» (1,3)	$N_2^+ + H \rightarrow N_2 (B^3\Pi g) (1,3) + H^+ - 8,8$ эв	3,10	1,25	0,46	3,7
5	3707	» (2,4)	$N_2^+ + H \rightarrow N_2 (B^3\Pi g) (2,4) + H^+ - 8,64$ эв	3,13	0,69	0,462	0,7
6	3576	» (0,1)	$N_2^+ + H \rightarrow N_2 (B^3\Pi g) (0,1) + H^+ - 8,76$ эв	3,10	3,84	0,46	0,1
7	3535	» (1,2)	$N_2^+ + H \rightarrow N_2 (B^3\Pi g) (1,2) + H^+ - 8,8$ эв	3,10	1,86	0,46	2,5
8	3500	» (2,3)	$N_2^+ + H \rightarrow N_2 (B^3\Pi g) (2,3) + H^+ - 8,84$ эв	3,10	0,605	0,46	0,8
9	3371	» (0,0)	$N_2^+ + H \rightarrow N_2 (C^3\Pi g) (0,0) + H^+ - 9,1$ эв	3,04	4,76	4,51	1,0
10	3341	» (1,1)	$N_2^+ + H \rightarrow N_2 (B^3\Pi g) (1,1) + H^+ - 9$ эв	3,06	1,64	0,454	2,8
11	3285	» (3,3)	$N_2^+ + H \rightarrow N_2 (B^3\Pi g) (3,3) + H^+ - 9,07$ эв	3,06	0,246	0,454	2,0
12	3270	» (4,4)	$N_2^+ + H \rightarrow N_2 (B^3\Pi g) (4,4) + H^+ - 9,09$ эв	3,06	0,52	0,454	0,9
13	3160	» (1,0)	$N_2^+ + H \rightarrow N_2 (B^3\Pi g) (1,0) + H^+ - 9,22$ эв	3,03	1,08	0,448	0,4
14	3134	» (2,1)	$N_2^+ + H \rightarrow N_2 (B^3\Pi g (2,1) + H^+ - 9,24$ эв	3,04	0,4	0,45	1,1
15	3914	N_2^+ 1 NG (0,0)	$N_2 + H^+ \rightarrow N_2^+ (B'^2\Sigma_u^+) (0,0) + H - 6,1$ эв	1,83	10,4	2,73	0,3
16	3882	» (1,1)	$N_2 + H^+ \rightarrow N_2^+ (B'^2\Sigma_u^+) (1,1) + H - 6,13$ эв	1,85	1,64	2,76	1,7
17	3857	» (2,2)	$N_2 + H^+ \rightarrow N_2^+ (B'^2\Sigma_u^+) (2,2) + H - 6,15$ эв	1,85	0,246	2,76	11,0
18	3285	» (3,3)	$N_2 + H^+ \rightarrow N_2^+ (B'^2\Sigma_u^+) (3,3) + H - 6,18$ эв	1,82	0,138	2,72	20,0
19	3582	» (1,0)	$N_2 + H^+ \rightarrow N_2^+ (B'^2\Sigma_u^+) (1,0) + H - 6,39$ эв	1,80	0,94	2,68	3 0
20	3684	» (1,11)	$N_2^+ + H \rightarrow N_2 (X'\Sigma_g^+) (1,11) + H^+ - 5,47$ эв	3,82	0,026	0,572	22,0
21	3425	» (1,10)	$N_2^+ + H \rightarrow N_2 (X'\Sigma_g^+) (1,10) + H^+ - 5,72$ эв	3,74	0,65	0,580	0,9
22	3466	N1 $^2p \rightarrow {}^4s$	$N_2 + H^+ \rightarrow N (^2p) + N^+ + H (3s) - 25,3$ эв.	0,892	0,433	1,33	3,1

1) Emission wavelength, λ A; 2) identification; 3) reaction. = ev = electronvolt.

energy.

In the transition from the ground level ^4S to the excited level ^2P the multiplicity changes. In this case [14]

$$U_m = U_a + 1. \tag{21}$$

The effective cross section of excitation by electron impact of the metastable level of the atom may be determined from the relationship [12]:

$$\sigma_{on} = 3{,}62 \cdot 10^{-15} \cdot \frac{\pi^5 \cdot m^2 \cdot e^4}{Uh^4} \cdot f_{on}^2 U_0, \tag{22}$$

where m, e and U are, respectively, the mass, charge and energy of the striking electron; f_{on} is the oscillator force of the transition $^4S \rightarrow$ $\rightarrow {}^2P$ of the atom N; E_0 is the energy of the ground state of the atom:

$$E_0 = \frac{2\pi^2 e^4 z^2}{h^2}, \tag{23}$$

where z is the charge of the atomic nucleus. For the atom N we have $E_0 = 1.09 \cdot 10^{-9}$ ergs. The oscillator force f_{on} for the metastable level can be found on the basis of the lifespan τ of this level from the relationship [12]:

$$\frac{1}{\tau} = \frac{8\pi^2 e^2}{mc} \cdot \frac{\Sigma g_n}{\Sigma g_m} \cdot \frac{1}{\lambda^2} \cdot f_{on}, \tag{24}$$

where c is the speed of light; $\tau = 2.1$ sec is the lifespan of the metastable level ^2p of the atom N. For the transition $^4S \rightarrow {}^2P$ of the atom N the formula yields $f_{on} = 6.3 \cdot 10^{-10}$. In this case, when $U = U_m = U_a + 1 = 4.58$ ev from Formula (22) we obtain $\sigma_{on}(U_m) = 8.3 \cdot 10^{-21}$ cm^2 which is the maximum effective cross section of the excitation of level ^2P by electron impact.

The maximum effective cross section of the de-exciting collisions in this case will, according to Formula (20), be equal to: $\sigma_{on}(U_m) = 1.5 \cdot 10^{-22}$ cm^2, i.e., extremely small.

It must also be taken into consideration that when $T = 2500^\circ K$ the

number of electrons exhibiting energy U_m according to the relationship

$$\frac{\Delta n_e}{n_e} = e^{-\frac{U_m}{kT}}\left(1 + \frac{U_m}{kT}\right) \qquad (25)$$

amounts to only 10^{-9} of their total number.

On the basis of these considerations, the process of extinction by electron impact is extremely ineffective.

Thus, consideration of all possible processes of extinction for the line 3466 A of atomic nitrogen shows that the most probable is the process of the extinction of $N(^2P)$ on collision with oscillation-excited molecules N_2.

8. With an effective cross section for Process (17) of $\sigma_\tau = 1.3 \times \times 10^{-15}$ cm^2 from Relationship (10) we will obtain the concentration of oscillation-excited molecules N_2

$$n_{N_2}(v'=10) = 3{,}3 \cdot 10^8 \text{ cm}^3.$$

The quantity $n_{N_2}(v' = 10)$ may be derived out of other considerations as well.

The total number of de-exciting collisions required for the transition of the oscillation-excited molecule N_2 from a higher level v' to a lower level v", on the one hand, is determined by the relationship [15, 16]:

$$z = \frac{1}{\gamma_{1\to 0}} \cdot \left(\frac{1}{v'} + \frac{1}{v'-1} + \ldots + \frac{1}{v''+2} + \frac{1}{v''+1}\right) \cdot e^{\frac{h\nu}{kT}}, \qquad (26)$$

where $\gamma_{1\to 0}$ is the probability of the oscillation transition $v'' = 1 \rightarrow \rightarrow v'' = 0$ ($\gamma_{1\to 0} = 10^{-4}$ [15, 16]); hν is the quantum energy for the transition $v' = 10 \rightarrow v'' \rightarrow 9$.

On the other hand, this same number of collisions

$$z = \tau_0 \cdot z_1, \qquad (27)$$

where z_1 is the total number of collisions experienced by the molecule N_2 within 1 sec; τ_0 is the time required for the transition of the mole-

cule N_2 from the level v' to the level v".

$$z_1 = 4\sqrt{2}\cdot v\cdot\sigma_c\cdot n_{v'=10}, \tag{28}$$

$$\tau_0 = \frac{3}{8\pi^3}\cdot\frac{c\cdot\mu\cdot r_0^2}{p^2}\cdot\lambda^3. \tag{29}[16]$$

In (29) $\mu = \frac{m_N\cdot m_N}{m_N + m_N}$ is the reference mass of the molecule N_2; $r_0 = 1.55 \times$ $\times 10^{-8}$ cm is the equilibrium distance between the atoms N in the molecule N_2; $p = 1.03\cdot10^{-18}$ CGSE [16, 17] is the dipole moment of the molecule N_2; $\lambda = 3620$ A is the wavelength for the transition v" = 10 → v' = = 9.

Having denoted $\left(\frac{1}{v'} + \frac{1}{v'-1} + \ldots + \frac{1}{v''+1} + \frac{1}{v''+1}\right)$ by B and having equated (26) and (27) to one another, we obtain

$$4\sqrt{2}\cdot\sigma_c\cdot n_{v'-10}\cdot\bar{v}\cdot\tau_0 = \frac{1}{\gamma_{1\to0}}\cdot B\cdot e^{-\frac{h\nu}{kT}}, \tag{30}$$

from which we obtain

$$n_{N_2}(v'=10) = 4{,}1\cdot10^8 \text{ cm}^{-3}.$$

Therefore the earlier derived quantity $n(v' = 10) = 3.32\cdot10^8$ cm^{-3} may be regarded as promising.

The concentration n_0 of neutral N_2 nitrogen molecules in the ground oscillatory state can be found from the relationship [10]:

$$n_{v'=10} = n_0\cdot\exp\left(-\frac{27\cdot\pi^2\cdot r_0^2\cdot kT}{2h}\right)^{1/3}. \tag{31}$$

With T = 2500°K Relationship (31) yields $n_0 = 1\cdot10^9$ cm^3, which corresponds to the height of the lower polar auroral boundary h = 185 km [18] assuming that the atmosphere below 300 km consists of molecular nitrogen and atomic oxygen O [1,].

The great height of the indicated polar aurorae is confirmed also by the presence of the hydrogen line H_α in their spectra, since a number of facts speak in favor of the contention that the hydrogen emission appears at heights considerably above 100-110 km [3].

9. Let us now determine the magnitude of the proton concentration

at the lower polar auroral boundary. The quantity I_{H_α} can be found by proceeding from the fact that generally $I_{H_\alpha}/I_{5577} = 0.15$ [19], and since $I_{5577} = 20$ kR, $I_{H_\alpha} = 3$ kR.

The most effective reactions for the excitation of the H_α line in polar aurorae may be those of charge transfer with excitation:

$$H^+ + N_2 \rightarrow H(3s) + N_2^+ - 14{,}3\ \text{ev}, \tag{32}$$

$$H^+ + O \rightarrow H(3s) + O^+ - 12{,}1\ \text{ev}. \tag{33}$$

The effective cross sections found for these reactions on the basis of Formula (4) are respectively equal to $\sigma_1 = 1.9 \cdot 10^{-16}$ cm^2 and $\sigma_2 = 4.1 \cdot 10^{-16}$ cm^2.

Since molecular nitrogen is a more abundant component of the terrestrial atmosphere than atomic oxygen O [1, 2], in the computations of n_{H^+} we can assume $\sigma = \sigma_1$.

The height of the homogeneous atmosphere for the height h = 185 km amounts to $H = 3 \cdot 10^6$ cm [20]. Now substituting the values of I_{H_α}, H, n_O, v_{N^+} and σ_1 into Relationship (5) we obtain

$$n_{H^+} = 137\ \text{cm}^{-3}.$$

10. To calculate the intensity 1NG N_2^+ it is also necessary to know the magnitude of the molecular ion concentration $n_{N_2^+}$.

According to Chamberlain's calculations [21] to produce the observed brightness in the polar auroral rays a current with a density of $i = 6 \cdot 10^{12}$ electrons/cm^2·sec must pass. The current of N_2^+ ions must be the same. With a velocity of $v = 1.38 \cdot 10^5$ cm/sec, corresponding to T = = 2500°K, the concentration $n_{N_2^+}$ will be

$$n_{N_2^+} = \frac{i}{v} = 4{,}35 \cdot 10^7\ \text{cm}^{-3}.$$

The quantity n_H was assumed to be equal to n_{H^+} [19].

11. In addition, Table 2 shows the most probable excitation reactions for lines and bands of intensity I^0 of emissions computed in ac-

cordance with Relationship (5). The table shows that in a number of cases the ultraviolet polar auroral emissions may be satisfactorily explained by reactions of charge transfer with excitation during the collision of N_2 molecules and N_2^+ ions with neutral and ionized atoms of hydrogen.

12. Can the electrons in polar aurorae be sufficiently effective in the excitation of the emissions 2PG N_2 and ING N_2^+? The effective cross section of excitation for the $C^3\Pi_u$ level of an N_2 molecule which serves as the origin for the emission of the bands 2PG for the maximum of the excitation function can be computed in accordance with the formula [10]:

$$\sigma_m = \frac{\pi e^4}{U_m U_a} \cdot f \cdot \ln\left(\frac{4U_m}{U_a}\right).$$

when $U_m = U_a + 1$ [14], $U_a = 11.2$ ev and $f = 0.033$ [22]

$$\sigma_m = 4{,}1 \cdot 10^{-17}\ \text{cm}^2.$$

Since Formula (34) is valid when $U \geq 7U_a$, and for lower values of U yields σ greater approximately by an order of magnitude than the true value [10], for $U_m = 12.2$ ev we can assume

$$\sigma_m = 4{,}26 \cdot 10^{-18}\ \text{cm}^2.$$

However, the number of electrons with energy equal to U_m with $T = 2500^\circ K$ according to (25) amounts only to 10^{-21} of the total number, i.e., the efficiency of the electrons in the excitation of the bands 2PG at this temperature will be negligibly small.

However, even at a temperature of $15{,}000^\circ K$ the number of electrons having an energy equal to U_m amounts to 10^{-4} of the total number and $I^0_{2PG} = 4.5$ kev.

If a temperature on the order of $15{,}000^\circ K$ is developed in the polar aurorae under conditions of gas discharge, it is possible to state that electron excitation will make a noticeable contribution to the ex-

citation of the bands 2PG N_2.

For the excitation of bands 1 NG N_2 the oscillator force $f = 0.1$ [23]. Since $U = U_m = 49$ ev [24], $U_a = 19.6$ ev, according to (34)

$$\sigma_m = 2{,}03 \cdot 10^{-17} \text{ cm}^2.$$

If we take into consideration that condition $U \geq U_a$ is not satisfied, we can assume $\sigma_m = 2 \cdot 10^{-18}$ cm^2.

At a temperature $T = 10^5$ K $\frac{\Delta n_e}{n_e} = 10^{-6}$ and $I_{N_2^+ 1NG} = 10^{-6} kR$,

i.e., even at so great a temperature as 10^5 K the electron impact cannot be responsible for the observed intensity of the bands 1NG N_2^+.

REFERENCES

1. Collection entitled "Atmosfery Zemli i planet" ["Atmosphere of the Earth and Planets"], edited by D.P. Koyper, 209 Foreign Literature Press, Moscow, 1951.
2. S.K. Mitra. Verkhiyaya atmosfera [The Upper Atmosphere], 388, IL [Foreign Literature Press], Moscow 1955.
3. Collection entitled "Spektral'nyye, elektrofotometricheskiye i radiolokatsionnyye issledovaniya polyarnykh siyaniy i svecheniya nochnogo neba"["Spectral, Electrophotometric and Radar Investigations of Polar Aurorae and Luminescence of the Night Sky"], 45, Izd-vo AN SSSR, [USSR Acad. Sci. Press], Moscow, 1959.
4. P. Swigs. Scientia, 89, 5, 1954.
5. V.I. Krasovskiy. Astr. zhurn. [Astronomy Journal], 35, Issue 2, 1958.
6. V.I. Cherednichenko. Astr. zhurn., 36, Issue. 2, 254.
7. V.I. Cherednichenko. Byull. komissii po komet'am i meteoram Astr. Soveta AN SSSR [Bulletin of the Commission on Comets

and Meteors of the Astronomical Council of the USSR Academy of Sciences], No. 2, 10, 1958.

8. R.N. Il'in, V.V. Afrosimov, N.V. Fedorenko. ZhETF [Journal of Experimental and Theoretical Physics], Vol. 36, Issue 1, 41, 1959.

9. V.L. Granovskiy. Elektricheskiy tok v gaze [Electrical Current in a Gas], Vol. 1, GITTL [State Publishing House for Theoretical and Technical Literature], Moscow-Leningrad, 1952.

10. G. Messi and Ye. Barkhop. Elektronnyye i ionnyye stolknoveniya [Electron and Ion Collisions], IL, Moscow, 1958.

11. I.A. Khvostikov. Svecheniye nochnogo neba, [The Luminescence of the Night Sky], izd. AN SSSR, Moscow-Leningrad., 1948.

12. N. Mott and G. Messi. Teoriya atomnykh stolknoveniy [Theory of Atomic Collisions], IL, M., 1951.

13. G. Gertsberg. Atomnyye spektry i stroyeniye atomov [Atomic Spectra and Atomic Structure], IL, M., 1948.

14. P. Bates, A. Fundaminsky, H. Massey, F. Leech, Phil. Trans. A, 243, 93, 1950.

15. V.I. Krasovskiy. UFN [Achievements in Physical Sciences], Issue 3, 483, 1954.

16. V.N. Kondrat'yev. Elementarnyye khimicheskiye protsessy [Elementary Chemical Reactions], ONTI, Khimteoret [Joint Scientific and Technical Publishing Houses, Publishing House of Theoretical Literature in Chemistry], Leningrad, 1936.

17. Uoters. Khimiya svobodnykh radikalov [The Chemistry of Free Radicals], IL, M., 23, 1948.

18. Collection entitled "Iskusstvennyye sputniki Zemli" ["Artificial Satellites of the Earth"], Issue 2, Izd. AN SSSR, M., 30, 1958.

19. B.A. Bagaryatskiy, UFN, 65, vyp. 4, 631, 1958.

20. M. Nicolet. L'etude optique de l'atmosphere terrestre, Mem. Soc. Roy. Scien. Liege Quatrieme Serie, t. 12, Fase, I-II, 1952.

21. J.W. Chamberlain. Ap. J. 122, No. 2, 349, 1955.

22. I. Stephenson, Proc. Phys. Soc., A., 64, 99, 1951.

23. Harrison, Ap. J. 112, No. 2, 353, 1950.

24. F.P. Bundy, Phys. Rev., 52, No. 7, 698, 1937.

CERTAIN FEATURES OF POLAR AURORAL FORMS WITH RAY STRUCTURE

N.I. Dzyubenko

The study of the structural features of the various polar auroral forms is presently a matter of pressing urgency. Together with the results of morphological, spectral, photoelectrical and spectrometric investigations such a study will doubtlessly serve to promote a more thorough understanding of the essence of the polar auroral phenomenon. The majority of the polar auroral forms are extremely dynamic and the problem, in final analysis, reduces to the taking of motion pictures having adequate spatial and time resolution. This will make it possible to study both the instantaneous characteristics of the structure as well as their time variations. The photographic methods in use to the present time for the study of polar aurorae (including motion pictures) are only slightly effective in terms of the possibilities of studying the structure (the great exposures of individual frames, the small image scale, limited frequency of frame repetition, etc.). However, certain average characteristics of the structure of certain forms of polar aurorae can be studied even with such photographs, which is the purpose of the present paper.

The observational material used in this paper was obtained in March 1959 at the AANII Geophysical Station and the KGU [Kiev State University] at Tiksi Bay. A NAFA-3S/25 aerial camera was used ($f = 25$ cm; relative aperture 1:2.5; photograph 18 × 24 cm^2; field-of-view angle along the 18-cm side of the photograph, 40°; along the 24-cm side of the photograph, 51°; along the diagonal, 62°). The observer was D.P.

Duma.

We know that the gray auroral forms, which in this case are of greatest interest, are marked by their great mobility. According to the visual observations of S.K. Vsekhsvyatskiy [1] a ray exists in a ray arc for several seconds, and sometimes for fractions of a second. For a clear picture the exposure should not exceed this length of time. However, the NAFA-3S/25 camera was not fast enough in order to ensure this exposure even in the case of the very brightest auroras. The exposures for the processed photographs range from 5 to 30 seconds.

A total of 12 photographs were selected for evaluation; the effects of blurring due to the motion of the rays were least pronounced in these photographs. The exposure time as well as the cleanness of the photographs were taken into consideration. In certain cases it was not the entire ray arc that was studied, but rather only that portion which in our opinion had been least subject to the effects of blurring and overlapping.

Fig. 1. Photograph of the aurora described in Item 3.

Let us present a brief listing of the auroras whose structure

were studied, and their characteristic in accordance with the notes made in the observation log.

1. 1.3.1959. 14^h42^m UT. Exposure 7 seconds. Portion of ray arc. Average height of ray base above horizon h = 11°. Azimuth 214°. Judging from photograph aurora very bright. Four bright rays stand out, possibly representing bundles of individual thin rays.

2. 1.3.1959. 14^h45^m UT. Exposure 15 seconds. Bright ray arc consisting of a large number of thin rays forming several bundles along the arc and these are outstanding because of the elevated luminosity brightness (Fig. 1). The average height of the lower border of the studied segment of the arc above the horizon is 15°. A = 222°.

3. 1.3.1959. 14^h48^m UT. t = 8 seconds. Arc with ray structure. Ray brightness along the arc exhibits outstanding periodicity. This periodicity stands out particularly clearly in the closer portions of the arc where the structure is not nearly so affected by distortions of perspective and similar phenomena. The average height above the horizon for the subject part of the arc is 17°. A = 243°. Isolated thin rays stand out rather clearly only on certain segments of the arc.

4. 1.3.1959. 14^h50^m UT. t = 15 seconds. The height of the lower border of the subject region above the horizon is 15°. A = 239°. The aurora exhibits a rather unique form – two arcs of ray structure positioned one above the other, with the outline of the lower border of one completely duplicating the outline of the lower border of the second. Moreover, the rays of the lower arc are seemingly an extension of the rays of the upper arc and similar to these not only in terms of mutual position but also with respect to relative brightness. One gets the impression that we are dealing with a single arc of ray structure, of great extent in height and exhibiting a strange brightness depression through the middle. The structure is extremely diffuse; however, on

certain segments of the arc it is possible to isolate regions suitable for evaluation.

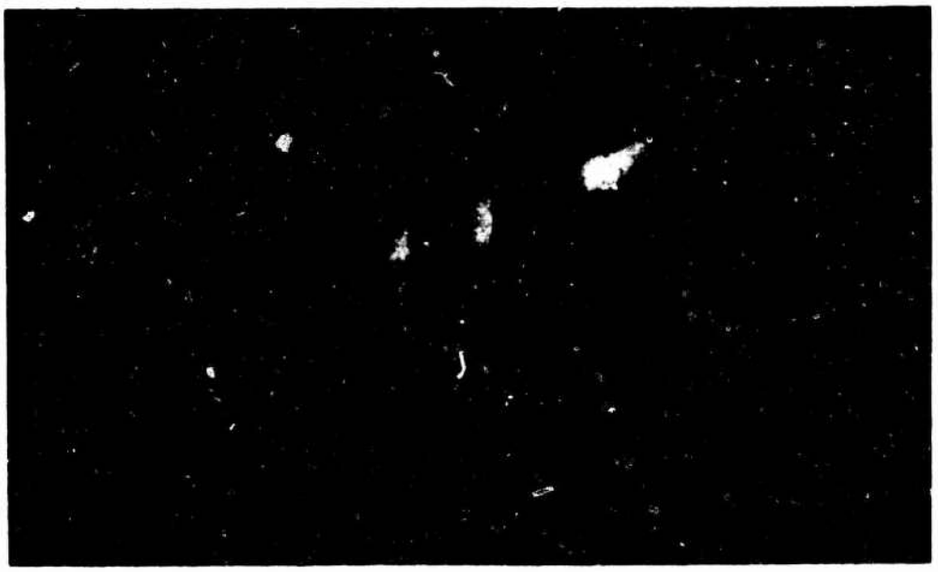

Fig. 2. Photograph of aurora described in Item 6 at $15^h38^m20^s$ Universal Time. Exposure 15 seconds.

5. 9.3.1959. $15^h34^m30^s$ UT. t = 20 seconds. Eastern part of arc with ray structure passes through zenith. Average height of lower border of rays above horizon 13° (from 6° to 20°). A = 288°. Pulsating arc, rapidly changing. Brightness 3 points. Rays exhibit great vertical extension. Photograph apparently shows only bright portions of arc close to horizon, reflecting large-scale structure. Finer structure not seen, on the one hand, because of blurring, and on the other hand, because of the great atmospheric absorption at the horizon.

6. 9.3.1959. $15^h37^m45^s$ UT. t = 15 seconds. Bright arc of ray structure rated at 3-4 points. Individual rather broad rays stand out clearly, possibly exhibiting fine structure which, however, is difficult to ascertain because of the effects of rapid motion. There are five successive photographs of this aurora taken in a time interval of about 3^m and these photographs make it possible to draw certain conclusions regarding the motion of the aurorae. On the first photograph ($15^h37^m45^s$

UT) the lower border of the rays is situated at a height of 56° above the northern horizon. The aurora subsequently rises to the zenith at a rate of 3°-5° per minute. On the basis of the characteristic appearance of the rays (western edge of the ray diffuse, eastern edge sharp) we can draw the conclusion that all rays (possibly with rare exceptions) moved as a single structural formation in one direction (Fig. 2).

7. 9.3.1959. $15^h38^m50^s$ UT. t = 10 seconds. The aurora described in Item 6, but at another instant of time.

8. 26.3.1959. 12^h39^m UT. t = 25 seconds. A part of the corona at zenith. Ordinary aurora of moderate brightness (underexposure at t = = 25 seconds).

9. 26.3.1959. 12^h48^m UT. t = 5 seconds. Arc of ray structure. Underexposed. Height above horizon 31°. A = 354°. Two waves in the brightness along the arc can be seen, apparently reflecting the small- and large-scale structure.

10. 26.3.1959. 14^h51^m UT. t = 30 seconds. Arc with ray structure on N1 of ordinary light. Long rays extend to the zenith. Despite the pronounced effect of overlapping and blurring, we note the periodicity of the structure with two spatial periods.

11. 30.3.1959. 14^h25^m UT. t = 15 seconds. Homogeneous arc changing into arc with ray structure. Height above horizon 29°. A = 139°. Brightness 3 points. Structural periodicity noted.

12. 30.3.1959. 14^h30^m UT. t = 20 seconds. Arc with ray structure. h = 20°. A = 171°. Structure very clean, but great underexposure. The exposure probably failed to cover the entire aurora or the rays exhibited great stability and low brightness. The clarity of the structure makes it possible clearly to detect the periodicity.

To all of the foregoing we should add that all examined aurorae were of conventional green coloration and the brightness, except for

rare instances, did not drop below 3 points. The photographic measurements were carried out with a ruler and grid accurate to 0.5 mm, which corresponds to 7' in angular measure. To determine the absolute values of the distances of interest to us in a polar aurora the slant ranges of the border points were determined on the basis of their height above the horizon. The height (zenith distances) and azimuths were determined from stars which stood out clearly on all of the photographs. In determining the slant ranges it was assumed that the lower borders of all the rays of an arc are situated on a surface concentric to that of the earth and situated at a height of 110 km above the ground. The curvature of the terrestrial surface was taken into consideration in the case of aurorae low over the horizon. The effects of perspective and mutual spatial position of auroral details were taken into consideration in all cases. Distortion was regarded as insignificant, at least in a circle with a 50-mm radius at the center of the frame.

The measurements produced the following information:

1. The periodicity in the brightness distribution along the arc with ray structure is more or less reliably noted for all subject aurorae. In certain cases two spatial λ periods are noted. One of these, reflecting a large-scale structure, includes the second which reflects a finer structure which can still be made out photographically.

2. Assuming the periodicity in the structure of the auroral forms with ray structure to have been established, we determine the absolute values of the spatial periods for the aurorae examined. The results are given in Table 1. The fourth column of the table shows the mean error of each result. As we can see, the relative error is rather great (15-25%), which is basically governed by the inaccuracy in the determination of the position of the lower border of the rays blurred as a result of the rapid motion of the structural details, the approximation

of certain simplifying assumptions, etc. The fifth column shows the number of rays (structure bundles) on the basis of which the averaging was accomplished.

3. Table 1 shows that three values of λ are characteristic of the studied aurorae:

$$\lambda_1 = (4-8)\cdot 10^5 \text{ cm},$$

$$\lambda_2 = (1{,}5-2{,}5)\cdot 10^6 \text{ cm},$$

$$\lambda_3 = (4{,}5-6{,}0)\cdot 10^6 \text{ cm}.$$

TABLE 1

№ п.п. 1	Дата 2	Мировое время 3	λ ($\times 10^5$ см)	$\Delta\lambda$ ($\times 10^5$ см)	Число лучей 4	Примечания 5
1	1.3. 1959	14^h42^m	45	6	4	Учтена поправка за кривизну Земли 6
2	1.3. 1959	14^h45^m	60 5—6	9	5	То же, что и в п. 1 7
3	1.3. 1959	14^h48^m	25 5—6	3	7	То же, что и в п. 1
4	1.3. 1959	14^h50^m	4	1	4	То же, что и в п. 1
5	9.3. 1959	$15^h34^m30^s$	60	9	8	То же 8
6	9.3. 1959	$15^h37^m45^s$	8	1	9	Возможно, $H < 110$ км 9
7	9.3. 1959	$15^h38^m50^s$	8	1	10	То же, что и в п. 6
8	26.3. 1959	12^h39^m	4—5		5	Зенит 10
9	26.3. 1959	12^h48^m	4 15—20	1	7	
10	26.3. 1959	14^h51^m	4—5			Структура сильно смазана 11
11	30.3. 1959	14^h25^m	12	2	7	
12	30.3. 1959	14^h30^m	6	1	12	То же, что и в п. 1

1) Item No; 2) date; 3) universal time; 4) number of rays; 5) remarks; 6) correction factor for curvature of earth taken into consideration; 7) the same as in item 1; 8) the same; 9) possibly H < 110 km; 10) zenith; 11) structure extremely diffuse.

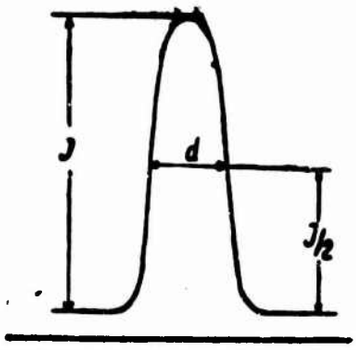

Fig. 3. For the determination of ray width.

Apparently both the physical state of those atmospheric layers in which the phenomenon occurs, as well as the conditions of observation, affect the presence of a given period in the arc under consideration. The large-scale structure (particularly λ_3) can be seen only in arcs with ray structures when observed at great distances. Since at low heights above the horizon the error in the determination of range increases, etc., the spatial period of the large-scale structure, in addition to the mean error, apparently is weighed down by a considerable systematic error.

To determine the width of the rays several microphotometric sections along the ray-structure arcs were made. We have selected rays which, in our opinion, were least subject to blurring. The ray width d was defined as the half-width of the ray contour on the trace (Fig. 3). The average values of d for two measured aurorae are presented in Table 2. On the basis of approximate estimates the width of the rays in other arc forms of ray structure is approximately the same. It is impossible to make any more precise determinations because of the influence of motion. For the same reason the widths which we have obtained apparently are somewhat exaggerated.

TABLE 2

1 № п. п.	2 Дата	3 Мировое время	4 Ширина луча-d ($\times 10^5$ см)	5 Δd ($\times 10^5$ см)	6 Число лучей	7 Примечания
1	1.3. 1959	14^h45^m	1,1	0,2	5	Учтена поправка за кривизну земли 8
2	1.3. 1959	14^h50^m	1,2	0,2	7	То же 9

1) Item No.; 2) date; 3) universal time; 4) width d of ray ($\times 10^5$ cm); 5) Δd ($\times 10^5$ cm); 6) number of rays; 7) remarks; 8) correction factor

for curvature of earth taken into consideration; 9) the same.

It is possible that the investigated structural features of arc forms with ray structures are associated with the phenomenon of horizontal electrical discharge in the upper atmosphere [2] and in a certain sense analogous to the stratification which takes place in gasdischarge tubes.

The author wishes to express his gratitude to S.K. Vsekhsvyatskiy and Ye.A. Ponomarev for their advice and comments, as well as to D.A. Andrienko and I.A. Rudenko for their assistance in the computations.

REFERENCES

1. S.K. Vsekhsvyatskiy. Collection of works on the IGY, Issue 1, Izd-vo KGU [Kiev State University Press], 1961.

2. A.I. Lebedinskiy. DAN [Proc. Acad. Sci.], 86, No. 5, 913, 1952.

CERTAIN PROBLEMS RELATING TO THE LOCAL GEOGRAPHIC DISTRIBUTION AND DYNAMICS OF POLAR AURORAE

Ye.A. Ponomarev, I.A. Rudenko

From the time of Fritz, numerous investigators have occupied themselves with the question of the geographic distribution of polar aurorae, primarily in connection with the development of an observational basis for the theory of polar aurorae. This latter circumstance left its mark on the methodology of the work. Primary attention was devoted to questions pertaining to the global distribution of polar aurorae. Appearance frequencies were studied for aurorae at various geomagnetic latitudes as functions of local time. The deflection of polar auroral arcs from geomagnetic parallels was investigated in detail [1]. This trend had a pronounced effect on the selection of the observational material. Stable quiet arcs, primarily of the homogeneous kind, were sought for evaluation. With the development of the S-180 wide-angle cameras and the establishment of an extensive network of stations during the period of the IGY a more detailed investigation of global and local features in the distribution of polar aurorae became possible with greater time resolution and more reliable conditions of simultaneity. However, the use of the S-180 cameras for these purposes is associated with certain additional difficulties which are brought about by the distortion of the mirror-optical system of this camera.

D.P. Duma [2] studied the positions of 80 polar auroral arc forms on the basis of materials provided with an S-180 camera at Tiksi Bay during the 1957-1958 observation season. In brief, the treatment method

involved the following. Arc forms with a sharp lower border were chosen on a strip of motion-picture film. Along the entire lower border a sufficient number of points were marked to provide for a comparatively complete characteristic of the projection of this arc on the frame. The broken line which was produced by connecting these points was then transferred point by point onto a geographic map prepared in Mercator projection. For each of the points a determination of its distance on the frame from the instrumental zenith was determined, and then recalculated for the range curve, with consideration of distortion, in kilometers. The azimuth of the points was determined directly by counting off from a meridian on a grid. No correction factor for the change in scale along the parallel was introduced for the plot of each of the points on the chart. The above-described method was excessively cumbersome and selective, since it did not permit the evaluation of polar aurorae with lower borders not clearly defined. Nevertheless, a number of extremely interesting and unexpected results were obtained. It turned out that the polar auroral arcs behave differently over water from their behavior over dry land. In certain cases there was a clear indication of a tendency on the part of the arcs to assume the outline of the coastline. D.P. Duma designated this phenomenon as the "shoreline effect."

Since a comparatively small quantity of material was used for purposes of evaluation, a need arose for a more careful study of the "shoreline effect" on considerably more extensive material, using more productive evaluation methods.

§1. THE EVALUATION METHOD. PLOTTING OF "TRANSFORMED" CHART

The method* used in the present paper involves the following: a chart of the surface of the earth within the limits of the field of view of the S-180 camera for Tiksi Bay was prepared so as to show dis-

tortions in accordance with the distortions of the camera's mirror-optical system. When projecting a frame of a motion-picture film onto such a "transform" chart it becomes possible to see how the luminosity is positioned relative to the coastline.

The actual projection onto the chart was accomplished by means of a D-1A slide projector. A drawing with a representation of the "transform" chart is attached to the plotting table, and this is then projected onto a wall.

The orientation of the photographs is accomplished with marks W and O to account for errors in the camera setting. Approximately 60,000 frames were examined for the present project in this manner, these pictures having been obtained during the 1957-1958 observation season.

The "transform" chart (Fig. 2) was prepared in the following manner: 117 points were marked on a blank chart of the Tiksi Bay region (Fig. 1) along the coastline and certain rivers; these points best represented the coastal outline. The point at which the S-180 camera was set up was taken as the center of the "transformed" chart. The calculation was carried out for points situated no farther than 900 km from the center, since beyond this distance the accuracy dropped below the permissible magnitude.

The coordinate axes X and Y were drawn through the projection onto the chart, and the coordinates of all of the points were determined relative to these axes. Since the blank chart was drawn in Mercator projection, consideration is given to the change in scale along the parallel (M 1:30,000,000 along parallel 75). The geographic coordinates were then determined for each point: latitude φ and longitude λ. The measurements were carried out with an accuracy of up to 1 minute of arc.

The problem involved the determination of the azimuth and distance for each point relative to the selected center. The calculation was

carried out on the basis of formulas from spherical trigonometry:

$$\sin\alpha = \frac{\sin\Delta\lambda\cos\varphi_1}{\sin l}, \qquad (1)$$

where α is the azimuth of the point; φ_1 is the geographical latitude of the point; l is the distance in angular measure; $\Delta\lambda = \lambda - \lambda_1$, where λ and λ_1 are, respectively, the geographic longitude of the center and the point.

$$\cos l = \sin\varphi_1\sin\varphi + \cos\varphi_1\cos\varphi\cdot\cos\Delta\lambda, \qquad (2)$$

where φ is the geographical latitude of the center.

Fig. 1. Blank chart of the Tiksi Bay area, with the magnetic parallels and meridians shown.

The distance obtained from Formula (2) in angular measure is converted into linear measure and expressed in km. The error in the calcu-

lations did not exceed: for the azimuth, 30'; for distance, 15 km.

For points situated no farther than 150 km, the distances were calculated with sufficient accuracy by means of formulas from plane geometry. Note should also be taken of the fact that according to the calculations that were carried out, consideration of the auroral heights above the surface of the earth would have influenced the final results insignificantly.

For purposes of studying auroral positions relative to the magnetic parallels on the "transformed" chart (Fig. 2) a magnetic coordinate grid was plotted on the blank chart (Fig. 1), for which purpose use was made of the magnetic charts of the seas of the Soviet Arctic, prepared in 1944 by the AANII [not identified in standard references] [3], and then on the basis of the points the magnetic grid was transferred to the "transformed" chart by the method described above.

Fig. 2. "Transformed" chart of the Tiksi Bay region with the magnetic

parallels and meridians plotted.

§2. INFLUENCE OF GROUND SURFACE ON DEVELOPMENT OF POLAR AURORAE

The method described above made it possible to trace the motion of various auroral forms, the transition of one form into another and to evaluate the change in auroral brightness during the process of its development.

In terms of structural features the investigated auroral forms were conveniently divided into the following types:

Arc of ray structure	LD
Arc of ray structure, with inter-ray diffuse luminosity	LD*
Homogeneous arc with ray structure	OD*
Homogeneous arc	OD
Diffuse luminosity	DS

The analysis of the observational material made it possible to establish the following quantitative relationships for the behavior of polar aurorae:

1. Homogeneous arcs (OD) 1-2 on the point scale, over water to the north of Tiksi Bay, generally quiet, little mobility, frequently showing signs of regular drift to the south. In the overwhelming majority of cases OD follow the magnetic parallel, with the eastern border of the arc generally deflected from the magnetic parallel through an angle of about 10°. Very frequently the western border of the arc shows a characteristic bend which, in general, corresponds to the bend in the magnetic parallel to the west.

A noticeable depression in OD luminosity is seen at the point where one of the western branches of the Lena enters the sea and at the entrance to Buorkhaya Inlet.

2. OD of great brightness (3 and higher on the point scale), generally speaking, are few in number and the above-described quantitative

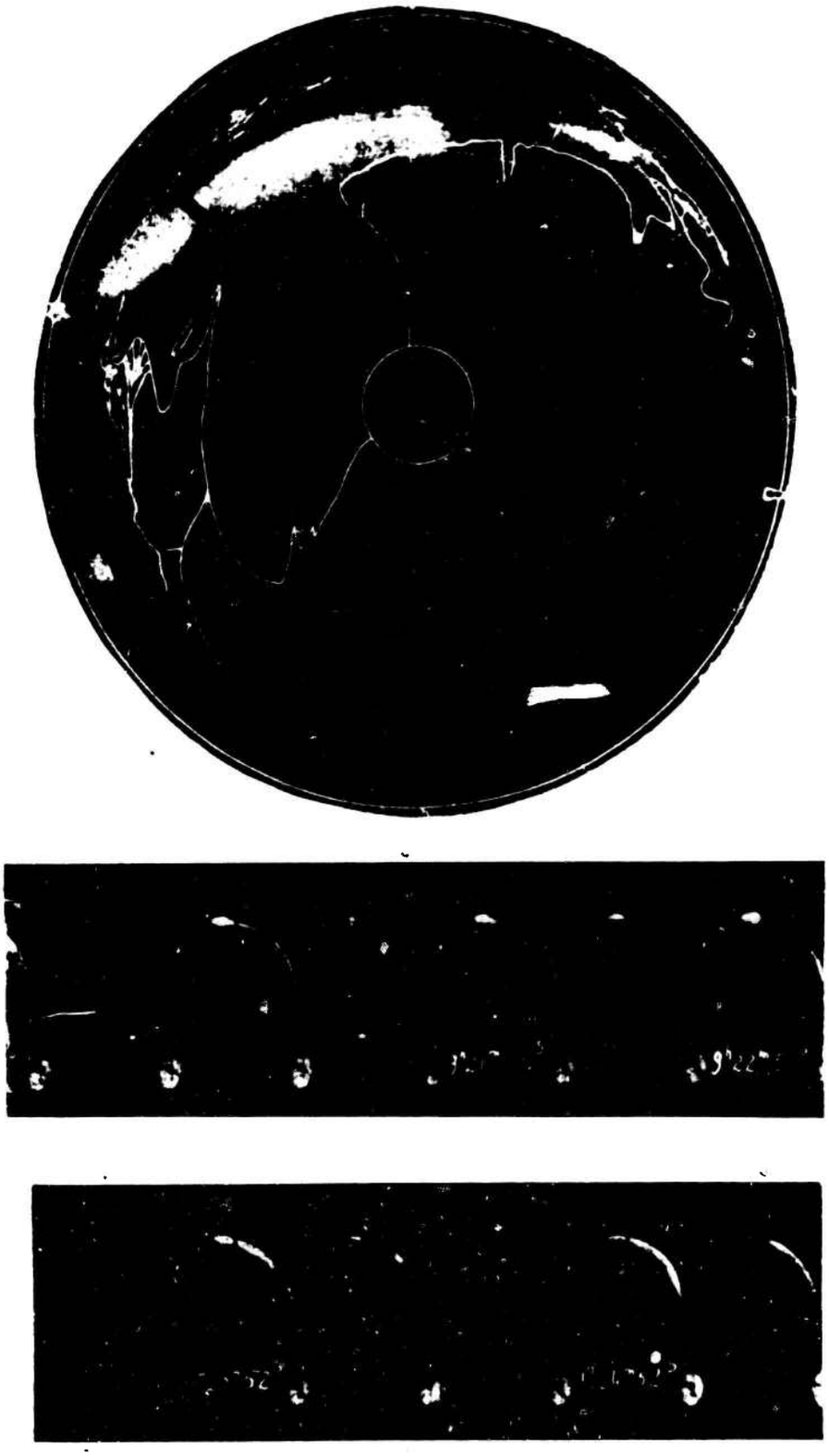

Fig. 3. Homogeneous arc with ray structure; depression in luminosity observered in the area of the Tumatskaya channel of the Lena River delta.

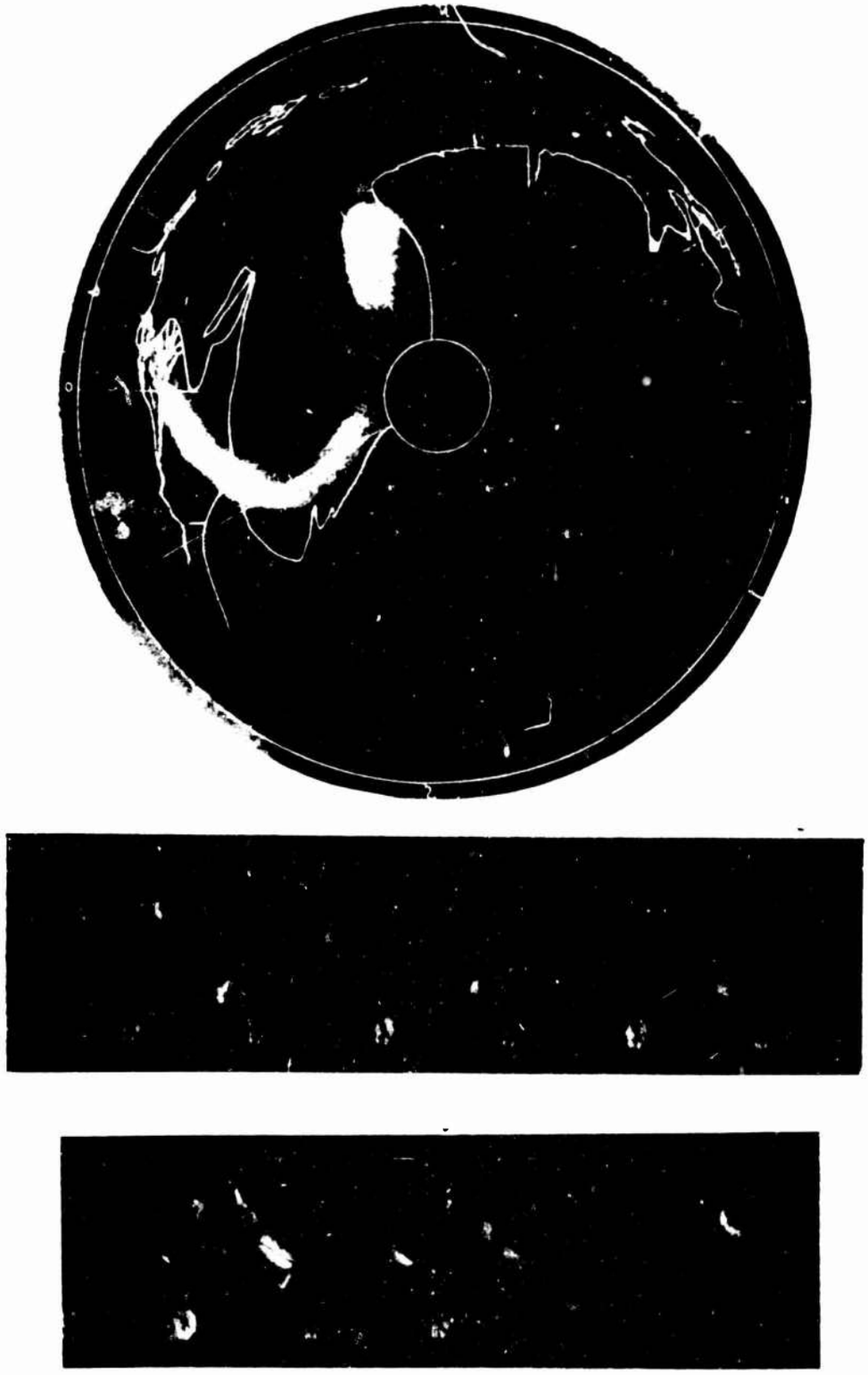

Fig. 4. Arc with ray structure and intra-ray diffuse luminosity, following the coastline of Buorkhaya Bay; discontinuity observed in the area of the Bykovskaya channel of the Lena River delta.

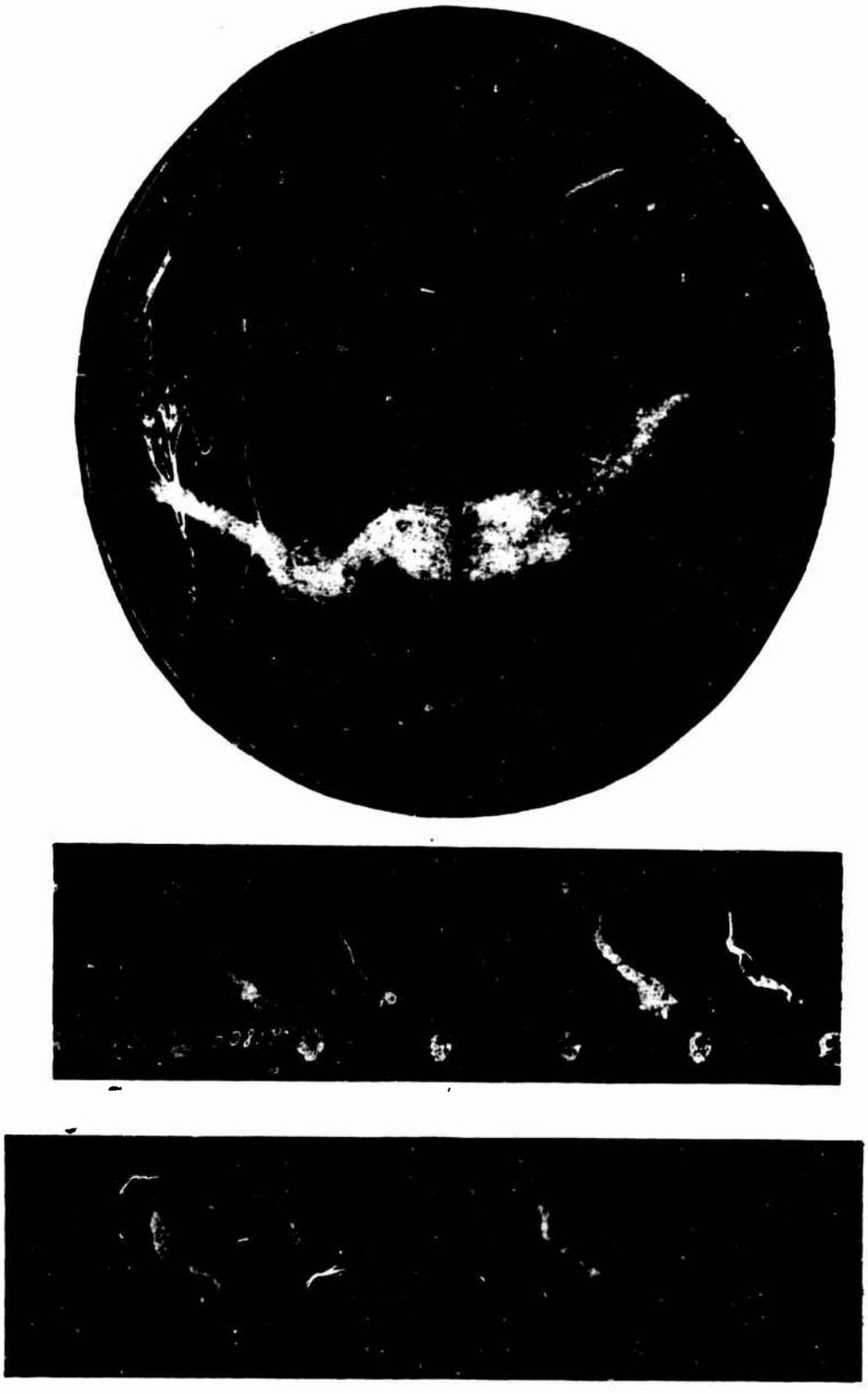

Fig. 5. Bright arc of ray structure with inter-ray diffuse luminosity, following the coastline of the Buorkhaya Inlet.

relationships are not characteristic of these.

3. Homogeneous arcs with ray structure (OD*) do not follow the magnetic parallel, although OD* which are rated 1-2 on the point scale continue to exhibit the tendency to assume positions in a west-to-east direction at some distance from coastlines.

In the overwhelming majority of cases OD* form stable discontinuities where OD show depressions in luminosity (Fig. 3).

4. Arcs with ray structure showing inter-ray luminosity (LD*) as a rule, exhibit "complete" stable discontinuities, i.e., luminosity at those points where OD exhibit depressions does not occur in the case of LD*. If LD* have formed immediately out of OD, the discontinuities arise simultaneously.

Note should be taken of the fact that at the zenith in the NO direction LD and LD* rarely bend (within several seconds after appearance), following approximately the coastal outline. This effect occurs in 20-25% of all arcs and is seen in the area of the Buorkhaya Inlet, and in the area of the Gulf of Yana and Khatanga (Figs. 4 and 5).

The LD* are oriented approximately as the OD (see item 3).

5. The behavior of the LD seems very complex and little governed by the presence of a coastline and the direction of the magnetic parallels, so that any conclusions are difficult.

These results lead to the conclusion that the properties of the ground surface somehow affect the development of polar aurorae. The role of the magnetic field as a factor governing the direction of polar auroral arcs varies with the auroral forms and is particularly pronounced in the case of feeble homogeneous arcs.

REFERENCES

1. S.K. Mitra. Verkhnyaya atmosfera [The Upper Atmosphere]

2. D.P. Duma. Informatsionnyy byulleten' [Informational Bulletin], No. 3, Komitet MGG USSR [IGY Committee of the UkrSSR], 1961.

3. Magnetic Charts of the Seas of the Soviet Arctic, prepared in 1944 by the AANII.

Manuscript Page No.

[Footnotes]

130 The idea for this method had been simultaneously and independently put forward by Yu.A. Nadubovich.

SIMILARITIES BETWEEN THE AURORAE BOREALIS AND AUSTRALIS

G.A. Rubo

Data produced in 1958 in accordance with the IGY program at Mostakh and Mirnyy Stations by means of S-180 cameras were used to study similarities between the northern and southern polar aurorae, a study proposed and headed by Professor S.K. Vsekhsvyatskiy.

The nature of polar auroral observations is such that there are only brief intervals of time for which the northern and southern aurorae can be compared. These intervals are symmetrical with respect to the equinox nodes and are functions of the geographic coordinates of the stations. The observations of the aurorae are not conducted around the clock, thus even further limiting the possibilities of comparison. The selection of stations in the northern and southern hemispheres is governed by the requirement that the geomagnetic characteristics of these stations not differ markedly from one another.

The Mostakh and Mirnyy Stations which we selected are found on markedly different geomagnetic longitudes, with a slightly less pronounced divergence in geomagnetic latitudes and geographic coordinates, thus permitting comparison of the progress and nature of polar aurorae at these stations for three months of the year, and namely from March through the first half of April and from September through the first half of October.

The processing of the survey material used for this paper showed that there are 16 nights suitable for direct comparison (the observations were carried out simultaneously at both stations). For the sta-

tistical evaluation (analysis of auroral forms, course of diurnal and seasonal activity) the possibilities were greater and cover a complex of 45 nights for Mostakh Station and 49 nights for Mirnyy Station.

Forms. In virtually all cases of aurcral photographs it is possible to classify them according to a given structural form. In addition, motion-picture photography makes it possible to employ the dynamics of auroral development to the problem of determining auroral forms. As a rule, active polar auroral forms (arcs with ray structures, rays, coronas) undergo extensive changes within brief intervals of time, which makes it possible to distinguish these virtually without error from the quiet forms (quiet arcs, diffuse surfaces, horizon glow).

The most frequently encountered active polar auroral forms both for Mostakh Station and for Mirnyy Station are the arcs of ray structure (RA) and [homogeneous] quiet arcs (HA), as well as rays (R). From among the quiet forms, special mention should be made of the [feeble] glow (G) at the horizon. However, in all probability, the pulsating surfaces (PS) which were visually observed frequently at Mostakh Station and Tiksi Bay do not show up on the photographs taken with the S-180 camera.

The development and change in the auroral forms at Mostakh and Mirnyy Stations show no pronounced differences. The most extensive continuous forms at these stations are the following:

$$G-RA(HA)-G,$$
$$R-RA-R-RA,$$
$$RA-C-R,$$

where C is the corona.

Diurnal activity. The variations in polar auroral activity at night were studied in an analysis of plots produced for these stations on the basis of motion-picture films for the above-indicated periods.

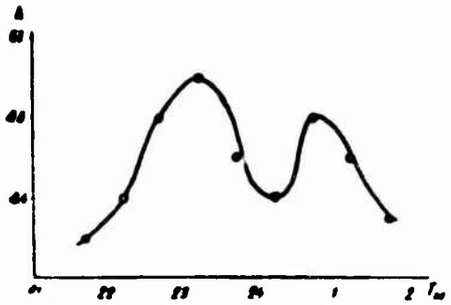

Fig. 1. Curve showing diurnal polar auroral activity for Mostakh Station.

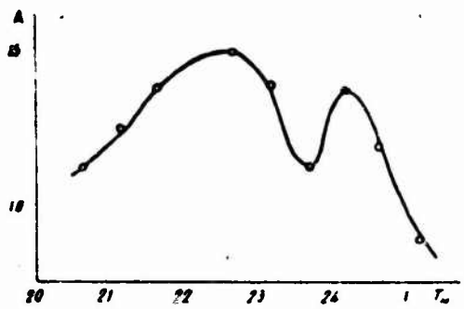

Fig. 2. Curve showing diurnal polar auroral activity at Mirnyy Station.

A motion-picture plot is a qualitative index of the intensity of polar aurorae. In the preparation of the motion-picture plots consideration is given to the auroral form (active or quiet) and their position (aurora overhead or at the horizon).

The number of plot squares filled at half-hour intervals of time for all days of observation was computed, and then averaged over the number of days (A). The pattern of the diurnal auroral activity yielded the function $A = A(t)$, where t is local time.

An analysis of the derived curves (Figs. 1 and 2) shows that the diurnal activity curve for Mostakh and Mirnyy Stations yields a maximum at around 23^h local time – the so-called main diurnal-activity maximum for polar aurorae, studied in detail by Vegard. In addition to an indication that the diurnal polar auroral activity is similar for the subject stations, the result which is in good agreement with the results obtained by other investigators [1] is important from the standpoint that it characterizes the objectivity of the motion-picture plot as a descriptive index of polar aurorae.

Seasonal polar auroral activity. The A-index for an evaluation of the integral activity of polar aurorae during a single day was found by a method analogous to that described above. To eliminate the influence of diurnal changes in polar auroral activity on the preparation of the A-index, specific intervals of time were selected for Mostakh and Mirnyy stations, and this index was established for these. The selection

of the intervals was based on the curves showing the diurnal activity of the polar aurorae. For Mostakh Station the chosen interval was from 12 to 18 hours universal time, corresponding to 21^h-3^h local time; for Mirnyy Station, from 15 to 21 hours, universal time, also corresponding to 21^h-3^h local time.

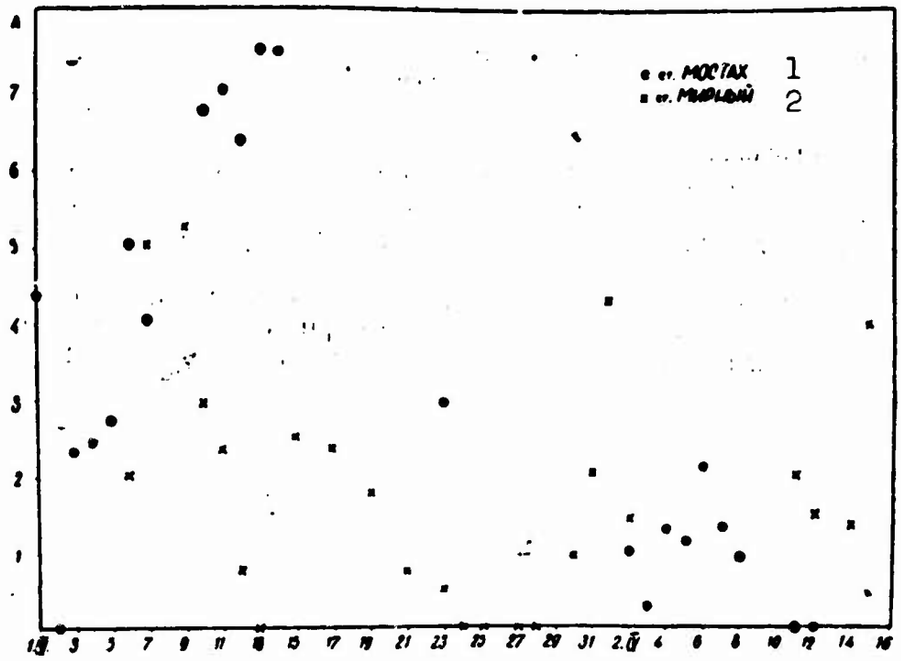

Fig. 3. Polar auroral activity in March-April 1958 at Mostakh and Mirnyy stations. 1) Mostakh; 2) Mirnyy.

The derived results are shown in Figs. 3 and 4. An examination of these leads to the conclusion: 1) that the polar auroral activity in March-first half of April at Mostakh Station (northern hemisphere) is greater than at Mirnyy Station (southern hemisphere); 2) that the polar auroral activity from September to the first half of October at Mirnyy Station is greater than at Mostakh Station.

An analysis of the durations of continuously recurring polar auroral forms also bears out this conclusion. Namely: from March through the first half of April there are more of these forms and they last longer in the northern hemisphere, whereas from September through the

first half of October this is the trend of the southern hemisphere.

It has also been noted that the draperies (D) and the corona (C) are forms which are not very extensive, but stand out because of their ray structure and are visible for a longer period of time in the northern hemisphere from March through the first half of April and not encountered at all from September through the first half of October, whereas the exact opposite is true for the southern hemisphere.

Finally, we examined the curves of diurnal polar auroral activity for the northern and southern hemispheres, taken from [2].

We found correlations between these curves for the intervals from January through May and from August through December. These proved, respectively, equal to 0.72 and 0.65. Then correlations were found for the curves shifted by half a year, i.e., between the polar auroral activity curves for January-May for the northern hemisphere and for August-December for the southern hemisphere, as well as correlations between the polar auroral activity curves for August-December for the northern hemisphere and for January-May for the southern hemisphere. The correlations were, respectively, 0.82 and 0.85. Thus the correlations between the polar auroral activity curves in the northern and southern hemispheres, shifted by half a year are systematically higher than the correlations between the activity curves which coincide in time.

This conclusion serves as a new argument in favor of significant differences in seasonal polar auroral activity for the northern and southern hemispheres. Essentially these differences involve the following: polar auroral activity near the vernal equinox is higher in the norther hemisphere, whereas near the autumnal equinox this activity is greater in the southern hemisphere.

Polar-auroral and polar activity. The polar auroral activity in-

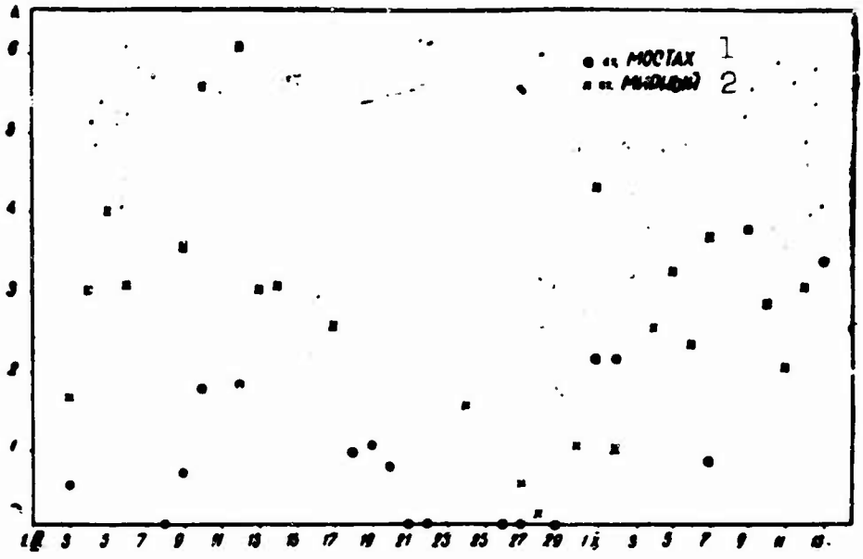

Fig. 4. Polar auroral activity in September-October 1958 at Mostakh and Mirnyy stations. 1) Mostakh; 2) Mirnyy.

dicated in Figs. 3 and 4 demonstrates that in addition to the above considered differences in auroral activity for the northern and southern hemispheres, it is possible also to note the following:

1) There are days in which aurorae are observed at Mostakh Station, but not at Mirnyy Station, and vice versa (13 March, 11 September, 27 September).

2) The auroral activity at Mostakh Station on 13 March was maximum whereas at Mirnyy Station on this same day a clear activity minimum is indicated.

It would be interesting to examine solar activity for these same periods and to establish a relationship between this and the polar auroral activity. Descriptions of solar activity were used for this purpose [3].

After an examination of the relationship between the existence on the sun of active regions (spot groupings accompanied by flares, facular and floccular fields, etc.) and the polar auroral activity, it can be demonstrated that: a) from March through the first half of April the

presence of active fields on the sun and an increase in polar auroral activity at Mostakh Station, whereas the polar auroral activity at Mirnyy Station fails to follow this rule; b) from September through the first half of October the existence of active regions on the sun can be associated with an increase in polar auroral activity at Mirnyy Station; the attempt to relate solar activity for this period with the solar auroral activity at Mostakh Station yields a negative result.

If we take into consideration that the polar auroral activity at Mostakh Station from March through the first half of April is greater than at Mirnyy Station, and that from September through the first half of October the opposite is found to be true, we can draw the following definitive conclusion: the course of solar activity better reflects the activity of polar aurorae in the hemisphere in which the activity during the given half year is greater.

Simultaneous appearance of polar aurorae. A comparison of the instants of polar auroral [illegible] at Mirnyy and Mostakh Stations shows that the predominant number of auroral appearances at these stations at instants of universal time [illegible] established only five cases in which the appearance of aurorae at Mostakh Station was accompanied by the appearance of aurorae at Mirnyy Station. In three cases these were [illegible] at Mostakh and at Mirnyy Stations. In one case [illegible] with ray structure was observed, while [illegible] time rays appeared. The opposite case [illegible] established at Mirnyy Station, [illegible] appearance of an arc with ray structure at [illegible] from rapidly disintegrating into [illegible] on a total of 16 nights both at Mirnyy and Mostakh Stations. As a result there are very few [illegible] simultaneously at Mirnyy and

at Mostakh Stations.

Investigations of polar aurorae carried out in the USA, Canada and in the Antarctic led to the conclusion that polar aurorae occur simultaneously in the northern and southern hemispheres [4]. Aurorae whose times of onset differed by no more than 1 hour, universal time, were regarded as occurring simultaneously. However, we included among the simultaneous aurorae only those whose times of onset according to universal time differed by no more than one minute – the limit of determination for the instant of aurora onset when working with a camera shooting 1 frame per minute.

Unfortunately, the interpretation of the derived results is made particularly difficult because of the substantial differences in geomagnetic coordinates of the stations. Nevertheless, the conclusion in [4] is doubtful. Further investigation of this problem is necessary.

The azimuths of polar auroral arcs. Based on photographic materials obtained at Mostakh and Mirnyy Stations, we found the average deflections of the magnetic azimuths of the ends of the arcs as seen on the motion-picture frames from the magnetic parallels ($\Delta\alpha_m$) for a unit interval of time, set at one hour. We considered only the rather quiet arcs which passed through the zenith or in the immediate vicinity of it. There were about ten arcs on the average which served as the basis for the determination of the deflections for an interval of one hour. The determination accuracy for the azimuths of the arc ends did not exceed $2\text{-}3^\circ$, which is explained by the great distortion at the edge of the field for the S-180 camera and the fact that the ends themselves were diffuse.

The derived value of $\Delta\alpha_m$ served as the basis for the construction of the function relating this quantity to local time (Fig. 5). The magnetic declination for Mostakh Station was assumed to be equal to (-10°)

and that for Mirnyy Station (-78°).

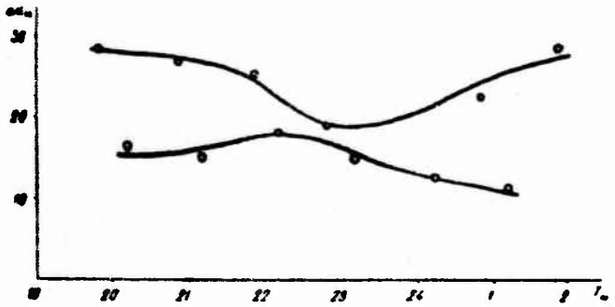

Fig. 5. Deflection of the ends of polar auroral arcs from the parallel. The upper curve is for Mirnyy Station; the lower curve is for Mostakh Station.

An analysis of this figure shows that for Mostakh Station the deflection of the azimuths of the arcs from the magnetic parallel amounts to 13-15°, which is in rather good agreement with the Vegard results [5]; he obtained results indicating that this deflection was of the order of 10°. For Mirnyy Station the deflection reaches 20-25°. In addition, while at Mostakh Station the maximum of the average deflections for the arc azimuths of the polar aurorae from the magnetic parallel coincide with the maximum of the diurnal polar auroral activity, i.e., onset at around 23 hours local time, at Mirnyy Station at this time a minimum of deflection is observed.

Conclusions. A study of the forms, behavior and polar auroral activity at Mostakh and Mirnyy Stations shows that in addition to the great similarity of these phenomena there exist substantial differences between the characteristics of the polar aurorae in the northern and southern hemispheres.

The similarities are indicated by the following:

1 the main maximum of diurnal activity for Mostakh and Mirnyy Stations sets in at around 23 hours local time;

2 significant differences in auroral forms and their development

are not observed;

3) polar auroral arcs follow the magnetic parallels.

The differences lead to the following:

1) from March through the first half of April the polar auroral activity at Mostakh is greater than at Mirnyy; from September through the first half of October the opposite is the case;

2) the systematic deflection of the ends of the polar auroral arcs from the magnetic parallel for Mostakh Station amounts to 13-15°; for Mirnyy Station the corresponding figure is 23-25°;

3) the deflection of the ends of the polar auroral arcs from the magnetic parallel is at its maximum for Mostakh Station and at its Minimum for Mirnyy Station close to the main maximum of the diurnal polar auroral activity.

The study of the aurorae at Mostakh and Mirnyy Stations also shows that:

1) the course of solar activity is in better agreement with the activity of polar aurorae in the hemisphere in which this activity in the given half year is greater;

2) there are days on which at Mirnyy Station aurorae were seen, while none were observed at Mostakh Station; the opposite phenomenon was also encountered;

3) aurorae occurring simultaneously at Mostakh and Mirnyy Stations are very few in number;

4) forms and development of forms for simultaneously occurring polar aurorae are not necessarily identical.

REFERENCES

1. B.W. Currie H.W. Edwards. Terr. Magn. and Atmos. Elec., 39, 293, 1934.

2. S. Chapman, J. Bartels. Geomagnetism, Oxford, Vol. I, page 474, 1951.

3. Kosmicheskiye dannyye [Cosmic Data] NIIZMIR [not identified in standard references], Nos. 3, 4, 9, 10, 1958.

4. Sky and Telescope. 18, No. 12, 672, 1959.

5. S. Mitra. Verkhnyaya atmosfera [The Upper Atmosphere], 1955, page 311.